# IDENTIFICATION OF POTENTIAL BIOMARKERS OF CARDIOTOXICITY INDUCED BY DOXORUBICIN THERAPY IN A TUMOUR BEARING MODEL BY TARGETING SPECIFIC MICRO-RNAs

by

**Temitope R. Ogundipe**

*Dissertation presented in fulfilment of the requirements for the degree of Doctor of Science in the faculty of Physiological Sciences at Stellenbosch University*

**Supervisor**: Dr Balindiwe JN Sishi

March 2021

*The financial assistance of the National Research Foundation (NRF) towards this research is hereby acknowledged. Opinions expressed and conclusions arrived at, are those of the author and are not necessarily to be attributed to the NRF*

## DECLARATION

By submitting this thesis electronically, I declare that the entirety of the work contained therein is my own, original work, that I am the sole author thereof (save to the extent explicitly otherwise stated), that reproduction and publication thereof by Stellenbosch University will not infringe any third party rights and that I have not previously in its entirety or in part submitted it for obtaining any qualification.

March 2021

# ABSTRACT

**Introduction**: Anthracycline-induced cardiotoxicity, a major side effect of chemotherapeutic drugs such as doxorubicin (DOX), has been a priority within the field of cardio-oncology for a number of decades. While multiple approaches and strategies have been utilized to understand and rectify this enigmatic condition, very little translatable research success has been achieved. Paramount to the reasons for this lack of utilizable return is that research has largely focused on the acute form of this disease, which is reversible, in contrast to the chronic form which has no cure. The majority of the tried and tested interventions have prioritized the oxidative stress theory, and the experimental models that have been developed have omitted the potential contributory effect of tumours within this context. Since their discovery, the elucidation of the primary roles of microRNAs (miRNAs) in the pathogenesis of oncological and non-oncological diseases has received much attention. As such, the detection of the existence of cell-free miRNAs in circulation has motivated researchers to investigate the role of these small evolutionary conserved endogenous single-stranded, non-coding RNAs as prospective non-invasive biomarkers. Therefore, this study explored the expression profile of a few miRNAs that have been observed in other pathologies that have the potential to be of significance in this context, by using a clinically relevant model that takes into account the plausible effects of tumour presence and the known DOX concomitant consequences.

**Methods**: Chronic DOX-induced cardiotoxicity was initiated through cumulative DOX injections (2.5 mg/kg/week) in 37 female Sprague-Dawley rats over the course of eight weeks. Prior to this, breast cancer mammary gland tumours were induced in these experimental animals through the injection of LA7 cells into the mammary fat pad following a carefully optimized protocol. Comparisons were carried out between groups that included a vehicle (control) (Hank's balanced salt solution), tumour, DOX and a combination of the tumour and DOX-treatment. A week after the last DOX injection, animals were euthanized, blood was collected and the heart was excised for molecular and biochemical analysis. To detect early changes in miRNA profile

expression, some animals were sacrificed after five weeks to represent early chronic modifications, whereas the rest of the experimental animals were sacrificed after nine weeks to represent late chronic adaptions. While miRNA manifestation was evaluated from plasma samples collected and assessed via quantitative PCR, the hallmarks of DOX-induced cardiotoxicity such as cardiac hypertrophy, fibrosis, oxidative stress and apoptosis were assessed via histological staining and western blotting techniques.

**Results and Discussion**: Mammary tumours were successfully induced and reached a peak volume (2563.00 ± 478.20 $mm^3$) after two weeks of LA7 cell inoculation. It was also evident from these results that DOX is an effective chemotherapeutic agent for breast cancer; as tumour growth was significantly lower (1523.00 ± 457.80 $mm^3$, $p< 0.01$) at this time point when compared to the tumour only group. Whilst miR-208a was significantly down-regulated in all treatment groups when compared to the vehicle (control) after eight weeks, plasma miR-29b expression was substantially upregulated across all groups after eight weeks versus the four week time point. This study observed no noteworthy changes in miRNA-133a and 133b following eight weeks of treatment. Together, these results, in amalgamation with increased collagen deposition (306.90 ± 52.62%, $p < 0.01$) vs control (100.00 ± 6.35%), cleaved caspase-7 (844.10 ± 166.21%, $p <0.05$) vs control (100.00 ± 3.40%) and MLC-2v (406.90± 47.18%, $p < 0.01$) vs control (100.00 ± 3.12%), in the combination group, demonstrated that miR-208a exhibits potential as a non-invasive biomarker of late chronic myocardial toxicity linked to fibrosis, apoptosis and cardiac hypertrophy, respectively. miR-208a and miR-133a remain the only miRNAs in this context that may have the potential to be utilized as early chronic biomarkers of cardiotoxicity in the presence of a tumour, however further investigations are warranted.

# OPSOMMING

**Uittreksel**:

***Inleiding***: Antrasiklien-geïnduseerde kardiotoksisieit, ‘n hoof newe-effek van chemoterapeutiese middels soos doksorubisien (DOX), is reeds vir dekades die prioriteit in die kardio-onkologiese veld. Terwyl daar verskeie benaderings en strategieë aangewend word om hierdie enigmatiese toestand te gebruik en te verstaan, is weinig verstaanbare navorsingsukses bereik. Die hoofredes vir die onsuksesvolle uitkoms is die fokus op navorsing van die akute vorm, wat omkeerbaar is, van hierdie siekte, eerder as die chroniese vorm, wat nie omkeerbaar is. Die meerderheid van die intervensies wat gedoen en getoets is, het op die oksidatiewe stres teorie berus, en die eksperimentele modelle wat ontwikkel is, het die potensiële bydraende effek van tumore binne hierdie konteks, weggelaat. Sedert hul ontdekking, het die primêre rolle van mikroRNAs (miRNAs) in die patogenese van onkologiese en nie-onkologiese siektes baie aandag verkry. Na die ondekking van selvrye miRNAs in die sirkulasie, het dit navorsers gemotiveer om die rol van hierdie klein evolusionêr gekonserveerde endogene enklestring, nie-gekodeerde RNA as potensiële, nie-ingrypende biomerkers te ondersoek. Daarom het hierdie studie die uitdrukkingsprofiele van ‘n paar miRNAs, wat in ander patologieë waargeneem is en moontlik relevant kan wees in hierdie konteks, deur gebruik te maak van ‘n klinies relevante model wat die waarskynlike effekte van die teenwoordigheid van ‘n tumor en die bekende DOX verwante gevolge in ag neem.

***Metodes***: Chroniese DOX-geinduseerde kardiotoksisiteit is in 37 vroulike Sprague Dawley rotte oor ‘n periode van agte weke geinisiëer deur middel van kumulatiewe DOX inspuitings (2.5 mg/kg/week). Voor dit, is borskanker borskliertumore in hierdie eksperimentele diere geinduseer deur LA7 selle in die borsvetarea in te spuit na ‘n optimaliserings protokol gevolg is. Tussengroep vergelykings is uitgevoer wat ‘n draergroep (kontrole) (Hank’s gebalanseerde soutoplossing), tumor, DOX en ‘n kombinasie van die tumor en DOX-behandeling ingesluit het. ‘n Week na die finale DOX inspuiting is die diere dood gemaak, bloed was versamel en die hart is gedissekteer vir molekulêre en biochemiese analises. Sommige diere is na vyf weke dood gemaak sodat vroeë veranderinge in die miRNA profiel uitdrukking ontleed kon

word om vroeë chroniese veranderinge te simuleer, terwyl die oorblywende eksperimentele diere na nege weke dood gemaak is om latere chroniese aanpassings te simuleer. miRNA manifestering is deur middel van plasma monsters verkry en deur kwantitatiewe PKR ontleed, en die kenmerkende DOX-geinduseerde kardiotoksisiteit soos bv. kardiale hipertrofie, fibrose, oksidatiewe stres en apoptose, is deur middel van histologiese kleurings, gical kleuring en westerse blattering tegnieke ondersoek.

***Resultate en Bespreking***: Borstumore is suksesvol verkry na selinokulasie met LA7, en na twee weke is piekvolume bereik (2563.00 ± 478.20 mm3). Dit is verder bevestig dat DOX ‘n effektiewe chemoterapeutiese middel vir borskanker is; omrede die tumorgroei betekenisvol laer was (1523.00 ± 457.80 mm3, p< 0.01) by hierdie tydsinterval, vergeleke met die tumorgroep. Terwyl miR-208a betekenisvol afgereguleer was in alle groepe, vergeleke met die draer (kontrole) groep na agt weke, het plasma miR-29b uitdrukking aansienlik verhoog oor alle groepe na agt weke vergeleke met die vier-week periode. Hierdie studie rapporteur geen beduidende veranderinge in miRNA-133a en 133b na ‘n agt weke behandeling nie. Gesamentlik demonstreer die resultate, tesame met verhoogde kollageen-neerlegging (306.90 ± 52.62%, p < 0.01) vs kontrole (100.00 ± 6.35%), gesplyte kaspase -7 (844.10 ± 166.21%, p <0.05) vs kontrole (100.00 ± 3.40%) en MLC-2v (406.90± 47.18%, p < 0.01) vs kontrole (100.00 ± 3.12%), in die gekombineerde groep, dat miR-208a potensiaal as ‘n nie-ingrypende biomarkers van latere chroniese miokardiale toksistiteit, wat gekoppel is met fibrose, apoptose en kardiale hpertrofie, vertoon. miR-208a en miR-133a is die enigste miRNAs in hierdie konteks wat potensiaal toon as vroeë chroniese biomerkers van kardiotoksisiteit in die teenwoordigheid van ‘n tumor, maar verdere ondersoeke word aanbeveel.

# ACKNOWLEDGEMENTS

First I would like to acknowledge **God's** guidance on my path so far.

To my supervisor and mentor, **Dr Balindiwe Sishi** for sticking with me this long, the trust and belief in me even when I have doubts. Always challenging me and pushing for more. I appreciate you immensely. Thank you for the incredible growth I have been able to achieve under your wing, for the extra mile gone and the mountains moved to get this project completed despite the multiple obstacles. I would always be grateful for your mentorship and friendship.

To my **dad, Dr Ogundipe**, **mom, Mrs Ogundipe** and **siblings, Tomi** and **Toyin**, you have been my sources of strength. Through the past years and the heavy toll it has taken on us all, you have remained supportive, loving and I could not even begin to repay you all for the sacrifices you have had to make. It's never easy, but I know it'll all work out for good. I love you all.

To **Nolu**, what a roller coaster it has been. The long late nights of grafting, writing, consistent support, care packages, motivation, absolute belief in me, the long conversations about both our progresses, the venting, strategizing and motivation. Thank you for the love and support, you are invaluable to me.

To **Prof Myburgh**, you are so knowledgeable and approachable. A wonderful human, I could not help but be flattered when you took interest in this work. I appreciate your guidance and contribution.

To **Dr Krygsman**, I thank you for always having your door open to listen. Your contribution to the tumour model of this study is immensely appreciated.

To **Dr Nell,** thank you so much for always being an ever present figure of support. Your assistance with translating the abstract was also invaluable.

To **Judith**, what would I have done without your assistance? Thank you for all the hours both working and after, you generously invested in helping execute the model.

To **Jonnifer**, I appreciate your friendship and support for the duration of my time at the department. Thank you for always making the space feel that more homely.

To **Jason,** I cannot tell you how appreciative I have been for your help and friendship during this period. From lab sessions filled with labelling tons of qPCR eppis, double-gloving to handle corrosive chemicals to Saturday surf sessions, I really appreciate you.

To **Tumi and Toni**, Thank you for continuing to be sources of support and friendship despite moving to the working world. Tumi, you would not understand how much I value the long phone calls. Toni, your friendship is invaluable, all the chats we have keep me going. Thank you.

To my **colleagues at the department** and the data hub scientists, I thank you for always making the lab a welcoming environment.

To the **NRF**, **South African Medical Research Council (SAMRC)** and the **Oppenheimer Memorial Trust (OMT)**, Thank you for the financial support to enable me complete this study. Without it, I would not have been able to.

# LIST OF COLLABORATIVE PUBLICATIONS

- Everson, F., Genis, A., Ogundipe, T, De Boever, P, Goswami, N, Lochner, A, Blackhurst, D, Strijdom, H., 2018. Treatment with a fixed dose combination antiretroviral therapy drug containing tenofovir, emtricitabine and efavirenz is associated with cardioprotection in high calorie diet-induced obese rats. *PLOS ONE*. 13, 1-27
- Strijdom, H., Goswami, N., De Boever, P., Westcott, C., Ogundipe, T., Everson, F., Genis, A., 2016. Cardiometabolic and vascular effects of treatment with a fixed-dose combination anti-retroviral drug containing nucleoside and non-nucleoside reverse transcriptase inhibitors (NRTIs and NNRTIs) in adult rats. *Abstracts/Atherosclerosis*. 252, e1-e196
- Genis, A., Everson, F., Ogundipe, T., Grandjean, T., De Boever, P., Goswami, N., Strijdom, H., 2016. Investigating the cardiovascular effects of antiretroviral drugs in a lean and high fat/sucrose diet rat model of obesity. *Cardiovascular Research*. 111, S74-S75.

# ABBREVIATIONS

| Abbreviation | Meaning |
|---|---|
| ADR | Adriamycin |
| ANOVA | Analysis of Variance |
| β-MHC | Beta Myosin Heavy Chain |
| BNP | Brain Natriuretic Peptide |
| CCL2/CCL5 | Chemokine Ligand 2/Chemokine Ligand 5 |
| cDNA | Complementary Deoxyribonucleic acid |
| CK-MB | Cytosolic Creatine Kinase |
| $CO_2$ | Carbon dioxide |
| cTI | Cardiac troponin I |
| Cq | Quantification Cycle |
| CuZnSOD | Copper Zinc Superoxide Dismutase |
| CVD | Cardiovascular Disease |
| DEX | Dexrazoxane |
| DNA | Deoxyribonucleic Acid |
| DOX | Doxorubicin |
| DRP1 | Dynamin Related Protein 1 |
| ECL | Enhanced Chemiluminescence |
| EDTA | Ethylenediaminetetra-acetic Acid |
| $Fe^{2+}$ | Iron ions |
| GAPDH | Glyceraldehyde 3-Phosphate Dehydrogenase |
| H & E | Hematoxylin & Eosin |
| HF | Heart Failure |
| HIV/AIDS | Human Immuno-deficiency Virus/Acquired Immune Deficiency Syndrome |

| | |
|---|---|
| HRP | Horse Radish Peroxidase |
| HSP | Heat Shock Protein |
| LVEF | Left Ventricular Ejection Fraction |
| MIQE | Minimum Information For The Publication Of Quantitative Real-Time PCR |
| miR | MicroRNA (naming abbreviation) |
| miRNA | MicroRNA |
| miRISC | Multiprotein RNA-Induced-Silencing Complex |
| MFN1 | Mitofusin 1 |
| MFF | Mitochondrial Fusion Factor |
| MGB | Minor Groove Binder |
| MnSOD | Manganese Superoxide Dismutase |
| MRI | Magnetic Resonance Imaging |
| MLC-2V | Myosin Light Chain - beta |
| NaCl | Sodium Chloride |
| NADH | Nicotinamide Adenine Dinucleotide |
| NADPH | Nicotinamide Adenine Dinucleotide Phosphate |
| NaF | Sodium Fluoride |
| NFκβ | Nuclear Factor Kappa-Light-Chain-Enhancer of Activated B Cells |
| NFQ | Non-fluorescent Quencher |
| NP40 | Non-ionic Polyoxyethylene 40 |
| $O_2$ | Oxygen |
| P53 | Tumour Protein P53 |
| PARP | Poly(ADP)ribose polymerase |
| PBS | Phosphate Buffered Saline |
| PI | Protease Inhibitor |

| | |
|---|---|
| PMSF | Phenylmethylsulfonyl Fluoride |
| Poly[A] | Polyadenylation |
| PVDF | Polyvinyldinefluoride |
| QPCR | Quantitative Polymerase Chain Reaction |
| QTc | Corrected QT interval |
| R | Reporter DYE |
| RhoA | Ras Homolog Family Member A |
| RhoK | Rho Kinase |
| RIPA | Radio-immunoprecipitation |
| RNA | Ribonucleic Acid |
| RNASE | Ribonuclease |
| ROS | Reactive Oxygen Species |
| RT | Reverse Transcriptase |
| SMN | Secondary Malignant Neoplasm |
| SOD2 | Superoxide Dismutase 2 |
| STAT3 | Signal Transducer and Activator of Transcription 3 |
| TBS-T | Tris Buffered Saline and Tween |
| TGF-β | Transformation Growth Factor-Beta |
| TNF-α | Tumour Necrosis Factor Alpha |
| TOMM20 | Translocase of Outer Mitochondrial Membrane 20 |
| US/USA | United States of America |

## UNITS

| | |
|---|---|
| **g** | gram |
| **mg** | milligram |
| **kg** | kilogram |
| **mM** | millimolar |
| **µM** | micromolar |
| **nM** | nanomolar |
| **$mm^3$** | millimetre cubed |
| **M** | molar |
| **nm** | nanometer |
| **L** | litre |
| **mL** | millilitre |
| **µL** | microliter |
| **g/mL** | gram per millilitre |
| **mg/mL** | milligram per millilitre |
| **ng/mL** | nanogram per millilitre |
| **$mg/m^2$** | milligram per metre squared |
| **mg/kg** | milligrams per kilogram |
| **µg/kg** | microgram per kilogram |
| **$^o$ C** | degrees celsius |
| **%** | percentage |
| **Hrs** | hours |
| **Mins** | minutes |
| **Secs** | seconds |

# TABLES

# FIGURES

# CONTENTS

## Contents

# Chapter 1. LITERATURE REVIEW

## 1.1. Introduction

Along with cardiovascular diseases (CVDs), cancer remains one of the two most prominent causes of global mortality. CVDs, the number one contributor, have accounted for a 17.3 million deaths globally (Mozaffarian *et al.,* 2015). It is also the most prevalent disease; more especially in more developed regions where lifestyle attributes contribute heavily to the development of the disease. An aging population, higher food consumption, and adopting a number of high-risk lifestyle behaviours such as sedentary lifestyles, alcohol consumption and abuse, westernized diets, and smoking have all contributed to the increased risk for the development of these diseases and complications related to them (Harikrishnan *et al*., 2014). As a result of these, CVD rates are on the rise, with mortality predicted to rise as high as 23.6 million within the next decade (Mozaffarian *et al.,* 2015). Cancers in their own right have also contributed immensely to global morbidity, with incidence and prevalence rates second only to CVDs, and mortality as high as 7.6 million deaths in the year 2008 (Bray *et al*., 2013), and 15 million by 2013 (Roth *et al*., 2015). These global statistics illustrate the immense nature of these diseases. More specifically, statistics in the region of sub-Saharan Africa, which South Africa falls under, demonstrate their local impact as well. Kingham *et al*., (2013) reported that cancer incidences are on the rise in low-and middle-income countries, due to the similar reasons responsible for the increase in CVDs. This fact is emphasized by reports that 80,000 women are diagnosed with cervical cancer annually in Africa, and that as many as 70% of the 24 million cases of cancer which have been forecast to be diagnosed by the year 2050, will occur in low-and middle-income countries. Kingham *et al*., (2013) also highlighted the illusion of cancers being a “western disease”, by reporting that while incidence rates are higher in western and high-income countries, the “overall case fatality”, which is defined as the mortality to incidence ratio, is as high as 75% in low-income countries, compared to 46% in high-income countries. This problem is compounded by a lower age of incidence, highlighted in South Africa, where the median age of diagnosis of colorectal cancer was 59 years (Wentink *et al*., 2010), compared with 71 years in the USA (Hornier *et al*., 2009).

In South Africa, at least 3127 years of life were lost per 100,000 people to cancer in the year 2008 alone according to the cancer atlas. Despite having a much lower incidence rate than the USA, South Africa has a significantly higher mortality rate with regards to breast cancer. This statistic is replicated in overall cancer mortality, where cancer mortality rates are similar per 100,000 in women, despite the US having an 11% higher projected incidence ("The Cancer Atlas", (2017, June 10). These statistics demonstrate just how significant the threat from cancers is, considering they are second only to CVDs.

CVDs are the highest contributors to preventable global mortality (Santulli, 2013). To place things into perspective, while global mortality related to HIV/AIDs is reported at three million people annually, CVDs have been reported to claim approximately 17 million lives globally, per annum. Both a costly expense economically and in terms of lives; Laslett *et al*., (2012) reported projections of close to 47 trillion dollars in economic cost related to CVDs, if proper investment is not undertaken to fortify current standards of prevention and treatment. Long considered diseases of the developed world, the rhetoric is exemplified by CVDs claiming more lives than the next 5 leading causes of mortality in the USA. This scheme is changing however, as CVD incidence is reported to have plateaued in developed nations, and this development has not been replicated in developing countries (Callow, 2006). Rather, it seems the opposite is happening, as increased migration from rural to urban areas experienced in developing countries has proven a risk factor, due to eating patterns and smoking associated with urban regions of these countries, as demonstrated in **Figure 1.1**. As a result, developing nations are currently experiencing a massive spike in incidence of CVDs (**Table 1.1**), akin to similar circumstances experienced by the more developed regions years ago (Callow, 2006). Already, the impact of these changes can be felt, since it has been reported that 80% of all mortality related to CVD occurs in low-and middle-income countries (Perk *et al*., 2012). This statistic is compounded by 87% of all CVD-related disabilities also occurring in these countries, with Kim & Johnston, (2011) reporting that diseases associated with CVDs like stroke, having higher mortality rates in Africa (**Figure 1.2**). With Physician density (global distribution of physician workforce per 10,000 population), and availability of essential medical care lacking in developing regions (**Figure 1.5**), the prognosis is negative for developing countries.

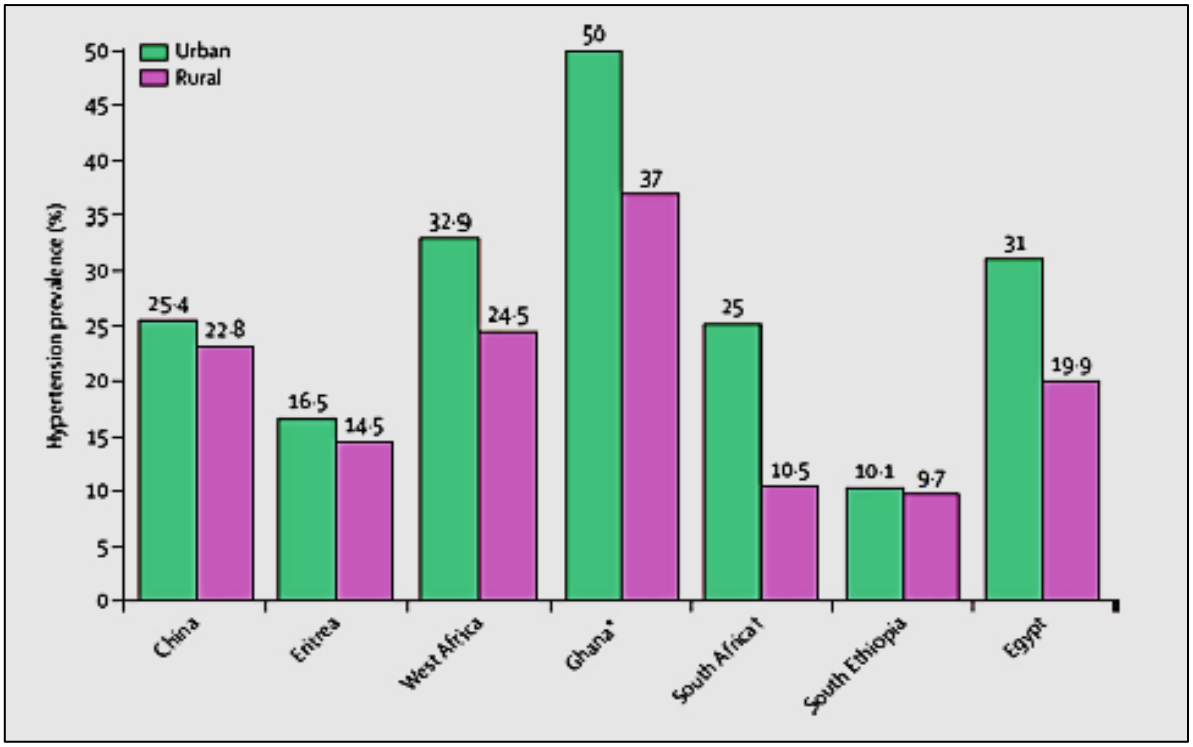


**Figure 1.1: Chart highlighting variations in prevalence of hypertension between urban and rural regions (Ibrahim & Damasceno, 2012).**

| Developing Countries | | Developed Countries | |
|---|---|---|---|
| Women | Men | Women | Men |
| 120% | 137% | 30% | 60% |
| | | | |

**Table 1.1: Age-related increases in incidence of Ischemic heart diseases between 1990 and 2020 (Callow, 2006).**

In these regions, health systems have been built around managing communicable diseases, especially HIV/AIDs, Tuberculosis and Malaria (Kingham *et al*., 2013). However, Smith *et al*., (2013) reported that these systems need to be transformed to address the impending dangers that CVDs pose, with regards to both mortality and morbidity. The economic burden (**Figure 1.5**) of these diseases in these regions is becoming more apparent, more especially because in the developing world, CVDs affect a large number of working-age adults. This is exemplified by the fact that of the 7.28 trillion dollars' worth of costs lost to non-communicable diseases in developing countries (**Figure 1.3**), 50% is accounted for by CVDs (Gaziano, 2007).

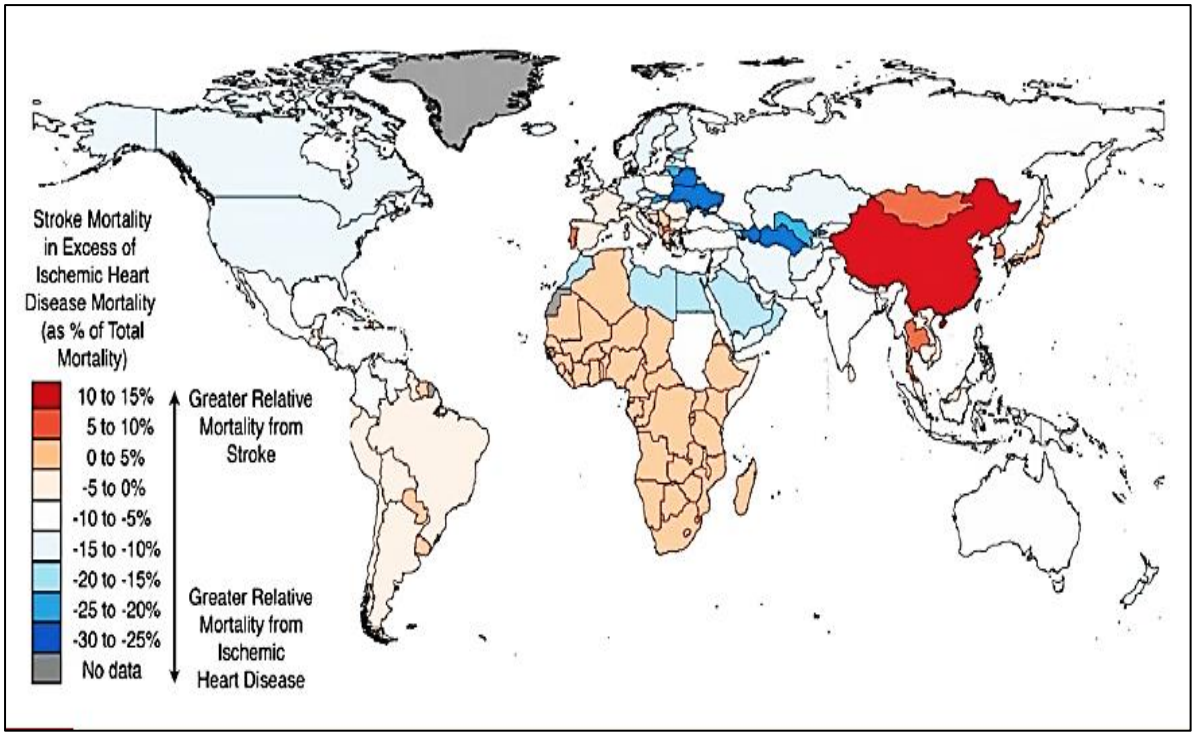


**Figure 1.2: Mapping Global mortality due to stroke and ischemic heart disease (Kim & Johnston, 2011).**

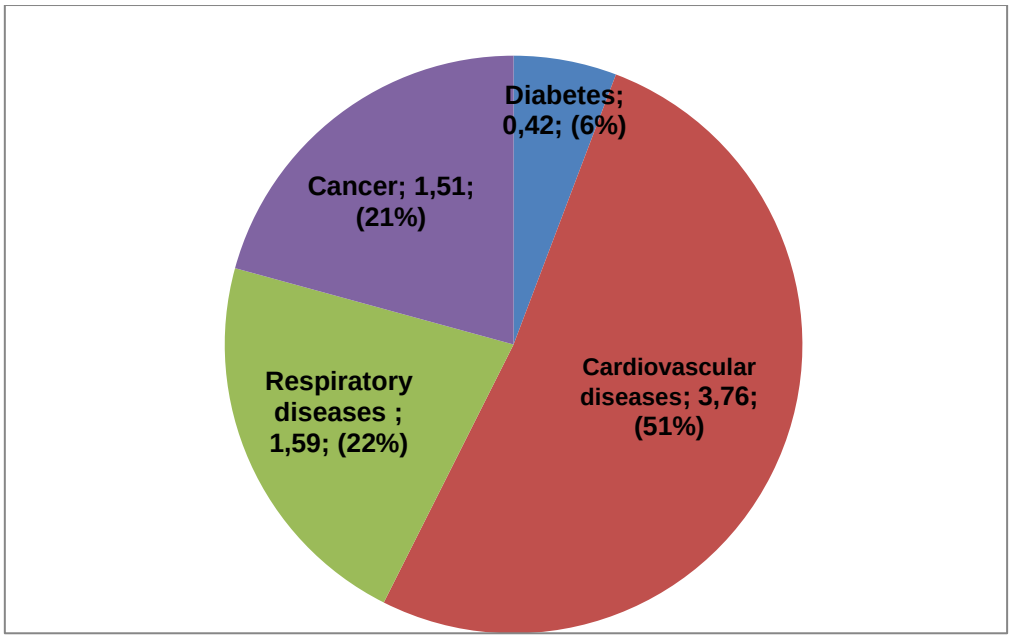


**Figure 1.3: Charting the economic loss in trillions of US dollars attributed to non-communicable diseases in developing countries from 2011 to 2025 (World Economic Forum & World Health Organization, 2011).**

South Africa has experienced a sharp increase of 25% in mortality risk due to hypertension in less than a decade (Ibrahim & Damasceno, 2012).

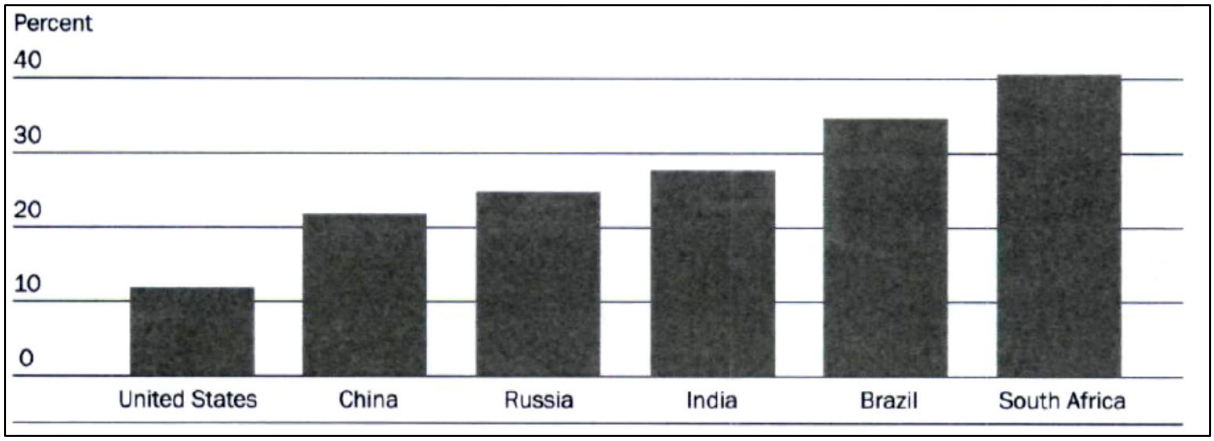


**Figure 1.4: Graphical comparison of projected CVD mortality amongst people between the ages of 35-64, from 2000 – 2030 (Leeder *et al*., 2004)**

With the HIV/AIDs pandemic being the focal point of most government interventions, the threat that CVDs pose cannot be overlooked. While HIV/AIDs has accounted for 41% of deaths in men, and 64% of deaths in women between the ages of 15-44 yrs, up to a third of deaths in people above the age of 65 years have been attributed to CVDs and stroke (Steyn *et al*., 2006). These numbers are worsening as is the trend with most of sub-Saharan Africa, and it is predicted that if the situation remains unattended, South Africa will experience four times more incidence of CVDs (**Figure 1.4**) in adults between 35 and 64 years of age than the USA (Gaziano, 2007). This is a distressing prediction considering the population ratio between the USA and South Africa is about 10:1, and the availability of medical resource and personnel to address such an exponential increase in CVD cases is largely limited in South Africa compared to more industrialized countries, as illustrated in **Figure 1.5**. The current situation is already economically damaging since CVDs already cost up to 25% of healthcare expenditure directly in South Africa, and up to double the value in indirect expenses (Gaziano, 2007).


**Figure 1.5: Mapping the global distribution of physicians, nurses/midwives per 10,000 people, from 2000-2009. (World Health Statistics 2010, WHO).**

These two diseases (CVDs and Cancer) have had a combined impact of 46.5% of all deaths in the year 2012 (Heron, 2015), exhibiting the immense extent of their devastating effects. All is not lost however, as Callow, (2006) proposed that there is a two decade window of opportunity for developing countries to address these issues and put structures in place to avoid future calamity. Considering that we are already a decade into this window, it is imperative to increase efforts towards curbing this trend.

These diseases have previously been treated in isolation; however, their impact has intricately interconnected links, traceable to their treatment and management. Treatment options such as radiation therapy, chemotherapy, and lifestyle choices such as diet and moderate exercise have contributed to an improved prognosis for most patients diagnosed with various cancers. Increasing survival rates for cancer patients, most evident in the treatments of breast cancers, where survival rates have been estimated to be as high as 85-90% (Ginsburg, 2013), illustrate the progress that has been made due to intensive research investment and output. While this serves as a positive trend, the increased survival of patients diagnosed with specific cancers have exposed other deadly complications of the disease and its treatment regimens; specifically complications affecting the heart (Minotti, 2004). To deal with these complications, the field of Cardio-Oncology was developed, as a multi-

dimensional approach which involves the collaborative effort by oncologists, cardiologists, haematologists and radiologists to treat cancer patients, especially patients who present with a high risk for cardiovascular events (Albini *et al*., 2010; Patane, 2014). These cardiovascular effects have largely been attributed to a side effect typical of chemotherapy known as cardiotoxicity.

## 1.2. Cardiotoxicity

This condition has confounded scientists for decades. There is little substantiated definition of the condition, and attempts to define it have been unable to completely characterize the condition, and largely vague. To rectify this, a symptom-specific definition was postulated by the Cardiac Review and Evaluation Committee. They defined cardiotoxicity as a condition induced by anti-neoplastic therapy, which presents with one of the following:

(i). Cardiomyopathy with a reduction in global left ventricular ejection fraction (LVEF), or to a more severe extent in the septum;
(ii). Symptoms associated with heart failure (HF), such as S3 gallop, tachycardia or both;
(iii). A reduction in LVEF, greater than or equal to 5% or less than 55% with accompanying signs or symptoms of HF or;
(iv). A reduction in LVEF that is greater or equal to 10% or less than 55% without accompanying signs or symptoms.

This definition, postulated in Seidman *et al*., (2002), while covering specificity, does not define cardiotoxicity in absolute terms. A more descriptive, however broad attempt was made by Minotti, (2004), who defined it as “a multi-factorial process which in the long run induces cardiomyocyte death as the terminal downstream event”. Moulin *et al*., (2015) described cardiotoxicity as deleterious and unwanted effects of therapeutic compounds on heart function, a definition markedly similar to that postulated by Montaigne *et al*., (2012), who described it as a broad range of deleterious effects on heart function induced by therapeutic molecules. Each one of these definitions presents essential descriptions of the concept, but lack in completeness; as such, an amalgamation of the definitions seems appropriate. It

could be defined as a deleterious multifactorial process, seemingly induced by anti-neoplastic treatment, which induces cardiomyocyte death, and presents with symptoms reminiscent of HF.

### 1.2.1. Early/Acute Cardiotoxicity

Also known as Type II cardiotoxicity, the mechanisms that guide this class of cardiotoxicity involve cardiomyocyte dysfunction, likely induced due to inflammation triggered by high/bolus doses of the drug administered (Montaigne *et al*., 2012). It is characterized by symptoms which include vasodilation, pericarditis, left ventricular dysfunction, hypotension, elevations in cardiac troponin I and cardiac rhythm disturbances in patients (Volkova & Russell, 2011; Barrett-Lee *et al*., 2009). This type of cardiotoxicity is less common, and can present during or immediately post-treatment. It is reversible, as it can either be treated or improves once chemotherapeutic administration is stopped (Simunek *et al*., 2009).

### 1.2.2. Chronic Cardiotoxicity

This type of cardiotoxicity is commonly classified as Type I cardiotoxicity, and is characterized by symptoms which present during therapy, within the year, or decades post-treatment as experienced in cases of early onset chronic cardiotoxicity and late onset chronic cardiotoxicity, respectively (Curigliano *et al*., 2012). These symptoms include dilated cardiomyopathy and systolic or diastolic left ventricular dysfunction induced by cardiomyocyte death through apoptosis or necrosis, as opposed to acute cardiotoxicity. Due to cell death governing this process, the damage to the myocardium is permanent, and its effects have been reported to resurface in childhood cancer survivors' decades after treatment is completed, where it induces severe congestive myopathy and eventually death (Simunek *et al*., 2009). These present as an obstacle to effective treatment and management of malignancies.

## 1.3. Doxorubicin, Cancer treatment and cardiotoxicity

Cancer therapy has evolved over the last few decades; treatment regimens such as radiation therapy and chemotherapy have increased cancer survival rates over time (Ginsburg, 2013). One of such treatment strategies is an anthracycline antibiotic known as Doxorubicin (DOX) (**Figure 1.6**). DOX, also known as Adriamycin (ADR)

has been utilized to treat a variety of cancers, more specifically breast cancer (Berthiaume & Wallace, 2007). First discovered in 1969, it was isolated from a mutated *Streptomyces* species (Pinedo & Smorenburg, 2006). Its efficacy and toxicity is intricately linked to its mode of action.

### 1.3.1. DOX mechanism of action

DOX has proven to be an effective anti-neoplastic agent, due to the variety of mechanisms through which it exerts its anti-neoplastic effects. The main mechanisms involve DNA intercalation, topoisomerase II inhibition, interference with DNA winding and lipid peroxidation. DOX inhibits DNA replication in neoplastic cells through the process of intercalation. Intercalation is described as “insertion or positioning between or among existing elements or layers” (Merriam-Webster’s Collegiate Dictionary, 2005). In this regard, DOX inserts itself in the DNA of neoplastic cells, where it inhibits transcription, and as such induces apoptosis (Minotti, 2004).

The second and most important mechanism through which DOX targets neoplastic cells is through the inhibition of topoisomerase II. This protein governs changes in DNA structure, and achieves this through the induction of single-or double-stranded breaks in DNA structure. Once broken, nucleotide sequencing can be modified around the site of the break, and once complete, topoisomerase II is responsible for resealing the site. DOX binds to topoisomerase II, and prevents resealing of broken DNA strands, which result in growth phase arrest, and apoptosis (Minotti, 2004)

Other mechanisms through which DOX has been reported to exert its anti-neoplastic effect include reactive oxygen species (ROS) production, P53 activation and inhibition of pro-growth pathways (Minotti, 2004; Mizutani *et al*., 2005).

### 1.3.2. Diagnosis

DOX-induced cardiotoxicity can exhibit numerous symptoms, including coronary heart failure, arrhythmias, QTc (corrected QT interval) wave elongation and myocardial ischemia, and as such, diagnostic tools for detecting this condition are important (Minotti, 2004). While the golden standard for detection previously was endomyocardial biopsy (Friedman *et al*., 1978), its invasive nature led to the

development of less invasive yet sensitive tools. Newer, less invasive diagnostic techniques include the use of transthoracic echocardiography to detect LVEF; tissue Doppler imaging, which evaluates global and regional cardiac function; cardiac magnetic resonance imaging (MRI) for global longitudinal strain, and finally stress echocardiography. Other techniques include the detection of blood biomarkers such as cardiac troponin I, creatine kinase (CK-MB) and the B-type natriuretic peptide (BNP), to determine cardiac damage and cardiac failure, respectively (Rosa *et al*., 2016, Yu & Ky, 2016).

### 1.3.3. Mechanisms behind DOX-induced Cardiotoxicity

Cardiotoxicity resulting from DOX therapy severely limits the therapeutic efficacy of this drug. The development of cardiotoxicity is dose-dependent and age-dependent (Barrett-Lee *et al*., 2009) as demonstrated in **Figure 1.7**. Cumulative DOX concentrations between the ranges of 275 - 399 mg/m$^2$ administered to patients resulted in a 4% decline in LVEF, with this number increasing exponentially with increases in dose concentrations. This was demonstrated by an 11% increase in this decline when doses ranged between 400 – 500 mg/m$^2$, and a LVEF decline of 28% in patients treated with cumulative doses that exceeded 500 mg/m$^2$ (Swain *et al*., 2003). These factors have limited the potential DOX has as an effective anti-neoplastic agent, since a dose cap was recommended as early as 1986, by Torti *et al*., who reported that lifetime cumulative dosages for DOX should be limited to approximately 450 mg/m$^2$.

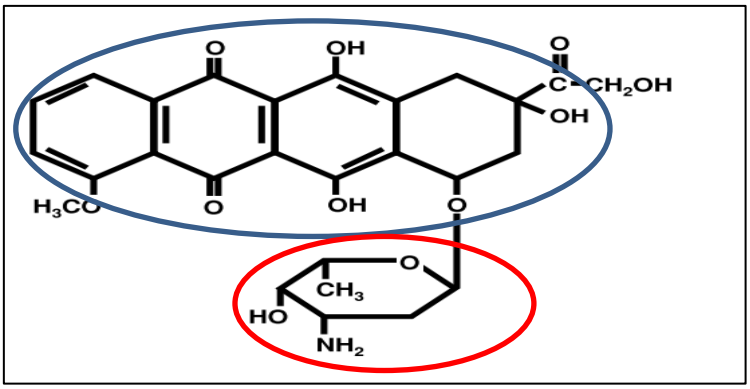


**Figure 1.6: Chemical structure of Doxorubicin (DOX) (Berthiaume & Wallace, 2007).**

Blue circle – Tetracycline quinone moiety, Red circle – glycosidic group

As a result of these factors, intensive research was executed towards elucidating and understanding the mechanisms behind this problem, in an effort to finding solutions or more effective therapeutic agents. While yet to be completely elucidated, it is evident that DOX exerts its cyto/cardiotoxic effects via a number of pathways, and does not have a singular main mechanism. A number of influential mechanisms have been identified however, and common consensus is that the mechanisms behind this side effect are linked to DOX's structure (**Figure 1.6**).

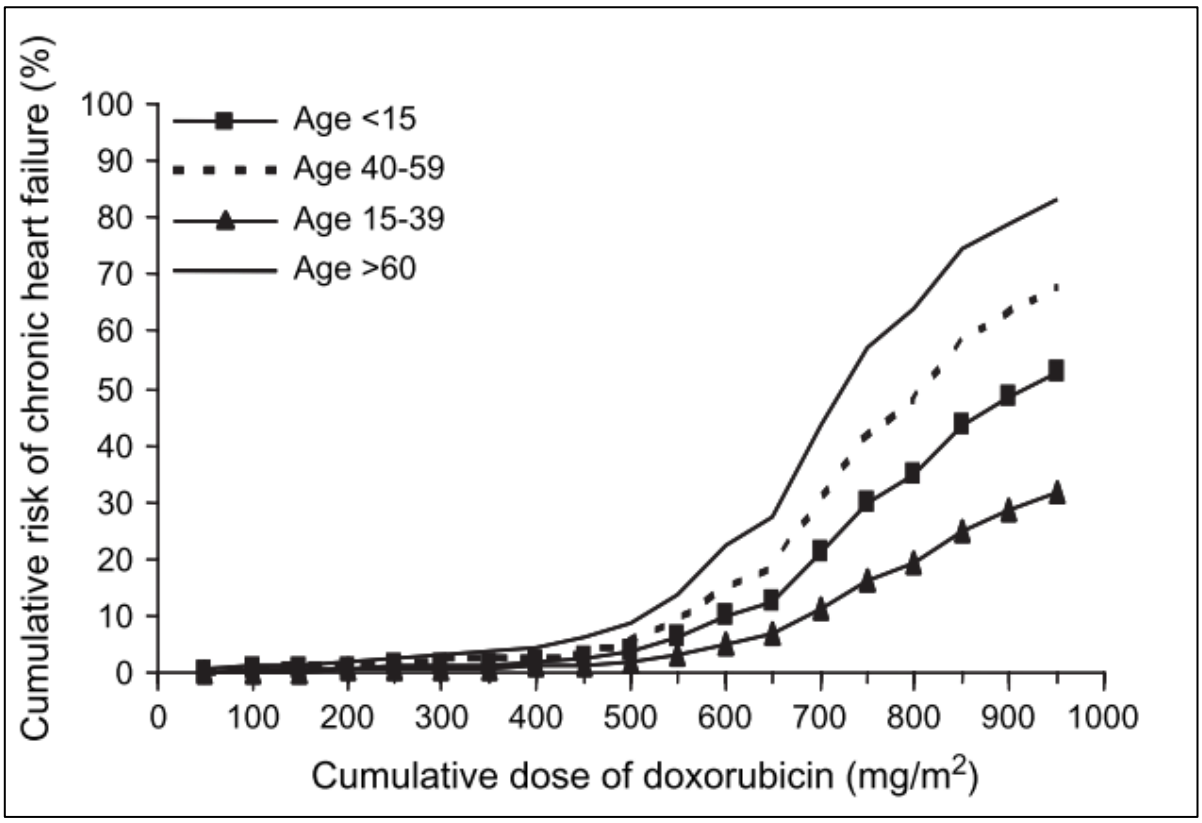


**Figure 1.7: Percentage risk of CVD relative to cumulative dose of DOX and age (Barrett-Lee *et al*., 2009).**

DOXs chemical structure is constituted by a tetracycline quinone moiety **Figure 1.6 blue**, and a glycosidic group **Figure 1.6 red**. It is metabolized to a number of molecules, including an alcohol which is produced through a carbonyl reduction, and other aglycone derivatives (Berthiaume & Wallace, 2007). It can be reduced by nicotinamide adenine dinucleotide (NADH)-dehydrogenases as complex I of the electron transport chain into a semi-quinone radical, which can react with oxygen in order to revert to its parent compound, and in the process produces the superoxide anion. This reaction forms the basis of one of the more influential mechanisms

identified, which is the oxidative stress theory. This theory revolves around continuous redox cycling between DOX and NADH-dehydrogenases, which produce ROS, in a never-ending cycle that culminates in oxidative stress (Bachur *et al*., 1978). Cardiomyocyte anti-oxidant defences are vulnerable to oxidative stress (Govender *et al*., 2014), and as such are overwhelmed by accumulation of ROS.

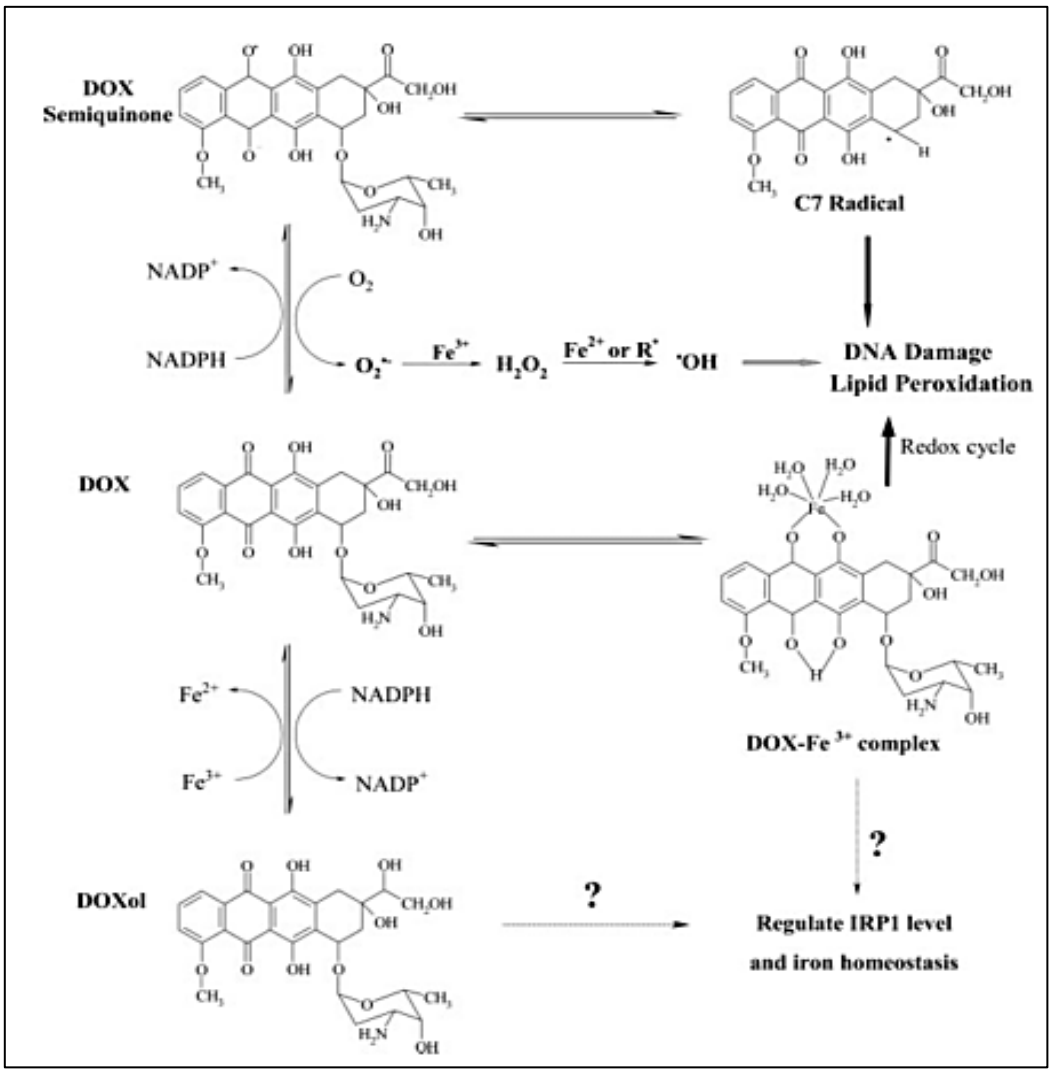


**Figure 1.8: The vicious redox cycle responsible for ROS formation with DOX administration (Xu *et al*., 2005).**

DOX can also contribute to oxidative stress through a reaction with iron, released from ferritin stores (**Figure 1.8**). Ferritin is a protein composed of 24 subunits, which are subdivided into heavy and light subunits. It is able to sequester approximately 4500 ferrous ($Fe^{2+}$) ions, and as such, free iron ions which are currently surplus to the requirements of the cell, are stored in ferritin (Xu *et al*., 2005). DOX binds favourably to iron released from ferritin stores; it does this to form a DOX-iron (II)

complex. This DOX-iron (II) complex can reduce oxygen to the superoxide anion, while cycling between the iron (II) and iron (III) states. These reactions continue since the iron (III) state of the DOX-iron complex can also be reduced back to the iron (II) state by reducing agents like NADPH cytochrome and glutathione. Semi-quinone radicals are produced in this process as well, compounding the vicious cycle (**Figure 1.8**) which continues to produce ROS. These, along with other ROS-producing reactions, such as DOX-eNOS associations (Vasquez-Vivar *et al*., 1997), contribute to a state of oxidative stress (Xu *et al*., 2005). This state leads to detrimental downstream consequences such as lipid peroxidation, mitochondrial dysfunction, calcium deregulation, and finally caspase cleavage and resulting cardiomyocyte apoptosis (Myers *et al*., 1977; Minotti, 2004; Ichikawa *et al*., 2014; Sishi *et al*., 2013b).

A number of therapeutic molecules have been developed or identified on the basis of these mechanisms, as potential interventions against cardiotoxicity. Current interventions include switching therapeutic doses to slower infusions rather than bolus therapy; attempting to develop structural analogues of DOX; liposomal encapsulation; and the use of cardio-protective agents (Dogru *et* al., 2013). However, with the overwhelming scientific consensus being that oxidative stress is at the root of deleterious effects attributed to DOX, the large majority of interventions have targeted the pathways through which DOX could induce oxidative stress, or by targeting ROS itself. A few noteworthy interventions developed so far include:

***Anti-Oxidants***

- Flavaglines: These compounds, which have been isolated from medicinal plants, were identified to be cytoprotective. In the context of DOX-induced cardiotoxicity, flavaglines were determined to exert cardio-protective effects in cultured cardiomyocytes (Bernard *et al*., 2011). They were reported to achieve this by inducing phosphorylation of Heat shock protein 27 (Hsp27). Hsp27 is essential for regulating chaperone activity, mRNA stabilization, regulating redox homeostasis, and inhibiting apoptosis (Kostenko & Moens, 2009). A flavagline analogue, FL3 was demonstrated to prevent DOX-induced apoptosis and fibrosis in mice hearts, protected calcium handling genes, and reduced animal mortality to 44% following a single dose of DOX.

Flavaglines demonstrated significant cardio-protective benefits against DOX-induced cardiotoxicity (Bernard *et al*., 2011)

- Sesamin, a lignin extracted from the oil of sesame seeds, has been demonstrated to exert pharmacological functions. Sesamin ameliorated DOX-induced cardiomyocyte stress and mitochondrial damage, as well as possessing anti-neoplastic properties. It was demonstrated to exert its cardio-protective effects by upregulating manganese superoxide dismutase (MnSOD or SOD2) expression, thereby protecting against oxidative stress, and preserving cell viability (Su *et al*., 2014).
- Tamoxifen, a non-steroidal selective estrogen receptor modulator, has been reported to also mediate cardio-protective effects. Its effects are linked to increased expression of antioxidants. Daosukho *et al*., (2005) demonstrated that Tamoxifen protected against DOX-induced cardiomyocyte injury, and reduced apoptosis through the induction of SOD2.
- Nebivolol, a $\beta_1$-selective adrenergic receptor antagonist which possesses vasodilatory effects, was also demonstrated to be protective *in vitro* and *in vivo* against DOX-induced cardiotoxicity by preventing apoptosis, and reducing oxidative stress (Nigris *et al*., 2008; Kaya *et al*., 2013)

These are just a few of the numerous anti-oxidants and oxidative stress targeting agents which have been identified as potential adjuvants to be utilized during cancer therapy to prevent or reduce the onset of DOX-induced cardiotoxicity. However, while they have been demonstrated to be effectively cardio-protective in laboratory studies either *in vitro* or *in vivo,* there has been a translational disconnect between these positive results to clinical utilization. Most of these anti-oxidants have demonstrated no clinical benefits, with others even proving to be detrimental to patients. Issues such as dosage, specificity and organ targeting limit the therapeutic potential of these anti-oxidants, and D'Andrea (2005) even went on to report that anti-oxidants should be avoided during cancer treatment. In this meta-analysis, anti-oxidants have demonstrated no significant clinical benefit, and may actually impinge on the therapeutic efficacy of anti-neoplastic drugs. An example of this is vitamin C, which while being a highly recommended anti-oxidant, is more effectively absorbed by cancer cells (Vera *et al*., 1995). This effect compromises chemotherapeutic efficacy, as neoplastic cells could be protected against oxidative damage.

The focus is therefore shifting to sourcing alternative avenues for preventing DOX-induced cardiomyocyte damage without compromising its efficacy. Another potential avenue identified was by preventing the formation of the DOX-iron complex, and, as such, reducing cardiomyocyte oxidative stress. To achieve this, the utility of iron-chelators within this context was explored (Van Dalen *et al*., 2008).

***Iron Chelators***

These agents were targeted as alternative adjuvants to anti-oxidants. Their mode of action involves sequestering free iron atoms, and preventing them from binding to DOX. One in particular, known as Dexrazoxane (DEX), initially developed as a chemotherapeutic agent, was demonstrated to be cardio-protective when used in combination with DOX (Van Dalen *et al*., 2008). It has anti-oxidant properties, and could scavenge superoxide and hydroxyl radicals (Junjing *et al*., 2010). Choi *et al*, (2010) were able to demonstrate cardio-protective benefits of DEX, as they reported it to reduce both the incidence and severity of cardiotoxicity in children receiving DOX treatment, a finding backed up by Lipshultz *et al.,* (2010). It was recommended by Swain & Vici, (2004), that patients who have stable disease should be identified and treated with DEX from early DOX administration. While it seems there is overwhelming evidence in favour of the cardio-protective attributes of DEX, not everyone agrees, and there is growing scepticism in the literature about the practicality of utilizing DEX as an adjuvant in this context. Van Dalen *et al*. (2008) reported hesitancy in the routine utilization of DEX due to side effects that could include potential interference with anti-tumour efficacy of chemotherapeutic drugs. Another study by Tebbi and colleagues (2007) found that the incidence and risk of developing acute myeloid leukaemia and secondary malignant neoplasms (SMNs) could be attributed to incorporating DEX into chemotherapeutic treatment. They found that this risk was likely due to DEX interfering with DNA repair, due to its topoisomerase II inhibition properties. The risk of developing SMNs escalated when DEX was utilized in combination with multiple topoisomerase II inhibitors, of which DOX happens to be one (Tebbi *et al*., 2007). While evidence demonstrating DEX to induce the development of SMNs when used in combination with DOX is lacking, the use in combination with another topoisomerase II inhibitor such as Daunorubicin (Albini *et al*., 2010), could overcome the DNA-repair deficiency threshold, and induce

the development of SMNs. As such, caution is recommended when prescribing DEX in such situations (Tebbi *et al*., 2007).

## 1.4. Redirection

Taking all these into consideration, it is evident that no completely satisfactory cardio-protective agent has been developed. With the underlying basis for the development and assessment of these numerous adjuvants being the current understanding of the mechanisms behind the development of cardiotoxicity, it is imperative to return to the drawing board. It has become necessary to re-examine the mechanisms behind the development of cardiotoxicity, in order to uncover and address potential ambiguities compromising the fundamental knowledge available, and at the root of the failure, to develop any comprehensively successful intervention up to date. An oversight by current literature is the failure to assess the effect of cancers and the cancer micro-environment on cardiac homeostasis. Current opinion is that these detrimental and cardiotoxic effects are induced solely by the anti-neoplastic treatment regimens (Minotti *et al*., 2004); however, literature also agrees that the cancers produce a wide variety of signalling molecules (Li *et al*., 2011). These signalling molecules regulate inflammation, tumour metastasis, recurrence, and influence signalling pathways such as cell proliferation and apoptosis (Fukuda *et al*., 2011; Lesina *et al*., 2011)

Little is known about the incidence of potential cancer-associated heart disease, and this is likely due to cancer mortality preventing the potential development of this disease (Kingham *et al*., 2013). As a result, incidence of HF due to cardiotoxicity is assumed to be due to cancer therapy. An investigation into the tumour microenvironment and its influence on cardiac health would enable the identification of potential pathways through which malignant neoplasms could predispose individuals to the development of cardiotoxicity. Literature has already identified numerous signalling molecules peculiar to cancers, and a few of them are:

- Inflammatory signals which could affect tumorigenesis through the activation of nuclear factor kappa-light-chain-enhancer (NF-κB) and signal transducer and activator of transcription 3 (STAT3) (Grivennikov *et al.,* 2010; Li *et al*., 2011).

- Transformation growth factor-beta (TGF-β), whose receptors are expressed generously in tumour cells (Derynck *et al*., 2001)

However, protein expression alone does not sufficiently elucidate signalling patterns, as other factors, such as localization, glycosylation and phosphorylation, determine specific protein activity. As such, a molecular analysis of protein activity would enable the characterization of potential protein markers which could be detrimental to cardiomyocyte health (Gutkind *et al*., 2001). It would also provide an opportunity to examine the influence of cancer on novel biomarkers for cardiotoxicity (Yu & Ky, 2016). These would provide better insight into the field of cardio-oncology, by helping to fill the gaps between the development of cancer, chemotherapy, the development of cardiotoxicity, insight on why current therapeutics have largely failed to prevent cardiotoxicity in the clinical setting, and what could be done to improve the success rates of such interventions. It also opens the opportunity for research into the role novel markers and role-players such as microRNA's would play in this context.

### 1.4.1. MicroRNAs

Micro-ribonucleic acids (miRNAs) are important for cellular regulation. These endogenous regulators of gene expression consist of about 22 nucleotides (Van Rooij *et al*., 2007). They negatively regulate expression and induce cleavage and translational inhibition of target genes. This process is achieved through either their binding with close complementarity to protein sequences and induction of RNA interference, or by binding to non-complementary sites and repressing gene expression post-transcriptionally. miRNAs evolved from RNA produced by the gene Lin-4, and are generally conserved (Bartel, 2004). They are generated in a multistep process which begins with pri-miRNAs being transcribed by RNA polymerase II. Pri-miRNAs are processed into pre-miRNAs by two enzymes, "Drosha" and "Pasha", and then exported into the cytoplasm by exportin-5, where they are processed into a 22 nucleotide long double-stranded RNA. This double-stranded RNA, known as the miRNA-miRNA duplex, is excised by another processing enzyme called Dicer, and incorporated into the multiprotein RNA-induced-silencing complex (miRISC). This complex retains the mature miRNA, and initiates its downstream functions. miRNAs are usually either located within the introns of protein-coding genes (miRtrons), or independently between genes. This serves as a determining factor for their

regulation, as intron-localized miRNAs are regulated by the transcriptional mechanisms of their host gene, while independent miRNAs possess independent transcriptional control systems (Dorn II, 2011). Each miRNA has the potential to regulate hundreds of gene targets, and it has been projected that there are as many as 1000 miRNAs in the human genome. They regulate cell processes such as growth, differentiation and apoptosis, and as such are easily linked to cancers (van Rooij *et* al., 2007; Esquela-Kersher & Slack, 2014). miRNAs specific to cancer are known as oncomirs. Of the already characterized miRNAs in the human genome, 50% are located in sites which are associated with cancers (Calin *et al*., 2004).

While the role of miRNAs in carcinogenesis has been well characterized, they have also been demonstrated to play critical roles in both cardiac development and pathogenesis. They have the ability to regulate cardiac function, heart muscle contraction, growth and development (Li *et al*., 2014). Their importance is underlined by the findings of Goren *et al*., (2012), who were able to characterize four specific miRNAs, whose expression levels were increased in the serum of HF patients. While that may suggest that HF led to increased miRNA production, Chen *et al*., (2008) reported that deletion of Dicer in mouse hearts induced severe neonatal dilated cardiomyopathy. They were able to determine that this deletion at a later stage of cardiac development resulted in postnatal lethality. This demonstrated the importance of this enzyme and in essence the miRNAs that it processes, to normal cardiac development and function. Supporting research undertaken by Rao *et al*., (2009), revealed that deletion of the pri-miRNA processing enzyme Drosha in mice led to premature mortality, in combination with symptoms associated with HF and dilated cardiomyopathy, such as fibrosis, and changes in the ventricular diameters and thickness of mutant mice. They were able to conclusively demonstrate that changes in cardiomyocyte-specific expression levels of these miRNAs occurred prior to the pathophysiological aberrations developed within mutant hearts.

In addition to these, other miRNAs have been identified as critical to cardiomyocyte homeostasis. MiR-1, was reported to be upregulated in plasma following myocardial injury (Ji *et al*., 2009; Ai, *et al*., 2010) and miR-423-5p was upregulated in clinical subjects diagnosed with HF (Tijsen *et al*., 2010). Also, miR-23a, miR-27a, miR-208a and miR-24-2 were upregulated in cardiac tissue during cardiac hypertrophy (Lee *et al*., 2004; Van Rooij *et al*., 2007), while miR-133 was downregulated in the

myocardium (Care *et al*., 2007). MiRNAs have also been demonstrated to regulate more specific cellular processes important for cardiomyocyte homeostasis and some of them possess the potential to be utilized as targets for preventative intervention within this context. Van Rooij *et al*., (2007) postulated that due to miRNAs being able to determine cardiac phenotypes, changes in their expression are more likely to be the cause rather than the consequence of cardiac remodelling that occurs during pathological states. They demonstrated this by showing that the overexpression of miR-195 was sufficient to induce cardiac hypertrophy followed by HF, in *in vivo* experiments. This hypertrophy they found could also be reversed by downregulating miRNAs which are upregulated during hypertrophy.

MiR-21 and miR-29b possess anti-apoptotic properties (Chan *et al*., 2005; Jing *et al*., 2018), while miR-320 enhances apoptosis specifically in cardiomyocytes (Ren *et al*., 2009), and considering apoptosis is a critical hallmark of cardiotoxicity, both could serve as potential targets for therapeutic manipulation. This was demonstrated by Li *et al*., (2014), who were able to identify miR-140 as a pro-apoptotic miRNA, which exerts its effects through the suppression of mitochondrial fusion protein mitofusin 1 (MFN1). MiR-140 targets and downregulates MFN1 expression, leading to increased mitochondrial fission, and subsequent apoptosis. Inhibiting miR-140 via anti-sense knockdown was able to restore MFN1 expression, reduce miR-140-induced apoptosis, and attenuate myocardial infarct sizes (Li *et al*., 2014).

All these conclusively demonstrate the crucial roles miRNAs play in aetiology, progression, pathogenesis and potential treatment for cancer and heart disease. However, the miRNA profile governing the progression from cancer to chemotherapy, cardiotoxicity and eventually HF have not been elucidated. MiRNAs present as a critical target in this context, as they could serve as both markers for early development of pathological cardiomyocyte damage, and also provide potential targets for the prevention and regulation of cardiotoxicity. To address the crux of this issue, highlighting specific miRNAs influential within the context of DOX-induced cardiotoxicity is imperative. For the purpose of this study, the scope was thus narrowed to four specific miRNAs associated with a strong correlation to HF and similar cardiomyopathies.

### 1.4.2. miR-208a

A constituent of a three member miRNA family, miR-208a is highly conserved between species and is expressed in the heart by intron 29 of the *myh6* gene. In a study conducted by Oliveira-Carvalho *et al*., (2012), it was noted that miR-208a is relatively less expressed during early cardiac development and its presence is only augmented during adulthood.

### 1.4.3. miR-29b

In a similar fashion, miR-29b forms part of a family composed of miR-29a, miR-29b and miR-29c, of which miR-29b has been illustrated to be much more substantially expressed in the myocardium than the other members of this family. In contrast to the generally accepted translational regulation associated with miRNAs, miR-29b's natural function is speculated to be the regulation of transcription or splicing of target transcripts (Hwang *et al*., 2007). It is present in all bodily fluids including the pericardial fluid (Kuosmanen *et al*., 2015), and considering that this miRNA has been shown to be downregulated in the myocardium following acute DOX exposure (Jing *et al*., 2018), it remains an intriguing target of this study.

### 1.4.4. miR-133

This group of miRNAs is muscle-specific. miR-133a is abundant in human and rodent hearts (Small *et al*., 2010). Its importance towards cardiac development is emphasized by late embryonic or neonatal lethality that occurs as a result of deletion of both miR-133a genes (miR-133a-1 and miR-133a-2) (Liu *et al*., 2008). The distinguishing factor between miR-133a and its third family member, miR-133b, is that its sequence differs by two nucleotides at the 3' terminus. Although miR-133b is exclusively expressed in skeletal muscle (Van Rooij *et al*., 2007), its close relationship and similarity to miR-133a made it an interesting target to investigate in this context.

## 1.5. Study Rational

As DOX remains crucial to chemotherapeutic approaches utilized in the treatment of multiple cancer types, the question of DOX-induced cardiotoxicity has remained relevant. For years, extensive research into the context has resulted in numerous mechanisms being elucidated, and potential interventions for alleviating this burden being identified. However, successful clinical output has remained relatively poor, since *in vitro* and *in vivo* animal model laboratory successes have been beset by poor translational output into human patients (Tebbi *et al*., 2007).

A majority of the research effort has focused on tackling the mechanisms induced through the oxidative stress hypothesis, resulting in a plethora of anti-oxidants being identified as potential preventative or therapeutic interventions. However, the lack of tangible success utilizing this school of thought has made it necessary for a more extensive and innovative approach towards the problem (D'Andrea, 2005).

One way of improving the approach is targeting molecules responsible for governing the pathways through which DOX is reported to induce cardiotoxicity. An overarching approach, applicable to the multiple pathways, should provide increased opportunity for clinical translation. In this regard, miRNAs, relatively novel molecules which regulate gene expression are interesting targets. Demonstrated to be involved in both cancer and heart failure, they also play significant roles within the different independent cellular processes associated with DOX-induced cardiotoxicity, within other contexts. As such, determining their roles in this context will provide valuable insight into possible strategies for detection and management of cardiotoxicity.

A second avenue to improving the approaches currently utilized is assessing the current strategies and identifying the weaknesses these approaches possess, which could result in translational failure. Most studies which have investigated cardiotoxicity, aiming to either elucidate its mechanisms or develop intervening strategies or molecules, have followed rather similar models. Most have utilized *in vitro* and *in vivo* models of acute cardiotoxicity; and omitted the presence of tumours in their models. The rationale behind this is based on the belief that cardiotoxicity is induced only by the presence of DOX, and that tumour signalling, or the interaction between DOX, the tumour microenvironment and the heart is not responsible for the

development of this side effect; hence the title “DOX-induced cardiotoxicity”. However, in the clinical setting, patients are seldom exposed to acute doses of DOX, and the early onset cardiotoxicity induced by this type of dosage is often reversible and resolves on its own. Chronic cumulative doses of DOX have been identified as the responsible factor for long-term irreversible cardiotoxicity.

As such, we hypothesized that within a chronic model of DOX-induced cardiotoxicity, the presence of a tumour would influence the mechanisms through which DOX exerts its pathological effects on the heart.

We also hypothesized that miRNAs would play a significant role within this context, and could be utilized as early biomarkers for the development of chronic cardiotoxicity. To test these hypotheses, we aimed to:

(i). Implement and establish a chronic *in vivo* model of DOX-induced cardiotoxicity.
(ii). Successfully implement a model of mammary gland tumour within this model, utilizing cells grown in cell culture.
(iii). Determine if the presence of a tumour influences established mechanisms of DOX-induced cardiotoxicity within the chronic context.
(iv). Determine the effects of the DOX-treatment, with and without the presence of a mammary gland tumour on the expression of specific circulating miRNAs.

This model is novel within this context, and the investigation into its effects on circulating miRNA expression is also novel.

# Chapter 2. MATERIALS and METHODS

## 2.1. Animal Model Development and Implementation

## 2.2. Animal Care and Ethical Considerations

The experimental procedure for this animal study was submitted in its entirety for ethical consideration and was approved by the Stellenbosch University Animal Ethics Committee. Ethical approval was obtained (REC: ACU PROTOCOL NUMBER 1701), within the guidelines that conform to the guidelines for the utilization of animals in research and teaching prescribed by the South African National Standards 10386:2008. (APPENDIX K: ETHICS LETTER, pg. 148)

Thirty-seven three to four week old female Sprague-Dawley rats (average weight 110 g) were purchased from the Stellenbosch University animal unit, and given a week of acclimatization at the animal facility. The animals were housed in sterile and ventilated cages and maintained in an animal house environment with 12-hour day/night cycles and at a temperature range of 21 – 25 $^{o}$C. The animals were consistently monitored by both the researcher and the highly experienced animal house managers for the duration of the study. Animal distress was evaluated using a rat grimace scale. Food and water was provided to the animals *ad libitum*, with nutrition derived from standard rat chow. White perspex tubing and shredded paper was utilized to provide environmental enrichment.

The rats used in this study were age-selected to accurately represent a model of chronic cardiotoxicity as observed in humans, since this condition is more common within child-hood survivors of cancer. Female rats were also utilized in order to accurately achieve a model of breast cancer.

**Table 2.1: Absolute animal body weights per group at the start and end of the study duration.**

| | Vehicle | Tumour | DOX | DOX and Tumour |
|---|---|---|---|---|
| **Initial weights (g)** | 107.78 | 95.66 | 132.35 | 87.90 |
| **Final weights (g)** | 225.54 | 225.39 | 228.85 | 196.03 |

## 2.3. LA7 Adenocarcinoma-derived tumour cell culture

Rat mammary adenocarcinoma-derived LA7 tumour cells (P-10, ATCC No CRL2283) were obtained as a kind gift from Dr Annadie Krygsman (Stellenbosch University, South Africa). These cells were cultured in a 1:1 ratio of Dulbecco's Modified Eagle's medium and Ham's F12 nutrient mixture, supplemented with 15 mM HEPES (Thermofisher Scientific, 31330095, Massachusetts, USA). Additional supplementation was achieved with the addition of 10% fetal bovine serum (Invitrogen Gibco, 10438018, California, USA), 50 nM hydrocortisone (Sigma, H0888-1G, Missouri, USA), 0.005 mg/ml insulin (Sigma, I9278-5ML, Missouri, USA) and 1% Penicillin/Streptomycin (Invitrogen Gibco, 15140122, California, USA). Culture medium was prepared and aliquoted without hydrocortisone and insulin, both of which were supplemented into aliquoted media within an hour of use. Under sterile conditions, cells were seeded at a density of 1 x $10^6$ cells, maintained and allowed to proliferate in a monolayer in T175 flasks (Bio-Smart Scientific, 71175, Cape Town, South Africa) at 37 $^oC$ in a humidified atmosphere of 95% Oxygen ($O_2$) 5% carbon dioxide ($CO_2$). Cells were monitored daily, and culture media was refreshed every 48 hours (hrs). Sub-cultivation was performed at a ratio of 1:8. As soon as cellular confluency reached 80%, cells were harvested by trypsinization with 0.25% trypsin-ethylene-diaminetetra-acetic acid (trypsin-EDTA) (Invitrogen Gibco, 25200056, California, USA) for three minutes (mins) at 4 mL per T175. Upon confirmation of complete detachment under the light microscope, cells were aspirated and the suspension centrifuged at 1500 rpm for three mins before subsequent pellet re-suspension in fresh warm culture media. Cells were counted with a hemocytometer, cell viability was determined with the automated cell counter (Invitrogen Gibco, C10227, California, USA) and then cells were re-suspended at a density of 16 x $10^6$ cells in 300 µl Hank's Balanced Salt Solution (Sigma, H8264-500ML, Missouri, USA) for animal inoculation. All harvested cells were used within one hr of preparation.

## 2.4. Tumour inoculation and Induction

Once the experimental animals were acclimatized, they were separated at random into four (4) groups (7-10 per group). These groups included a vehicle control, DOX, Tumour, and Tumour + DOX group. Animals in the Tumour groups were inoculated

with LA7 breast cancer cells prepared as described in section **2.3** above. To achieve this, a protocol described by Abbasalipourkabir *et al.,* (2010) was utilized as a guide. Animals were oriented in a supine position and placed under anaesthesia by inhalation of 3% Isoflurane® (Isofor, Safeline Phamaceuticals, Johannesburg, South Africa), coupled with an oxygen regulator. The injection site was sterilized with ethanol, and the cell suspension aspirated using 1 ml unibody insulin syringes with 29 gauge needles (Stelmed Pharmacy, Stellenbosch, South Africa). Subcutaneous application of the suspended LA7 cell solution (section **2.3)** was injected 5 mm into the mammary pad approximately 3 mm lateral and 2mm anterior to the mammary pad on the right flank of each rat. Injections were carried out by qualified personnel, slowly administered in small volumes every 30 seconds, with a culminated injection time of five mins.

Upon inoculation, animals were taken off anaesthesia, and allowed to recover. The animals were closely monitored daily for tumour development. Tumours were palpable 2 days post-inoculation, and tumour volumes were taken weekly, and animal weight was measured bi-weekly. To calculate tumour volumes, the diameters of tumour masses were measured across horizontal and vertical planes with a digital calliper. Volume was calculated according to the formula:

$$Volume(V) = {}^{(ab^2)}/_{2}$$

Where ‘a’ and ‘b’ are representative of the longest and shortest diameter of the tumour, respectively (Carlsson *et al*., 1983).

## 2.5. Treatment Protocol

The female Sprague-Dawley rats were specifically selected for this study due to their successful history of use in studies focusing on cardiotoxicity (Nigris *et al*., 2008; Gharanei *et al*., 2013). As mentioned previously, the animals were monitored daily, and once tumour volumes of at least 250 $mm^3$ were achieved for both tumour groups, the experimental protocol was commenced. The DOX groups were treated with 2.5 mg/kg DOX (LKT Laboratories, D5794, Minnesota, USA) once a week for eight weeks, resulting in a cumulative dose of 20 mg/kg. According to the manufacturers report, DOX has a distribution half-life of 5 mins, and a terminal half-

life of 24 – 48 hrs, indicating rapid uptake by tissue, and slow elimination. This dose was calculated with reference to the range of 60 – 75 mg/m$^2$ utilized in the treatment of humans (Desai *et al*., 2013). Vehicle-control animals received an equivalent volume of Hank's salt solution weekly as well for the entire duration of the study.

All injections administered were delivered intraperitoneally (i.p), using 1 ml unibody insulin syringes, fitted with 29 gauge needles. Considering the negative impact expected of both the tumours and DOX on the animals, animals were monitored daily and humane endpoints were set to minimize animal suffering in the event of animal distress. These endpoints were regarded as factors that would prompt the consideration of euthanasia to prevent excessive animal suffering.

- A failure of animals to eat or drink for a time period longer than 24 hrs
- Excessive necrosis at site of tumour growth
- A failure of inflammation at sites of DOX injection to subside within 24 hrs
- A grimace scale was used, and signs of excessive pain or discomfort (Sotocinal *et al*., 2011)

## 2.6. Animal Sacrifice and Organ Harvest

To assess possible early miRNA peaks, this study utilized two end-points. On the 7$^{th}$ week, approximately half (n = 3 – 5 per group) of the animals in each group were anaesthetized with a lethal dose (2.6 - 3.2 % of inspired concentration) of Isoflurane (Kissin *et al*., 1983). The pedal reflex was examined and once absent, the animals were dissected rapidly with an incision at the xyphisternum, and extended to the lateral costal margins. The ribs were cut through on both axillary lines, and the chest wall was raised upwards. Blood was drawn from the abdominal aorta (**Figure 2.1**) using 10 ml syringes (Stelmed Pharmacy, Stellenbosch, South Africa) with sterile 25 gauge needles (Avacare, Johannesburg, South Africa) and collected in 6 ml EDTA tubes (Lasec, VGRV456043, Cape Town, South Africa). Upon completion of the blood draw, the hearts and livers were excised rapidly and weighed. The collected organs were cut into transverse halves, with one half snap-frozen in liquid nitrogen ($LN_2$) and the other stored in 4 % formaldehyde for histological analysis. Snap-frozen organs were stored at -80 $^{o}$C for molecular analysis. Upon completion of the treatment protocol, this process was repeated at the second endpoint on the 11$^{th}$

week (n = 5 per group), where the remaining animals were anaesthetized (**Figure 2.2**).

Images were taken of each harvested organ and no animals were lost during the duration of this study.

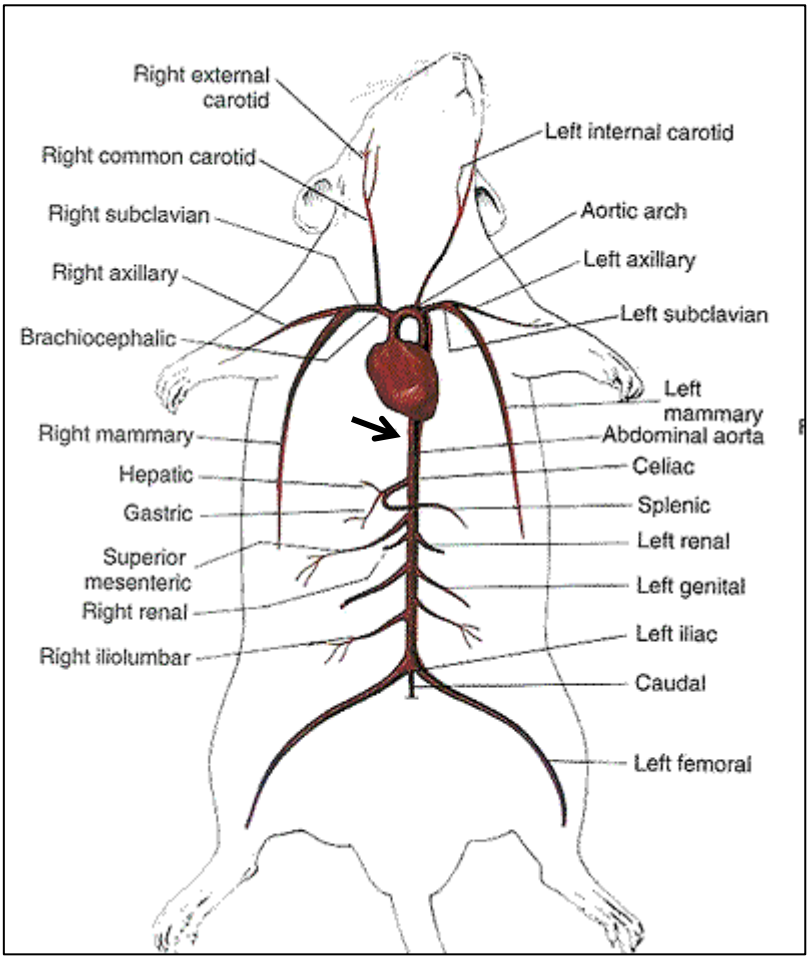


**Figure 2.1: Diagram illustrating the blood vessels from which blood was drawn (Biologycorner, 2020).**

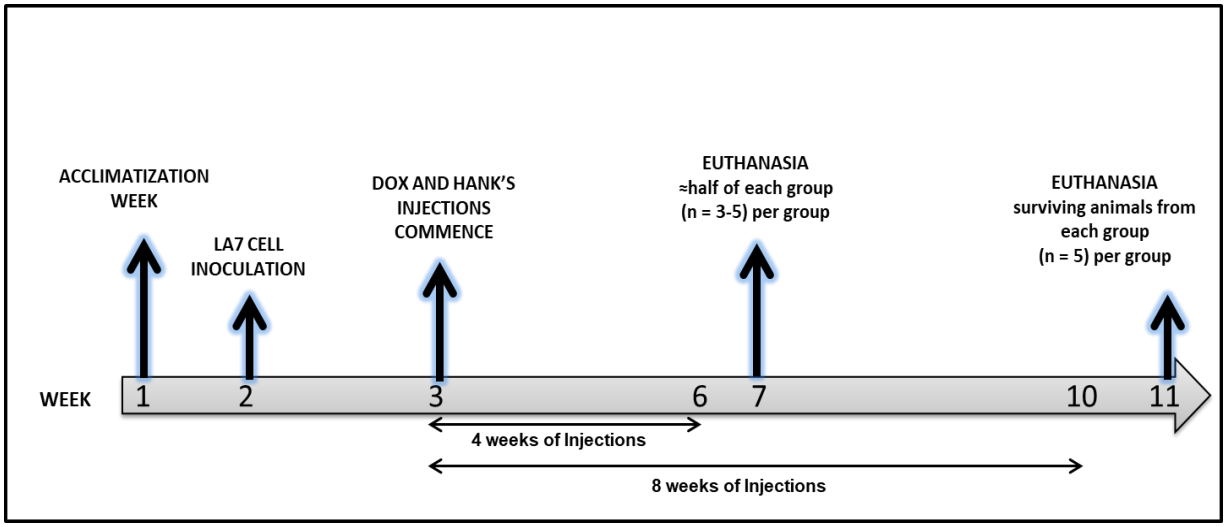


**Figure 2.2: Sprague-Dawley cancer and chronic cardiotoxicity model timeline (37 rats, 4 groups)**

## 2.7. Detection of Cardiac Troponin I, Creatine Kinase and B-type Natriuretic Peptide

To confirm the extent of toxicity of the treatment regimens on the myocardium, the expression levels of molecular markers for cardiac damage were assessed through specific enzyme-linked immunosorbent assays (ELISAs). Quantitative sandwich-type ELISA kits were purchased and used to evaluate plasma samples for cardiac troponin I (CTI) (Abcam, ab246529, Cambridge, United Kingdom), Brain-type natriuretic peptide (BNP-45) (Abcam, ab108816, Cambridge, United Kingdom) and tissue samples for cytosolic creatine kinase (CK-MB) (Abcam ab187396, Cambridge, United Kingdom). Kits were run according to the manufacturer's instructions. Briefly, frozen plasma and tissue samples were allowed to thaw on ice. Assay reagents delivered with the kits were prepared according to the manufacturer's instructions and equilibrated to room temperature (≈24 $^{o}$C). Standard dilutions were prepared, and 50 µL volumes of samples as well as standards were added in duplicates to assigned wells in the 96-well ELISA plate. Detection antibody was subsequently added to each well and the ELISA plate incubated on a shaking incubator at room temperature. Following a few wash and incubation steps, signal development reagents were added and the subsequent addition of a stop solution to each well signalled the end-point of the experiment. Colorimetric end-point readings were performed with the EZ Read 400 Microplate Reader (Biochrom, 80-4001-40,

Cambridge, United Kingdom) at 450 nm. Average readings were normalized with the zero reading and a standard curve was plotted. The best smooth curve with linear regression was fit, and unknown sample readings were interpolated and analysed. Results were normalized and presented as a percentage of the controls.

## 2.8. Quantitative Polymerase Chain Reaction

The existence of analytical tools that enable the measurement and monitoring of nucleic acids is a critical part of molecular biology (Raymond *et al*., 2005). This study understands that evaluating expression levels of components within plasma is potentially viable for assessing molecular patterns within the context of chronic cardiotoxicity; in a less invasive manner. In the case of miRNAs, their low abundance in bio-fluids prompts the need for an analytical technique which incorporates high sensitivity, and the ability to amplify a signal. Quantitative polymerase chain reaction (qPCR) provides an assay-based analytical avenue which possesses each of these qualities. It presents as a powerful tool for measuring and validating observations with sensitivity requirements beyond other easily available molecular techniques (Bustin *et al*., 2009). As such, this technique was selected as appropriate for the measurement of miRNA levels in this study.

To execute this technique, it was pertinent to take certain pre-analytical conditions into consideration. In line with peer-reviewed standards (Coenen-Stass *et al*., 2019), miRNA expression was analysed from plasma samples. A major consideration in this regard was the difference between plasma and serum. Plasma is the cell-free supernatant collected after the centrifugation of blood in the presence of an anti-coagulant, while serum is the cell-free supernatant collected after centrifugation of blood in the absence of an anti-coagulant (i.e. clotted blood) (Kroh *et al*., 2010). To collect suitable plasma for analysis with qPCR, EDTA tubes were utilized as they are more suitable for this process, while heparin inhibits the PCR process (Kroh *et al*., 2010). While literature has demonstrated miRNA expression to be highly correlated between plasma and serum (Mitchell *et al*., 2008), it was important that this study selected and maintained one specimen type for the duration of the study to ensure that variables were well matched.

Another pre-analytical condition that was taken into consideration was the period of time between collection of blood samples and processing to isolate plasma. Established literature reports that miRNAs are transported out of their native organs as part of the cargo exported by extracellular vesicles (Lovett *et al*., 2018) and they remain stable with extended room temperature incubation of plasma (Mitchell *et al*., 2008), however Kroh *et al*., reported in 2010 that samples maintained their integrity as long as they were processed within four (4) hrs of blood collection.

Upon blood collection, described in section **2.6**, EDTA tubes were inverted six times and centrifuged at 2000 *g* (3333 rpm) for 10 mins at 4 $^{o}$C for plasma separation. To maintain a strong standard for our model and maintain uniformity between samples, centrifugation was completed within an hour of blood collection. Subsequently, plasma (**Figure 2.3A**) was carefully aspirated and stored in Ribonuclease (RNASE)-free Eppendorf tubes (Invitrogen Gibco, AM12425, California, USA) at -80 $^{o}$C.

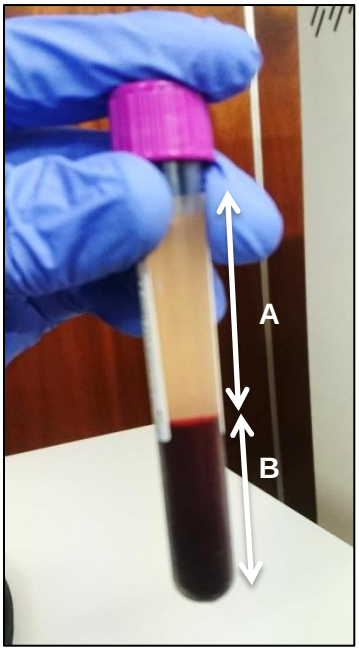


**Figure 2.3: Diagram demonstrating isolation and separation of plasma (A)**

### 2.8.1. Plasma RNA Isolation

miRNAs are much smaller than most other RNA types. For example, messenger RNAs consist of up to 1000 nucleotides compared to the 18-22 nucleotides possessed by miRNAs (Li *et al*., 2012). As a result, traditional RNA isolation

techniques come up short when the recovery of small-sized RNA is required. Therefore, to fulfil the specific requirements for this study, a specialized RNA extraction method was undertaken to generate a sufficient yield of small RNA types. Total RNA was isolated using the MIRVANA Paris kit as per the manufacturer's guidelines (Thermofisher Scientific, AM1556, Massachusetts, USA). As opposed to traditional methods, which utilize glass columns or alcohol precipitation to precipitate RNA, this kit utilizes glass-fibre filters to purify total RNA from protein, DNA and RNA mixtures recovered from experimental samples.

In summary, plasma samples were retrieved from the – 80 $^{o}$C freezer and allowed to thaw on ice. Once thawed, samples were centrifuged at 10000 *g* (≈9000 rpm) for ten (10) mins at 4 $^{o}$C, and the supernatant carefully collected and placed into new Eppendorf tubes. An equal volume of 2x denaturing solution was added to the collected samples and allowed to incubate on ice for five (5) mins. Post denaturing, an equal volume of acid-phenol:chloroform was added to the Eppendorf tube to separate DNA from RNA. Samples were subsequently centrifuged at 10000 *g* (≈9000 rpm) for ten (10) mins at room temperature, to separate the sample into the bottom phase, interphase and aqueous phase. The aqueous phase was carefully collected without disturbing the compact interphase and placed in fresh RNASE-free Eppendorf tubes on ice. At this point, the external spike-in control was introduced to each sample (discussed in section **2.8.3**).

Working on ice, a volume of room temperature 100% alcohol equivalent to a 1.25 volumes of the sample in each respective Eppendorf tube was added to the collected aqueous phase, and then the samples were passed through a glass-fibre filter (included in the kit) for a few wash steps to immobilize the RNA. To collect the immobilized RNA, a low ionic strength elution solution was passed through the filter. Eluted RNA isolates were collected in RNASE-free Eppendorf tubes and stored at -80 $^{o}$C for subsequent processing.

### 2.8.2. RNA concentration

To ensure sufficient RNA was isolated from the samples, RNA concentration was measured with the NanoDrop ™ Lite Spectrophotometer (Thermofisher Scientific, Massachusetts, USA). After washing of the optical measuring surface, 2 µL of each sample was added to the measuring surface. In duplicates, nucleic acid

concentration measurements were taken at 260 nm and purity determined using a ratio of 260/280.

### 2.8.3. RNA quality control and Normalization controls

miRNAs have been demonstrated to display remarkable stability in extracellular bio-fluids; thus justifying our decision to investigate the miRNA prevalence in plasma. As a standard with conventional RNA studies utilizing qPCR, total input RNA is standardized across samples. Subsequently, RNA expression is evaluated, and normalized to house-keeping reference genes/RNA (Roberts *et al*., 2014). This approach is unsuitable for our study model however, for two reasons:

1. Plasma RNA content is very low which essentially complicates the evaluation of specific miRNAs.
2. There is a lack of consensus on stably expressed reference miRNAs in plasma. Some normalization methods that have been evaluated as potential solutions include (Roberts *et al*., 2014):
    I. Normalization to average quantification cycle (Cq) values of all measured miRNA assays; this method is however restricted to models evaluating large numbers of miRNA assays.
    II. Normalization to endogenous reference miRNAs. This method has also been demonstrated to be flawed, as it assumes that the global miRNA abundance of individual samples to be approximately equal. Another short-coming of this method is the variable expression of proposed reference genes (Roberts *et al*., 2014).

Upon extensive literature consultation, it was determined that the most appropriate method of normalization would be to normalize against an external spike-in miRNA control, which was introduced into the aqueous phase, post separation using acid-phenol:chloroform. This method has been demonstrated to produce the most consistent results, as previous experiments showed that externally spiked-in controls demonstrated the least amount of variability across samples over time (Roberts *et al*., 2014).

For this protocol, this study utilized the cel-miR-39 synthetic miRNA (**Table 2.2**), a generous gift from Prof. Kathy H Myburgh's research group, as a spike-in control, which was introduced to the aqueous phase collected after the phenolic separation step during the RNA isolations. The amount of the spike-in recovered after the RNA isolation is proportional to the total RNA recovered from the sample. All reactions were normalized to cel-miR-39 Cq values.

### 2.8.4. Reverse Transcription cDNA synthesis and qPCR

Utilizing the Taqman advanced miRNA cDNA synthesis kit (Thermofisher Scientific, A28007); a number of critical steps were executed for this study which ensured high sensitivity and specificity for target miRNA. The primer and probe sets in this kit are capable of detecting miRNA from 2 µL of total RNA isolated from plasma. cDNA synthesis was achieved by the simultaneous addition of a polyadenylation (poly [A]) tail to the 3' end of the mature miRNA transcript and the adaptor ligation on the 5' end of the transcript. Poly [A] polymerase executes the polyadenylation step (**Figure 2.4**), and the adaptor acts as the forward-primer binding site in the amplification reaction.


**Figure 2.4: Diagram depicting polyadenylation.**

Subsequent to these, the reverse transcription primer binds to the poly [A] tail on the 3' end and the modified miRNA is transcribed by reverse transcriptase to produce suitable cDNA for the assays as demonstrated in Figure 2.5.

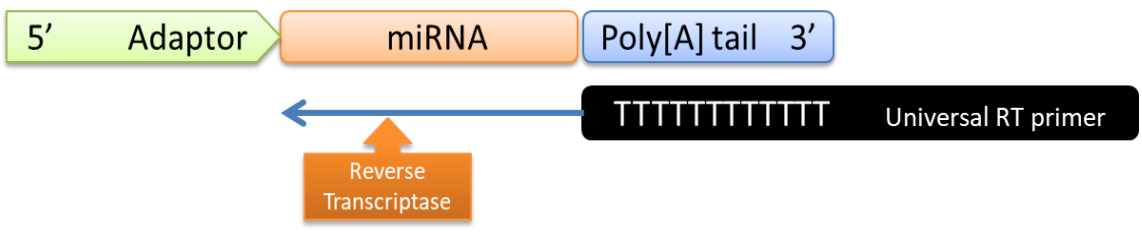


**Figure 2.5: Diagram depicting cDNA synthesis.**

In light of the low copy numbers for miRNA in bio-fluids, an important amplification step (**Figure 2.6**) that enables detection of small RNA molecules was then carried out by universal forward and reverse primers in the miRNA amplification step.

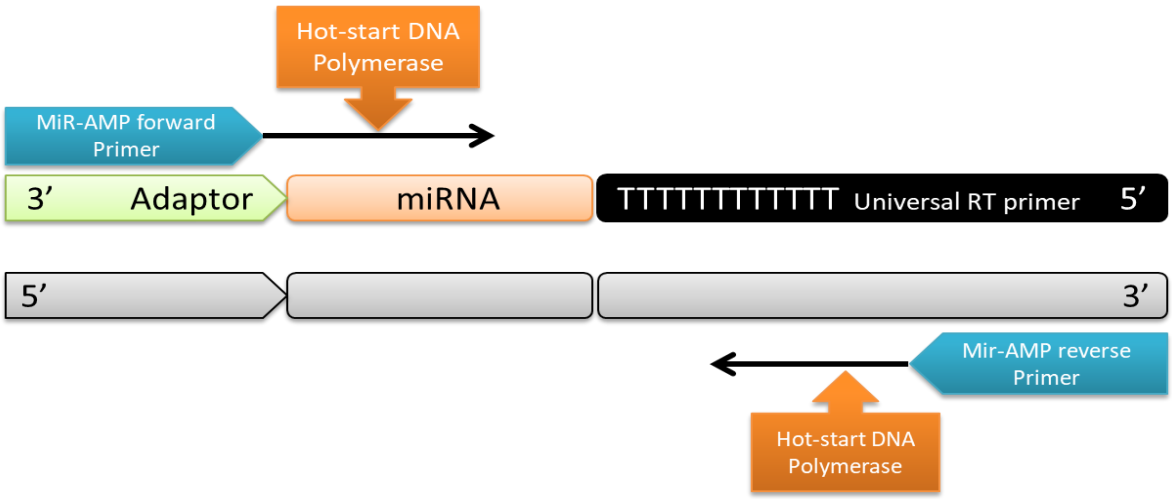


**Figure 2.6: Diagram depicting miRNA amplification.**

Once the above steps were completed, utilizing Taqman Fast Advanced Master Mixes (Thermofisher Scientific, 4444557), in combination with optimized thermal cycler steps (Thermal Cycler 2720, Applied Biosystems, USA); miRNA expression was evaluated utilizing Taqman advanced miRNA assays (Thermofisher Scientific, A25576). These assays utilize a probe design which consists of a reporter dye which is attached to the 5' end of the probe, a non-fluorescent quencher (NFQ) and a minor groove binder (MGB), which both attach to the 3' end of the probe (**Figure 2.7**). The MGB increases the melting temperature of the probe, without increasing its length and as such enables the design of shorter probes. The reporter dye and the NFQ work in tandem to produce the fluorescence measured as a representation of miRNA abundance.

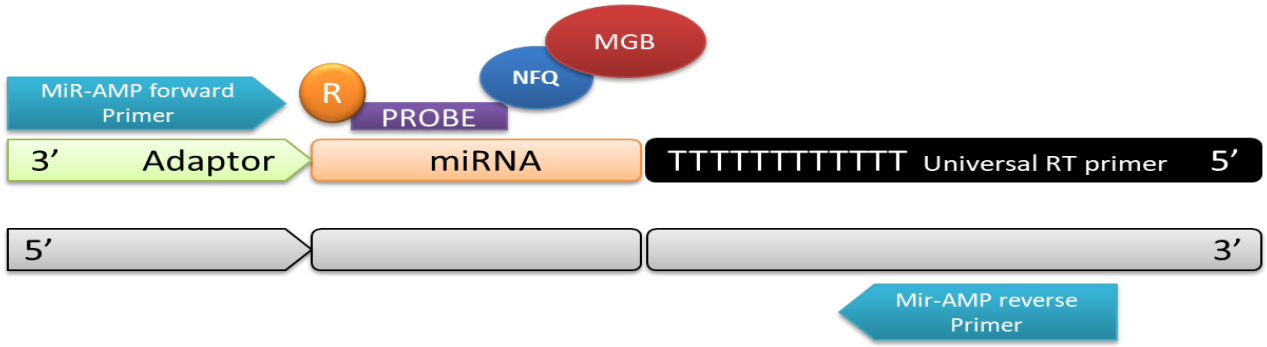


**Figure 2.7: Diagram depicting the initial binding of the hydrolysis probe.**

Abbreviations: **R** - Reporter Dye, **RT**- Reverse Transcriptase, **NFQ** – Non-fluorescent Quencher, **MGB** – Minor Groove Binder.

The mode of action of hydrolysis (Taqman) probes (**Table 2.2**) renders them more accurate than most other probes. No fluorescence is generated from intact probes as the proximity of the NFQ to the reporter leads to a repression of fluorescence. DNA polymerase only cleaves probes which have full complementary binding to the target miRNA sequence. Once cleavage of the hydrolysis probe is completed, the NFQ and the reporter are separated from each other (**Figure 2.8**).

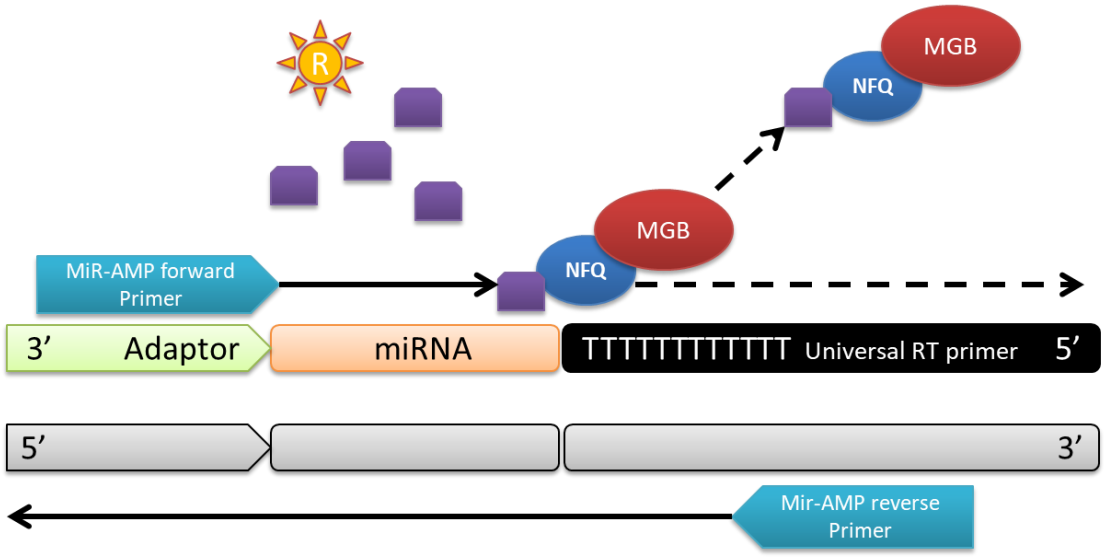


**Figure 2.8: Diagram depicting the mechanism of action of the hydrolysis probe.**

Abbreviations: **R** - Reporter Dye, **RT**- Reverse Transcriptase, **NFQ** – Non-Fluorescent Quencher, **MGB** – Minor Groove Binder.

**Table 2.2: A list of the specific hydrolysis probes utilized in this study, and their sequences.**

| miRNA | Species Name | Prime | Sequence |
|---|---|---|---|
| **miR-208a** | Rno-miR-208a-3p | 3p | AUAAGACGAGCAAAAAGC |
| **miR-29b** | Rno-miR-29b-3p | 3p | UAGCACCAUUUGAAAUCAGUGUU |
| **miR-133a** | Rno-miR-133a-3p | 3p | UUUGGUCCCCUUCAACCAGCUG |
| **miR-133b** | Rno-miR-133b-3p | 3p | UUUGGUCCCCUUCAACCAGCUG |
| **cel-miR-39** | Cel-miR-39-3p | 3p | UCACCGGGUGUAAAUCAGCUUG |

Their lack of proximity relieves the fluorescence repression causing the reporter to release fluorescent signals, which are detected by the StepOne™ PCR system (Applied Biosystems, USA). The assays were formulated on 96-well Microplates (Thermofisher Scientific, 4346906), which were sealed with optical adhesive covers (Thermofisher Scientific, 4311971).

In brief, 50 µl of the resulting product from the amplification step was diluted at a ratio of 1:10 with the miR-Amplification master mix. 5 µl of this diluted cDNA was loaded onto the 96-well microplate and the PCR master-mix was added to it. Analysis was performed in duplicates on the StepOne qPCR thermocycler (Applied Biosystems, North Carolina, USA). Both the four-week and eight-week groups were analysed at the same time to eliminate experimental bias, however, to achieve this, samples from the four-week groups had to be stored for longer.

Experiments were performed with as much adherence to the minimum information for the publication of quantitative real-time PCR (MIQE) guidelines as set out in Bustin *et al*., (2009). (Detailed protocol available in APPENDIX D: QUANTITATIVE POLYMERASE CHAIN REACTION, pg. 126).

## 2.9. Western Blotting

### 2.9.1 Preparation of Tissue Lysates

Snap-frozen tissue samples were retrieved from storage at – 80 $^{o}$C and pulverized into small pieces. These crushed samples were incubated in chilled radio-

immunoprecipitation (RIPA) buffer consisting of 50 mM Tris-HCl (pH 7.4), 150 mM NaCl, 1% NP40 (Sigma-Aldrich, 74385, Johannesburg, South Africa), 1 mM EDTA (Merck Millipore, SAAR2236020EM, Modderfontein, South Africa), 1 mM NaF (Merck Millipore, 1.93270.0500, Modderfontein, South Africa), 1 mM PMSF (Sigma-Aldrich, 94382, Johannesburg, South Africa), 1 mM Sodium Orthovanadate (Sigma-Aldrich, S6508, Johannesburg, South Africa) and a protease inhibitor (PI) cocktail (cOmplete, 11873580001, Sigma-Aldrich, Johannesburg, South Africa).

Briefly, in a process completed on ice, 450 µL RIPA buffer was added to the crushed tissue samples (100 mg) in 2 ml Eppendorf tubes. Following thorough laboratory etiquette to prevent cross contamination, these samples were subsequently individually homogenized with a polytron benchtop homogenizer (Kinematica, Luzern, Switzerland) for ±30 seconds at 30000 rpm (20124 *g*). Once completed, the Eppendorf tubes were centrifuged (Labnet, New Jersey, USA) at 4 $^{o}$C at 12000 rpm (13300 *g*) for 20 mins. The supernatant was carefully aspirated and preserved in sterile Eppendorf tubes and aliquoted and stored at -80 $^{o}$C, while the pellet was discarded appropriately. Detailed protocol can be found in APPENDIX F: WESTERN BLOTTING, pg.132.

### 2.9.2. Tissue Fractionation and Mitochondrial Isolation

Cardiomyocytes have been demonstrated to be rich in mitochondrial content (Hom & Sheu, 2009). Mitochondria destabilized by dysfunctional quality control systems have been implicated in a number of pathological states (Barbour & Turner, 2014). Mitochondria, crucial to cellular homeostasis and mediators of apoptosis; have also been proposed to play important roles within the context of DOX-induced cardiotoxicity (Karbowski & Youle, 2011). Determining the expression of mitochondria-specific proteins would help elucidate any adaptations or maladaptation induced by the varying conditions represented in our model.

To accurately determine mitochondrial state, mitochondrial/cytosolic fractionations were performed from cardiac tissue frozen for molecular analysis. The Mitochondria isolation kit for tissue (Thermofisher Scientific, 89801, Massachusetts, USA) was utilized and isolations/fractionations were performed according to the manufacturer's instructions.

Briefly, 80 mg of cardiac tissue was weighed out and allowed to thaw on ice. Tissue was washed twice in 1X Phosphate buffered saline (PBS, pH 7.4) and cut into smaller pieces. In lysis buffer provided with the kit and prepared according to the instructions, the small tissue pieces were homogenized in a dounce homogenizer. Subsequently, homogenized samples were centrifuged at 700 *g* (2600 rpm) to separate cell debris. Once completed, the supernatant was aspirated and transferred to a fresh Eppendorf tube. A subsequent centrifugation step was performed at 3000 *g* (5700 rpm) to separate the mitochondrial pellet from the cytosolic supernatant. Once the supernatant had been transferred into a specifically allocated tube, mitochondrial pellets were washed in prepared wash buffer. Mitochondrial pellets were subsequently dissolved in sample buffer and boiled for processing *via* western blots.

### 2.9.3. Determination of Protein Content

To determine protein concentration, the Direct Detect ™ system (Merck Millipore, DDHW00010-WW, Darmstadt, Germany) was utilized. This spectrometer accurately determines protein concentrations that range between 0.25 – 5 mg/mL by measuring amide bonds in protein chains. Since amide bonds are intrinsic properties of all proteins, the Direct Detect ™ system is able to eliminate the drawbacks of colorimetric techniques, such as the often used Bradford Assay, by accurately quantifying these intrinsic properties independent of amino acid composition, redox potential or dye-binding properties. Briefly, the system was calibrated using 2 µL RIPA buffer, which served as the blank standard. Subsequently, 2 µL of each lysate sample was pipetted onto assay-free cards made specifically for this purpose. Protein determination was executed once the cards were placed into the Direct Detect ™ machine, measured as protein concentration per sample in mg/mL. This process was carried out in triplicate.

### 2.9.4. Gel Electrophoresis

Using protein concentration values determined from section **2.9.3** above, aliquots containing 50 µg of protein samples were prepared in Laemmli's buffer. These samples were subjected to gel electrophoresis utilizing stain-free 12% graded acrylamide gels (Bio-Rad, 456-8084, California, USA). Once protein separation was conformed through gel-activation, the separated proteins were transferred onto

polyvinyldineflouride (PVDF) membranes (Bio-Rad 170-4156, California, USA). Successful protein transfer was confirmed by membrane activation and proteins were locked into the membrane by a short wash in methanol. Membranes were subsequently blocked in 5% milk for 1 hour (hr) at room temperature. Excessive milk was washed off, and membranes were incubated in specific primary antibodies (Table 2.3) prepared according to optimized dilutions in a Tris-Buffered Saline and Tween (TBST) detergent mix overnight at 4 $^{o}$C. Upon retrieval, incubated membranes were subjected to a few wash steps and incubated in appropriate secondary antibodies for 1 hr at room temperature. Following a few wash steps, enhanced chemi-luminescence (ECL) clarity substrate (Bio-Rad, 170-5061, California, USA) was applied to the membranes and chemiluminescence was measured in the Chemi-Doc ™ XRS system (Bio-Rad, California, USA). Band intensity was quantified on the ImageLab software version 5.0., and bands were normalized to total protein (**Figure 7.11**). (Detailed protocols in APPENDIX F: WESTERN BLOTTING, pg. 132)

**Table 2.3: A list of the various antibodies utilized in this study.**

| | | | | | | |
|---|---|---|---|---|---|---|
| **Name** | **Size (kDa)** | **Company** | **Catalogue Number** | **Primary** | **Secondary** | **Species** |
| SOD2 | 22 | Cell Signalling | 13141S | 1/1000 (5% BSA) | 1/10000 | Rabbit |
| DRP1 | 82 | ABCAM | AB56788 | 1/1000 | 1/10000 | Mouse |
| Caspase-3 | 32 | Cell Signalling | 9662S | 1/1000 | 1/2000 | Rabbit |
| Cleaved Caspase-3 | 17 | Cell Signalling | 9662S | 1/1000 | 1/2000 | Rabbit |
| Caspase-7 | 35 | Cell Signalling | 9491 | 1/1000 (5% milk) | 1/2000 | Rabbit |
| Cleaved Caspase-7 | 20 | Cell Signalling | 9492 | 1/1000 | 1/2000 | Rabbit |
| MYC-2V (MLC-2V) | 29 | Cell Signalling | 12975S | 1/1000 (5% BSA) | 1/2000 | Rabbit |
| PARP | 113 | ABCAM | Ab191217 | 1/1000 | 1/10000 | Rabbit |
| Cleaved PARP | 89 | ABCAM | AB191217 | 1/1000 | 1/10000 | Rabbit |

| | | | | | | |
|---|---|---|---|---|---|---|
| RhoA | 21 | Cell Signalling | 67B9 | 1/1000 (5% BSA) | 1/2000 | Rabbit |
| TOMM20 | 16 | Cell Signalling | 42406 | 1/1000 (5% milk) | 1/10000 | Rabbit |
| GAPDH | 37 | Millipore | CS204254 | 1-2000 | 1/10000 | Mouse |
| $2^{o}$ Anti-rabbit IgG, HRP-Linked | | Cell Signalling | CST7074s | | | |
| $2^{o}$ Anti-mouse IgG, HRP-Linked | | Cell Signalling | CST7076s | | | |

Indicated alongside the antibodies are the companies the antibodies were purchased from, their catalogue numbers, protein target sizes in kDa, as well as the primary and secondary dilutions utilized in obtaining protein expression expressed as band signal. Abbreviations: **DRP1** – Dynamin Related Protein 1, **GAPDH** – Glyceraldehyde 3-Phosphate Dehydrogenase, **SOD2** – Superoxide Dismutase 2, **TOMM20** – Translocase of Outer Mitochondrial Membrane 20, **MLC-2v** – Myosin Light Chain Beta, **HRP** – Horse Radish Peroxidase, **RhoA** – Ras Homologue Family Member A.

## 2.10. Histological Analysis

Cardiac tissue samples were isolated for the purpose of morphological analysis. These samples were preserved in 4 % formaldehyde solution (Merck Millipore, 1.00496.5000, Massachusetts, USA) for a minimum fixing period of 120 hrs.

### 2.10.1. Cardiac tissue processing and sectioning

Post fixation, tissue samples were processed to prepare them for wax embedding through a series of dehydration steps described in detail in APPENDIX G: HISTOLOGY, pg. 136. This process and subsequent infiltration of Paaplast® wax (Sigma-Aldrich, A6330-4LB, Johannesburg, South Africa) was executed in a tissue processor (Tissue Tek II, 4634, Sakura Finetechnical Co., Ltd Japan). Once processing was complete, tissue samples were retrieved and embedded in wax on histological cassettes (Lasec, PLPS191023, Cape Town, South Africa). This process was executed on a tissue embedding system (Leica Biosystems, Leica EG 1160, Wetzlar, Germany).

Upon successful embedding, 5 µm thick sections were carefully sectioned with a microtome (Leica RM 2125RT, Leica Biosystems, Wetzlar, Germany). The sectioned samples were subsequently place in a water bath and mounted onto microscope slides (Lasec, GLAS4S22M3000F, Cape Town, South Africa). Mounted slides were placed on a 20 $^{o}$C heating block and sections were allowed to adhere.

### 2.10.2. Hematoxylin and Eosin Staining

To visualize the gross morphological constitution and integrity of the cardiac tissue extracted from our *in vivo* model, this study utilized Hematoxylin and Eosin (H & E) staining.

A natural occurring compound, Hematoxylin is the most popular histological staining dye. It is extracted from the logwood tree, and is a versatile staining compound commonly utilized by pathologists in diagnostic procedures (Titford, 2005). It stains the nuclei with a blueish colour, and in this study, was utilized in combination with Eosin, which stains cytoplasmic components with a pinkish colour (Alturkistani *et al*., 2015). In combination, the H & E staining protocol can be utilized to study most histopathological processes.

For this study, this staining procedure was selected due to its cost efficiency, efficacy and ease of execution.

Briefly, 5 µm sections of heart tissue were prepared as described in section **2.10.1**, mounted onto microscope slides and allowed to dry on a heating block. Mayer's Hematoxylin (Merch Milipore, SAAR2822001LC, Modderfontein, South Africa), was prepared by filtering through Whatman's number 2 filter paper. A working solution of Eosin (Leica Biosystems, 3801600E, Illinois, USA) was prepared. The procedure was completed manually by placing the slides onto the slide holders on a Leica ST 4020 auto staining machine (Leica Biosystems, Wetzlar, Germany) and meticulously guided by submerging into appropriate consecutively ordered solutions as described in APPENDIX H: MANUAL HEMATOXYLIN AND EOSIN STAINING, pg. 138.

### 2.10.3. Picrosirius Red Stain

A hallmark of chronic inflammation is fibrotic damage which is characterized by the formation of collagen deposits. Collagen can be classified into three subtypes; Type I, which is collagen fibres, Type II which is constituted by hyaline and elastic

cartilage, and reticulin fibres and fibrillary collagen which constitute Type III deposits (Stephenson, 2015). Identifying and quantifying collagen provides an avenue for investigating fibrosis. As such, staining techniques targeting collagen deposits are an important part of histological analysis (Stephenson, 2015).

The Picrosirius red stain is a sensitive and specific stain for collagen deposits. It selectively stains Type I collagen and Type III reticulin, red and green birefringent fibres, respectively (Kiernan, 1995).

Briefly, 5 µm sections of heart tissue were placed on microscope slides, and allowed to dry. Subsequently, the required reagents were made up and poured into appropriately labelled staining baths. Dried sections on microscope slides were taken through xylene steps to clear and dewax the sections, followed by a few dehydrating steps and subsequent staining according to the protocol described in APPENDIX I: PICROSIRIUS RED STAIN, pg. 140.

Upon completion, stained slides were mounted and allowed to dry for 48 hrs prior to visualization.

#### 2.10.4. Visualization and Quantification

Visualization of stained slides was accomplished on the Nikon ECLIPSE E400 microscope (Nikon®, Tokyo, Japan). Digital images were obtained with a Nikon DS-Fi2 camera mounted on the microscope, which processed the images *via* a Nikon Digital Sight DS-U3 processor (Nikon®, Tokyo, Japan). Images were acquired and processed with the NIS elements v4.10 software. Image capturing was performed by capturing at 4x magnification; where several images were captured and stitched together to visualize the entire section. As a standard, images were also captured at 4x magnification and at 20x magnification around randomly selected blood vessels within the myocardium.

Quantification was accomplished using ImageJ 1.52a software version 1.8.0_112. To quantify fibrosis, the thresholding function on ImageJ was utilized to select the entire section at range of (9, 130 – 144) (**Figure 2.9B**). Pixel measurements for this selection was obtained and stored. Using the threshold slider, adjustments were made within a specified standard range (9, 70 – 90) until only the red collagen fibres

were selected (**Figure 2.9C**). Pixel measurements were again generated and expressed as a percentage of the entire section.

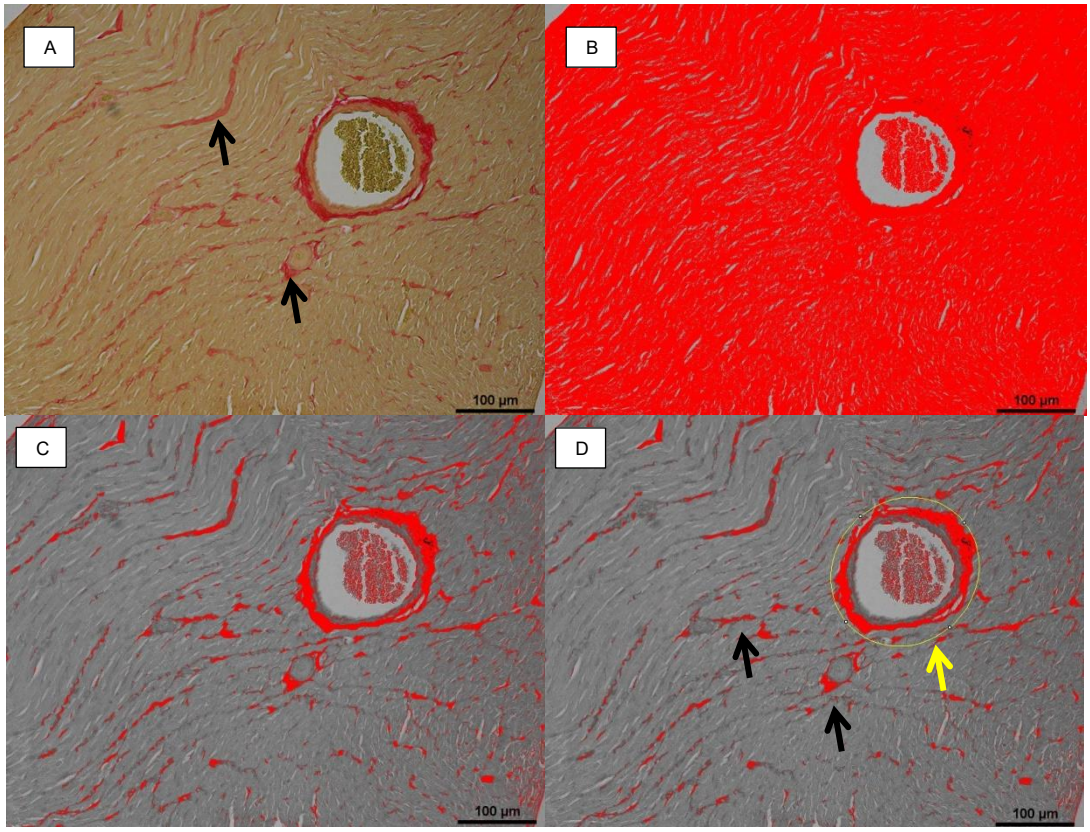


**Figure 2.9: Depiction of the process of color thresholding utilized for the measurement of fibrosis in the histological samples.**

The process of color thresholding (**Figure 2.9**) was utilized to determine pixel measurements for the entire myocardial tissue, and then the collagen depositions depicted with black arrows. Collagen deposition around the walls of blood vessels was measured (yellow arrow) and its pixel measurement was subtracted from the total fibrotic pixel measurements to account for normal distribution of collagen within the walls of blood vessels. Magnification: 20x, Scale Bar: 100 µm.

## 2.11. Statistical Analysis

Data was normalized to the control groups of the respective experimental groups and are presented as mean ± standard error of mean. P-values less than (<) 0.05 were considered statistically significant. Data obtained from multiple groups across two time points were analysed with the repeated measures Two-way analysis of variance (ANOVA) was followed by the Bonferroni post-test. Data obtained across

groups over one time point were analysed using the One-Way ANOVA followed by the Bonferroni post-hoc correction. All statistics were executed on Graph-pad Prism ™ software version 5 for analysis of statistical significance and visual representation.

# Chapter 3. RESULTS

## 3.1 Inoculation with LA7 cells successfully induced the development of mammary tumours.

Research conducted by Govender (2017) implemented the LA7 cell tumour-bearing experimental model. Their results demonstrated palpable tumours three days post cell inoculation and while these tumours persisted, they declined by the tenth day of the study. Since our entire treatment protocol was eight weeks long, we optimized the above-mentioned model to achieve better tumour stability (see Sections **2.3**, **2.4** & APPENDIX B: CELL CULTURE, pg. 121; APPENDIX C: TUMOUR INNOCULATION, pg.125.). The use of this model was appropriate because it is clinically relevant and takes into account not only the effects of the tumour alone, but also the effects of the tumour and DOX treatment. In this study, tumours were palpable as early as two days post-inoculation (**Figure 3.1**) and persisted beyond four weeks as showed in **Figure 3.2**. While peak tumour volumes were observed at week two, this study acknowledges that this model was not perfect, as tumour size started to decline beyond this point. It is also clear from **Figure 3.2** that DOX-treatment is an effective chemotherapeutic agent against breast cancer, as tumour growth was significantly arrested by week two and persisted to decrease at week three when the DOX and tumour group (week two: 1523.00 ± 457.80 $mm^3$, $p < 0.01$, week three: 529.3.00 ± 375.30 $mm^3$, $p < 0.01$) was compared to the tumour alone group (week two: 2563.00 ± 478.20 $mm^3$, week three: 1613.00 ± 319.20 $mm^3$).

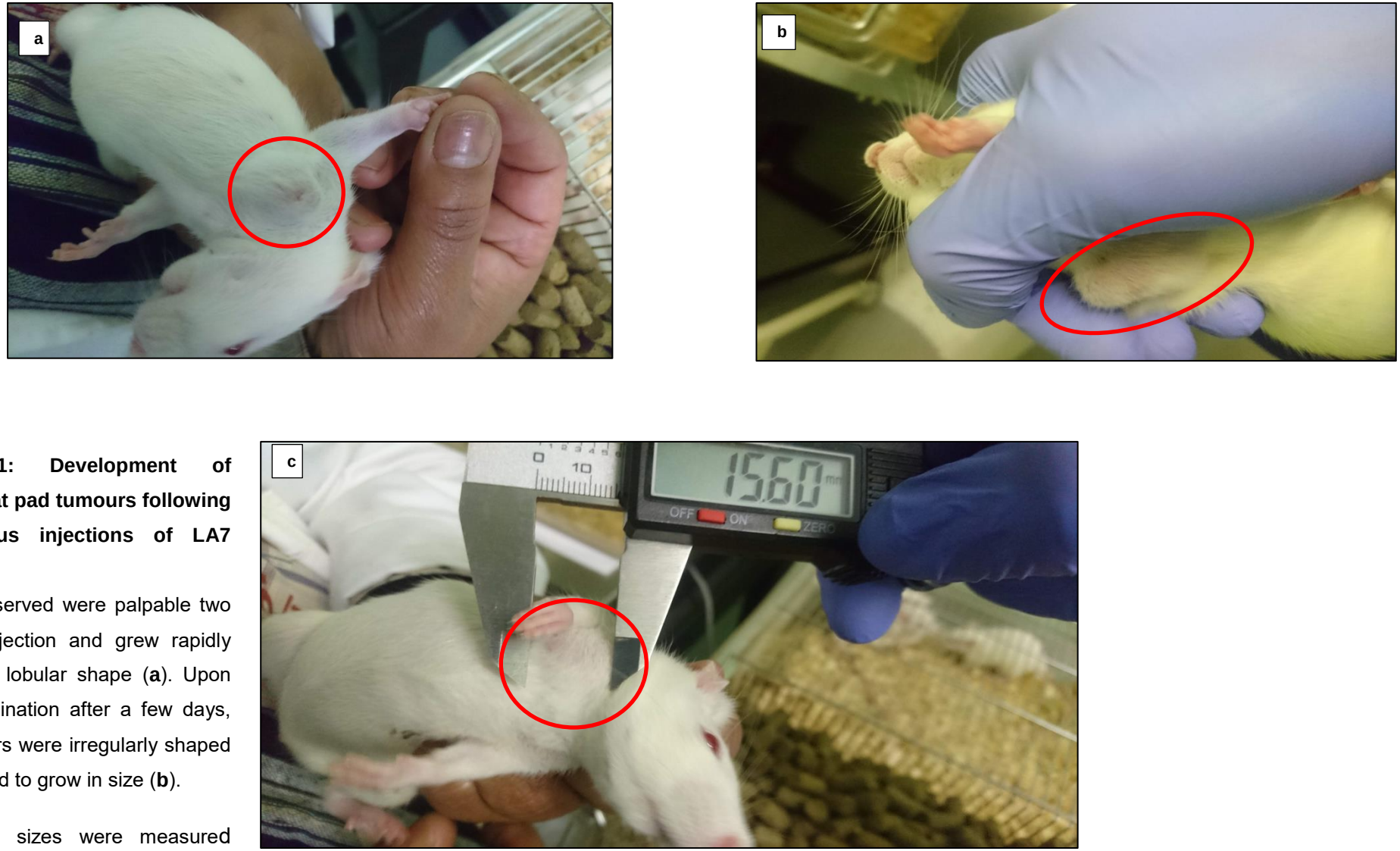


**Figure 3.1: Development of mammary fat pad tumours following subcutaneous injections of LA7 cells.**

Tumours observed were palpable two days post-injection and grew rapidly initially, in a lobular shape (**a**). Upon further examination after a few days, these tumours were irregularly shaped and continued to grow in size (**b**).

(**c**). Tumour sizes were measured with a digital calliper.

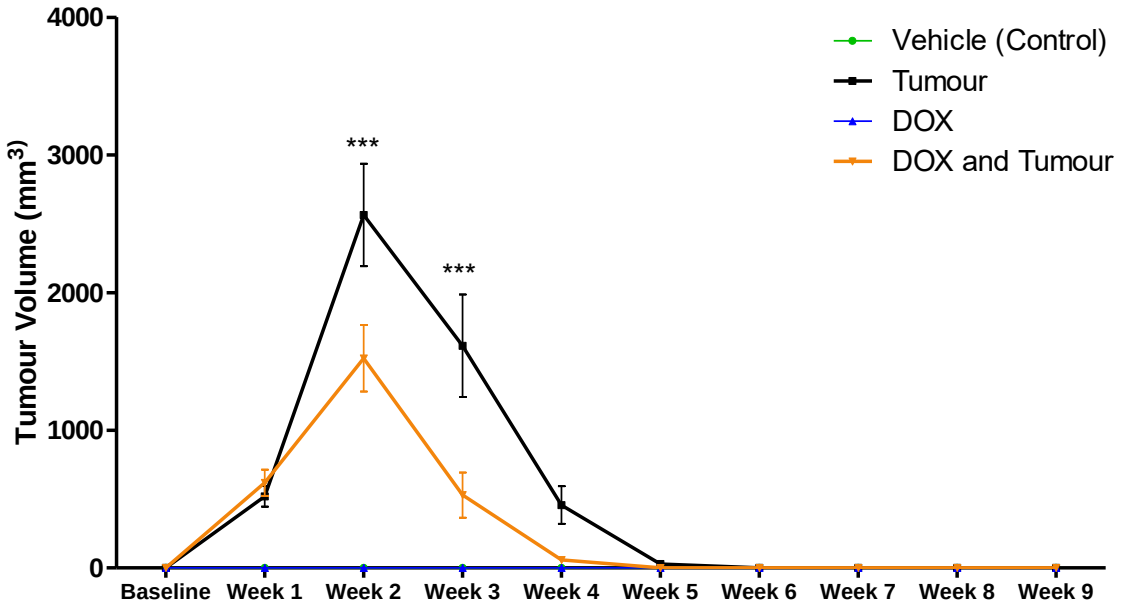


**Figure 3.2: Tumour volumes in mm$^3$ during the treatment protocol of all the models.**
Female Sprague-Dawley rats were randomly divided into four groups, and subjected to various treatment protocols over the course of eight weeks. Animals inoculated with LA7 cells exhibited mammary gland tumours and animals in the DOX groups were treated with 2.5 mg/kg DOX for eight weeks (cumulative dose: 20 mg/kg) starting at week 1. Results are presented as mean ± SEM (n = 9 - 10). ******* $p < 0.001$ vs DOX and tumour group. Abbreviations: **DOX** – Doxorubicin

## 3.2 Biometric Data

An important consideration of this study was the overall well-being of the animals utilized in the animal model. As such, body weight was monitored twice a week to evaluate the overall well-being of the animals, relative to those that were not treated. Moreover, to observe the early changes that took place, this study was conducted in two parts (treatment following four weeks and treatment following eight weeks). As such, the results are presented in this manner.

### 3.2.1. DOX treatment inhibits weight gain in otherwise healthy animals

Empirical body weight measurements obtained from this study gave varying results due to varying starting weights amongst the animals. To assess the effect of the tumour presence and DOX treatment on body weight, this study sought to determine

the percentage weight change over time. Data here indicates the change in body weight per week. Following the first week of treatment, both the tumour (25.81 ± 3.01%, p< 0.05), and DOX (18.27 ± 8.12%, p< 0.001) groups gained significantly less weight when compared to the vehicle (control) (30.26 ± 4.43%). This decrease was further exemplified in the DOX-treated group (5.84 ± 4.17%, p< 0.001) at week 3 relative to the vehicle (control) (12.00 ± 1.91%) (**Figure 3.3**).

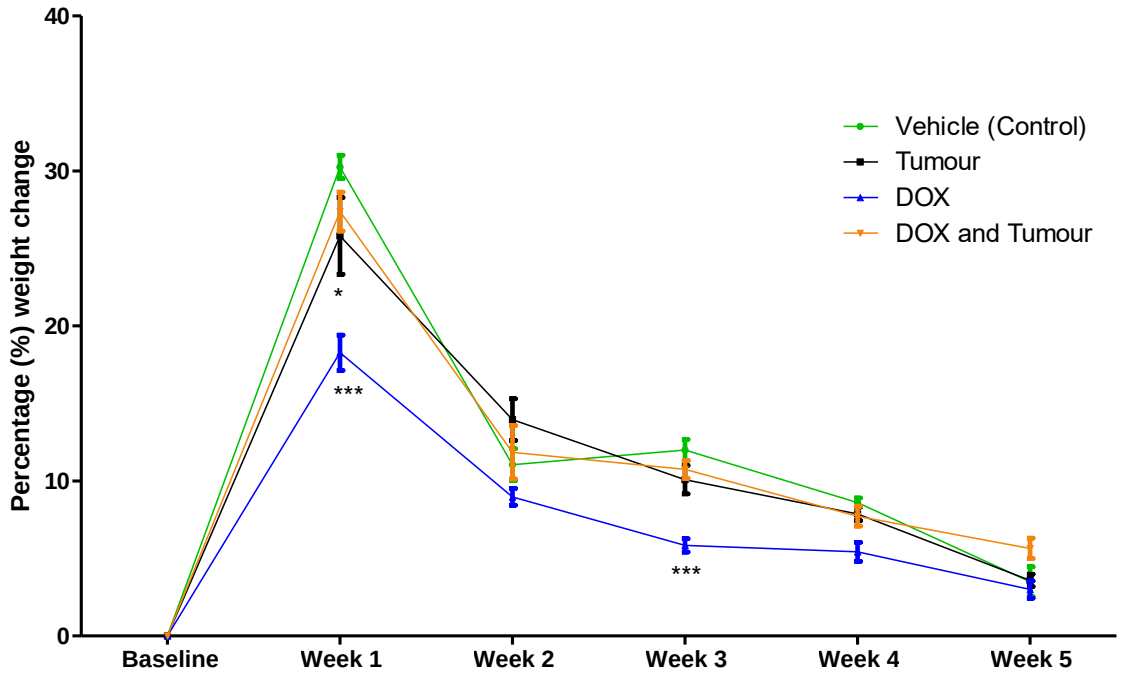


**Figure 3.3: Percentage (%) body weight change over the course of four weeks.**
Female Sprague-Dawley rats were randomly divided into four groups, and subjected to various treatment protocols over the course of four weeks. Animals inoculated with LA7 cells exhibited mammary gland tumours and animals in the DOX groups were treated with 2.5 mg/kg DOX for four weeks (cumulative dose: 10 mg/kg). Results are presented as mean ± SEM (n = 3-5) *p<0.05, *** p < 0.001 vs Vehicle control. Abbreviations: **DOX** - Doxorubicin

To gain a better understanding and a different perspective on the effect of the treatment on the animals, this study also plotted the percentage weight gain per week over the four week treatment protocol (**Figure 3.4**). Data for this section was obtained by comparing the weight gained per week as a percentage of the baseline weight. This analysis demonstrated that although the DOX-treated animals gained some weight over the treatment duration (5.84 ± 1.40 % at week 3); this was not to

the same extent as the other groups in this study. Considerable differences were observed not only between the non-tumour bearing DOX-treated animals and the vehicle (control) group, but also between the non-tumour bearing DOX-treated animals (5.84 ± 1.40% at week 3) and the tumour-bearing DOX-treated animals (10.75 ± 1.69% at week 3). These results thus suggest that irrespective of tumour presence in these animals, DOX treatment alone has a potent and negative influence on body weight gain, results which were also reported by Chandran *et al*., (2009).

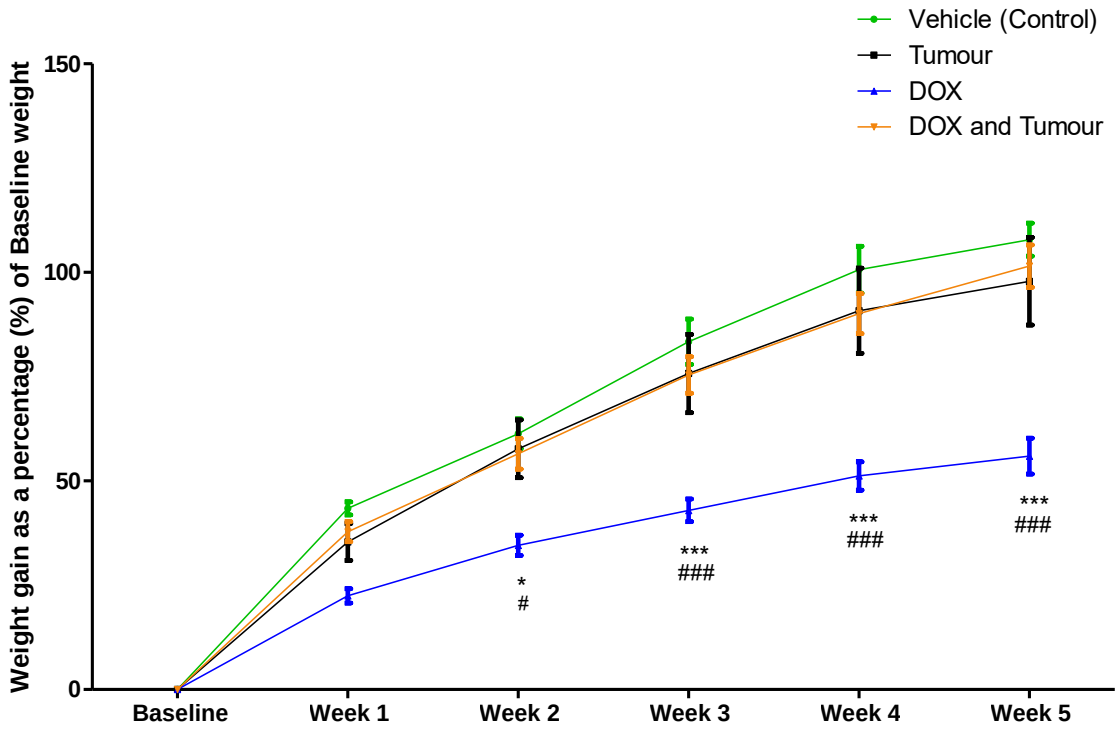


**Figure 3.4: Percentage (%) body weight gain over the course of four weeks.**

Female Sprague-Dawley rats were randomly divided into four groups, and subjected to various treatment protocols over the course of four weeks. Animals inoculated with LA7 cells exhibited mammary gland tumours and animals in the DOX groups were treated with 2.5 mg/kg DOX for four weeks (cumulative dose: 10 mg/kg). Results are presented as mean ± SEM (n = 3-5). *p<0.05, *** p < 0.001 vs vehicle control, $^{\#}$p<0.05, $^{\#\#\#}$p<0.001 vs Tumour. Abbreviations: **DOX** - Doxorubicin

In a similar manner, the animals that remained for the extended treatment protocol and treated for an additional four weeks, demonstrated comparable effects in that both the percentage weight change to an extent (**Figure 3.5**) and the percentage weight gain (**Figure 3.6**) were negatively influenced by DOX treatment.

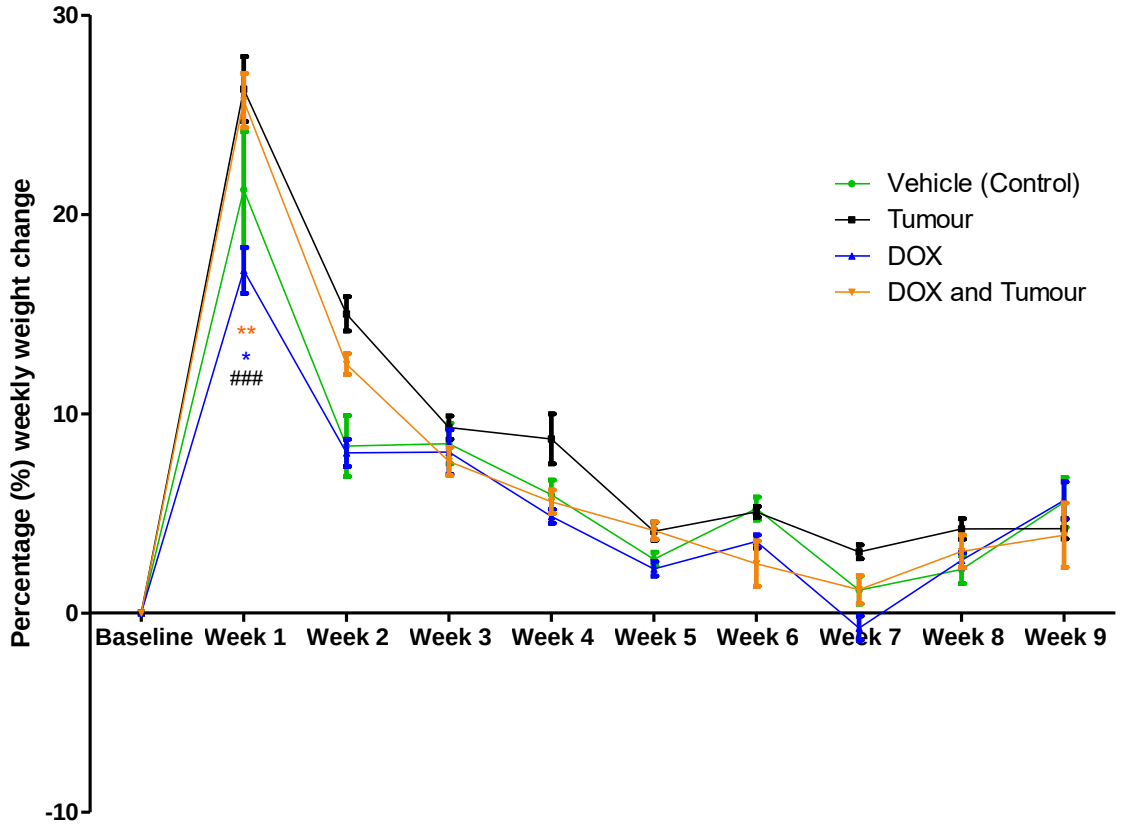


**Figure 3.5: Percentage (%) body weight change over the course of eight weeks.**

Female Sprague-Dawley rats were randomly divided into four groups, and subjected to various treatment protocols over the course of eight weeks. Animals inoculated with LA7 cells exhibited mammary gland tumours and animals in the DOX groups were treated with 2.5 mg/kg DOX for eight weeks (cumulative dose: 20 mg/kg). Results are presented as mean ± SEM (n = 5) *p<0.05 vehicle vs DOX control, **p < 0.01 Vehicle vs DOX and Tumour, ###p< 0.001 DOX vs DOX + Tumour. Abbreviations: **DOX** - Doxorubicin

As observed in the 4-week model, DOX-treated animals in the 8-week model gained less body mass from as early as the 4$^{th}$ week vs the tumour-bearing animals (6.96 ± 3.29%, $p < 0.05$), and the 6$^{th}$ week vs the vehicle controls (3.59 ± 2.96%, $p < 0.05$). By the 8$^{th}$ week, the tumour bearing DOX-treated animals began to demonstrate significantly less weight gain compared to the untreated tumour group (3.09 ± 3.18%, $p < 0.05$).

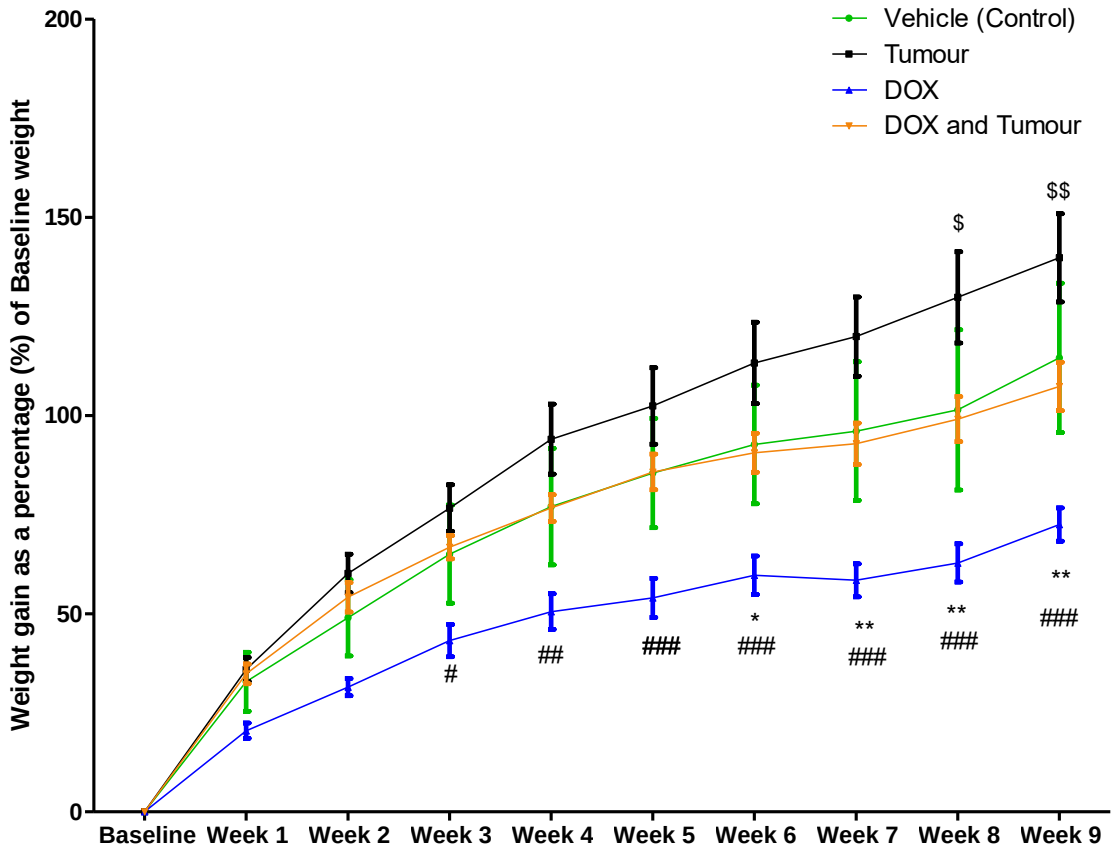


**Figure 3.6: Percentage (%) body weight gain over the course of eight weeks.**

Female Sprague-Dawley rats were randomly divided into four groups, and subjected to various treatment protocols over the course of eight weeks. Animals inoculated with LA7 cells exhibited mammary gland tumours and animals in the DOX groups were treated with 2.5 mg/kg DOX for eight weeks (cumulative dose: 20 mg/kg). Results are presented as mean ± SEM (n = 5) *p < 0.05, ** p < 0.01 vs vehicle (control), $^{\$}$p < 0.05, $^{\#}$p<0.05, $^{\#\#}$p<0.01, $^{\#\#\#}$p<0.001 vs Tumour, $^{\$\$}$p < 0.01 vs DOX and Tumour. Abbreviations: **DOX** - Doxorubicin

## 3.3 DOX-treatment induces fibrosis in cardiac tissue independent of tumour presence

In an effort to evaluate cardiac remodelling, which would indicate progression of HF, the end result of cardiotoxicity; this study assessed collagen deposition in the myocardial samples obtained. Cardiac remodelling can take place following several pathophysiological stimuli and may either be adaptive or maladaptive. In the adaptive stage, structural changes of the heart exert a compensatory effect to maintain normal cardiac function; however, if the stress is sustained, cardiac

remodelling advances to progressive and irreversible dysfunction of the heart (maladaptation). In the context of fibrosis, this occurs through fibroblast proliferation and extracellular matrix reorganization (Xue & Jackson, 2015). Myocardial fibrosis, as such, is regarded as a hallmark of cardiomyopathy (Payne & Nohria, 2017). Therefore, to determine the levels of maladaptation induced by the presence of a tumour and/or DOX treatment, cardiac tissue was stained for collagen deposition characteristic of fibrosis **Figure 3.7; Figure 3.8**.

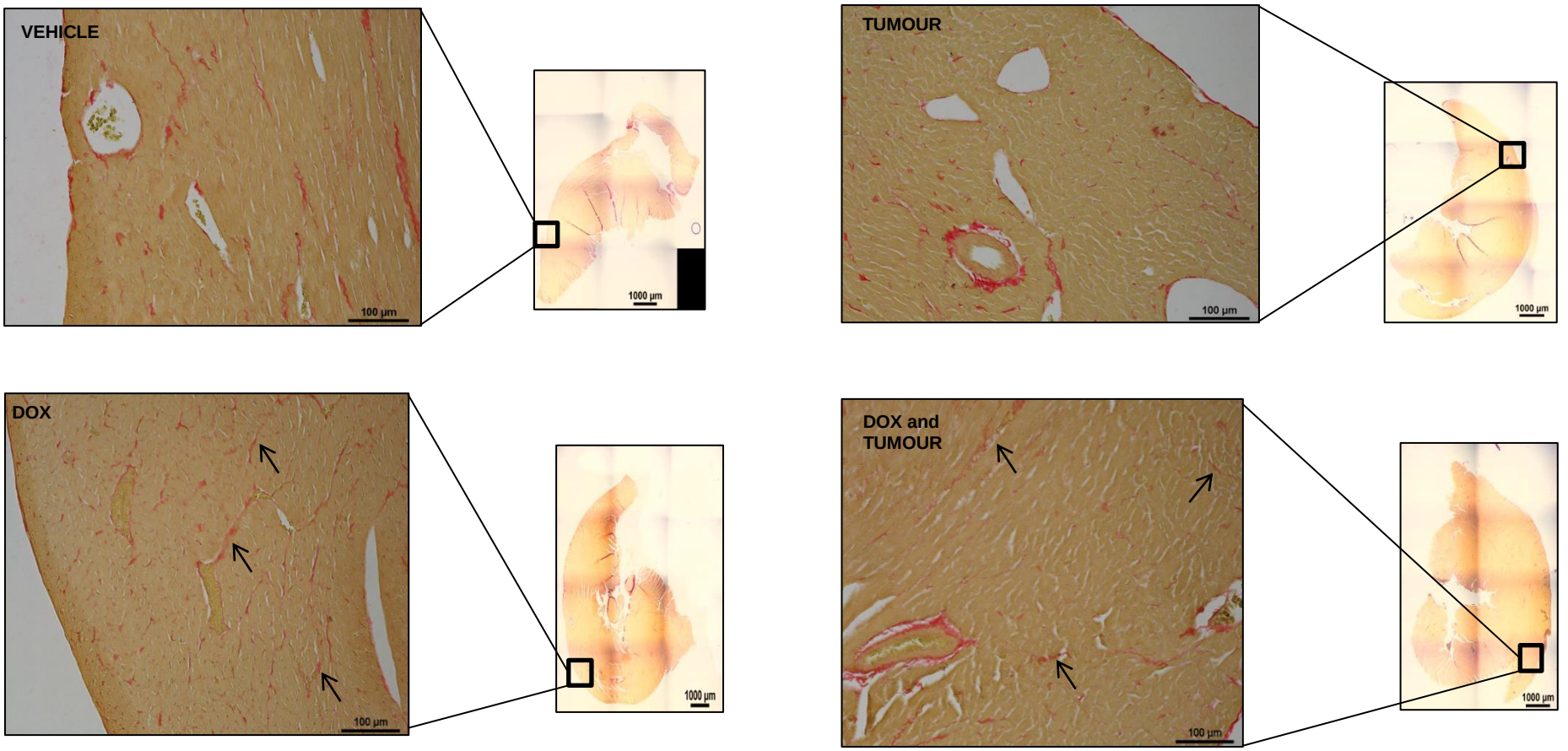


**Figure 3.7: Representative images of the Picrosirius red stain for fibrosis in the 4-week model:**

Female Sprague-Dawley rats were randomly divided into four groups, and subjected to various treatment protocols over the course of four weeks. Animals inoculated with LA7 cells exhibited mammary gland tumours and animals in the DOX groups were treated with 2.5 mg/kg DOX for four weeks (cumulative dose: 10 mg/kg). The left ventricular section of the myocardium in this model was red stained and collagen fibres (black arrows) were distinctly visible in contrast to the yellow/brown stain of the cardiomyocytes. Magnification: 4x for entire sections and 20x for the enlargements, Scale bars: 1000 µm for entire sections and 100 µm for the enlargements (n = 3-5). Abbreviations: **DOX** – Doxorubicin.

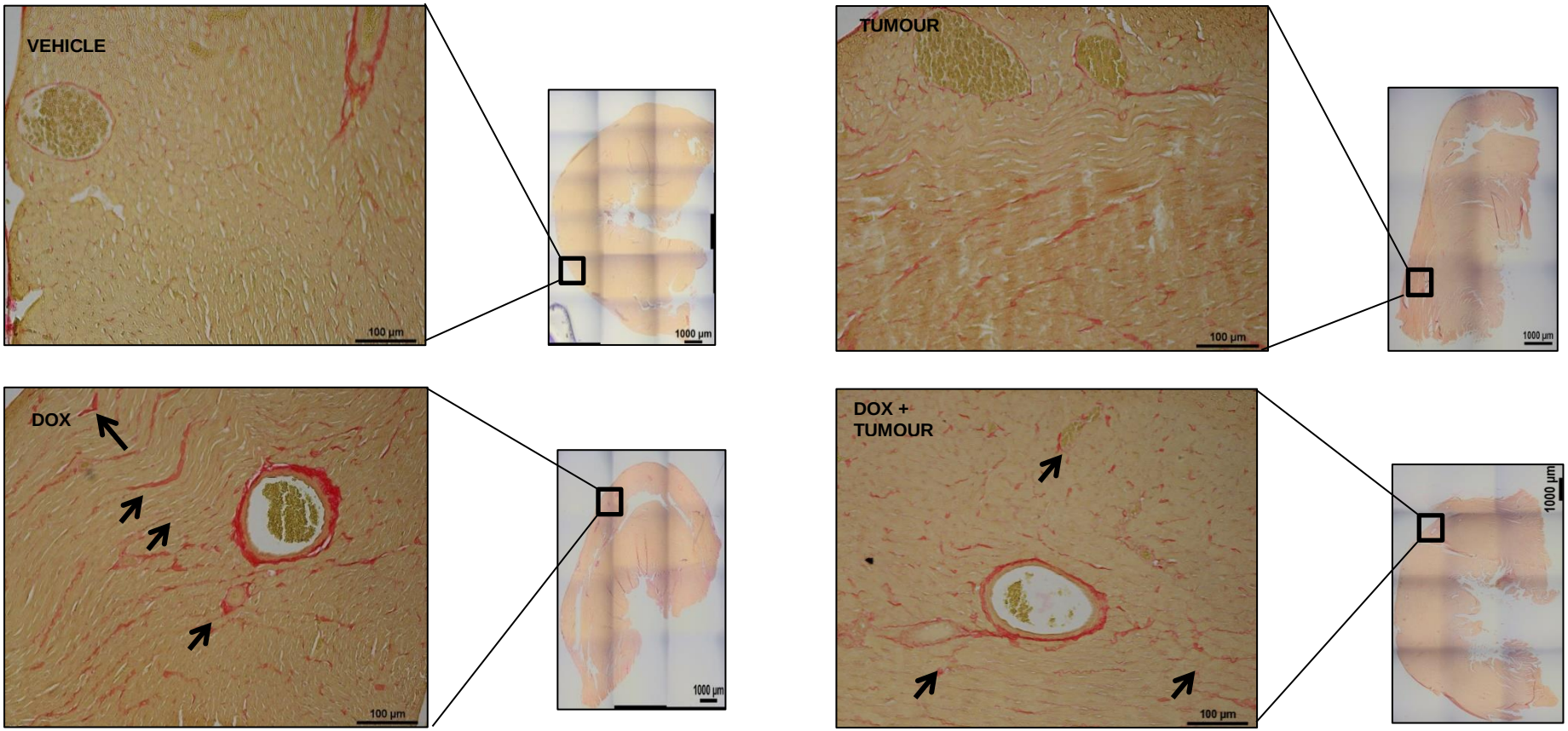


**Figure 3.8: Representative images of the Picrosirius red stain of collagen deposition indicative of fibrosis following eight weeks of treatment.** Female Sprague-Dawley rats were randomly divided into four groups, and subjected to various treatment protocols over the course of eight weeks. Animals inoculated with LA7 cells exhibited mammary gland tumours and animals in the DOX groups were treated with 2.5 mg/kg DOX for eight weeks (cumulative dose: 20 mg/kg). The left ventricular section of the myocardium in this model was red stained and collagen fibres (black arrows) were distinctly visible in contrast to the yellow/brown stain of the cardiomyocytes. Magnification: 4x for entire sections and 20x for the enlargements, Scale bars: 1000 µm for entire sections and 100 µm for the enlargements, (n = 5), Abbreviations: **DOX** – Doxorubicin.

To quantitatively assess fibrosis, results were expressed as a 'fold-increase' compared to the vehicle (control). In the early onset DOX-induced cardiotoxicity model represented by the four week protocol (**Figure 3.7**), DOX-treated animals presented with increased collagen deposition (3.05 ± 0.27%, $p < 0.05$) when compared to the vehicle (control) (1.00 ± 0.64%). This study did not observe any changes in the tumour alone group versus control nor the combination when compared to the DOX alone group (**Figure 3.9A**). In the late onset DOX-induced cardiotoxicity model represented by the eight week protocol, similar results were observed where the DOX-treated group (3.27 ± 0.52%, $p < 0.01$) displayed considerably higher levels of collagen deposition when compared to the vehicle (control) (1.00 ± 0.20%). Furthermore, significance was also observed when comparisons were made between the DOX and tumour group (3.81 ± 0.29%, $p < 0.05$) with the tumour only group (2.06 ± 0.29%). No changes were noted when the DOX and tumour group was compared to the DOX only group (**Figure 3.9B**). These results therefore suggest that the discerned changes in collagen deposition were a direct effect of DOX treatment and not the presence of a tumour, although in the late onset model, the combination of DOX and the tumour seemingly compounded the pathology.

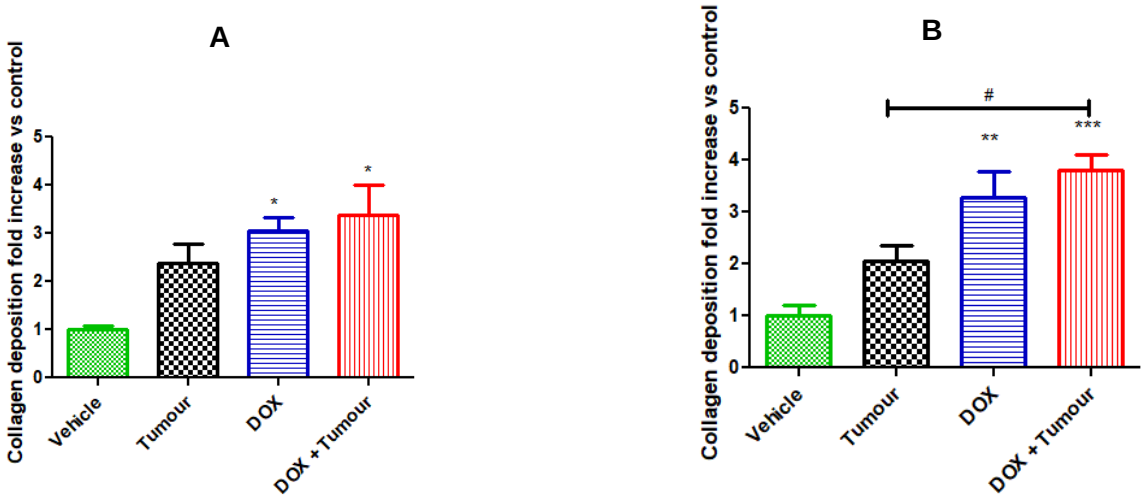


**Figure 3.9: Collagen deposition quantification as an indication of fibrosis following four and eight weeks of treatment.**

Female Sprague-Dawley rats were randomly divided into four groups, and subjected to various treatment protocols over the course of four and eight weeks. Animals inoculated with LA7 cells

exhibited mammary gland tumours and animals in the DOX groups were treated with 2.5 mg/kg DOX for four (**A**) and eight (**B**) weeks (cumulative dose: 10 and 20 mg/kg respectively). The percentage collagen deposition in the myocardium was measured using colour thresholding. Results are presented as mean ± SEM (n = 3-5). *****p<0.05 DOX vs vehicle (control), $^{\#}$p<0.05 Tumour vs DOX and tumour, **p<0.01 vs Vehicle (control), ***p<0.001 vs Vehicle (control). Abbreviations: **DOX** – Doxorubicin.

## 3.4. Expression of CTI, CKM and BNP-45 as measures of heart damage

A few methods have been utilized in literature to establish cardiac damage. Considering that the treatment protocols implemented by the present study were utilized to compare the outcomes of modifying a current model of chronic DOX-induced cardiotoxicity, measuring markers of cardiac damage was required to determine the extent of cardiotoxic damage inflicted by the treatment protocols. Cardiac troponins are the most widely studied markers of myocardial injury (Yu & Ky, 2016). The two forms of cardiac troponin (I and T) form part of the troponin complex responsible for regulating the interaction between the thin and thick filaments in striated muscle (Neves *et al*., 2016). Along with the troponins, natriuretic peptides have been studied extensively for their prognostic and diagnostic roles within heart failure. BNP-45, an N-terminal pro-brain natriuretic peptide (NT-proBNP) is a standard marker utilized for the diagnosis and management of HF (Yu & Ky, 2016). Creatine kinase (CK) is a dimeric enzyme that has four isoforms specifically localized within the mitochondria (Mt-CK), and the cytosol. The cytosolic isoforms are CK-MM (muscle type), CK-BB (brain type) and CK-MB (heart type). These isoforms work in tandem to form the CK phosphagen system that regulates energy supply in response to demand. Impairment in this system and reduction in total CK levels have been associated in the pathophysiology of chronic heart failure (Cao *et al*., 2020). This study investigated the expression of CTI, CK-MB and BNP-45 in order to establish the extent of cardiac damage inflicted by the treatment protocols. Whilst both troponin isoforms have similar diagnostic value, this study proceeded with the I-isoform since it has the advantage over T by not being influenced by renal failure (Immer *et al*., 1999; Neves *et al*., 2016).

This study found no significant difference in the expression of BNP-45 between the groups. On the other hand, a strong trend towards an increased expression of CTI in the other groups (Tumour: 927.30 ± 369.80%, DOX: 1134.00 ± 447.90%) compared

to the control (100.00 ± 179.40%), however this increase was only significant in the combination group (1970.00 ± 400.30%, $p < 0.05$). Conversely, total CK-MB was significantly downregulated within tissue in the combination group (72.70 ± 7.03%, $p < 0.05$) compared to the controls (100.0 ± 5.47%).

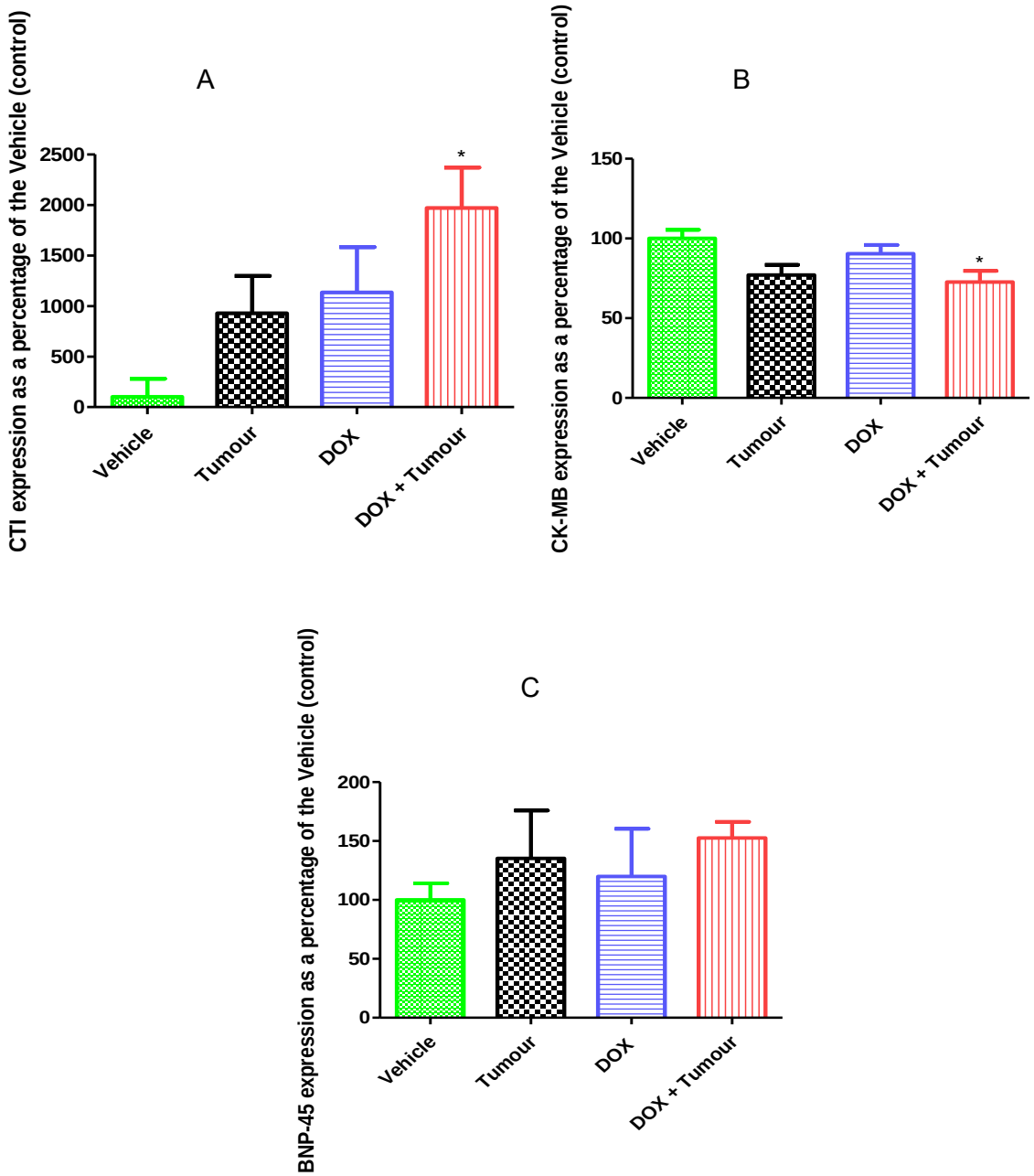


**Figure 3.10: Plasma expression of CTI (A), CK-MB (B) and BNP-45 (C) as markers of cardiac damage associated with the development of cardiotoxicity.**

Female Sprague-Dawley rats were randomly divided into four groups, and subjected to various treatment protocols over the course of four and eight weeks. Animals inoculated with LA7 cells

exhibited mammary gland tumours and animals in the DOX groups were treated with 2.5 mg/kg DOX for four and eight weeks (cumulative dose: 10 and 20 mg/kg, respectively). Luminescence readings taken at 450 nm were normalized to a zero reading and concentration readings extrapolated from a standard curve. Plasma concentration readings of CTI (A) and BNP-45 (C) as well as tissue concentration readings of CK-MB (B) are expressed as a percentage of mean vehicle concentration are represented as mean ± SEM (n = 3 - 5), * $p < 0.05$ vs Vehicle control. Abbreviations: **CTI** – cardiac troponin I, **CK-MB** – creatine kinase heart-type, **BNP-45** – Brain-type natriuretic peptide 45.

## 3.5. Heart Weight as a measure of hypertrophy

As cardiac remodelling is closely correlated with the progression of HF, and encompasses all the molecular, cellular, and interstitial events that contribute to the clinically relevant changes in the shape, size, and mass of the heart after cardiac injury, this study assessed whether cardiac hypertrophy took place as a result of the treatment regimens. To this end, the final heart weight measurements were taken at the end of experimental protocol. Since the animals had varying body weights at the time of sacrifice, it was necessary to standardize this measurement. To achieve this, this study expressed heart weight as a ratio of body weight and compared these as a percentage of the vehicle (control). As demonstrated in **Table 3.1**, no hypertrophy was evident across all groups. It should be noted that while heart to body weight ratios may have provided an indication of potential hypertrophy in this model, rodent body weights tend to fluctuate, and as such, a more stringent and accurate method of analysis for hypertrophy in cases where body weight fluctuates may have been to rather use heart weight to tibial length than to body weight (Yin *et al*., 1982).

**Table 3.1: Quantification of hypertrophy calculated as the ratio between heart weight to body weight.**

| | Vehicle (control) | Tumour | DOX | DOX and Tumour |
|---|---|---|---|---|
| **% Heart weight : Body weight ratio at four weeks (n = 3-5)** | | | | |
| | 100.00 ± 2.32 | 96.78 ± 4.40 | 90.31 ± 2.11 | 100.30 ± 5.94 |
| **% Heart weight : Body weight ratio at eight weeks (n = 5)** | | | | |
| | 100.00 ± 3.23 | 104.8 ± 3.30 | 97.50 ± 4.08 | 103.6 ± 4.61 |

Freshly excised hearts were weighed and their weight as a percentage ratio to body weight was calculated. Results are presented as mean ± SEM, (n = 3-5). Abbreviations: **DOX** – Doxorubicin.

## 3.6. qPCR profiling of specific microRNAs

As previously mentioned, miRNAs are small, highly conserved non-coding RNA molecules involved in the regulation of gene expression (Thum *et al*., 2007). Although there is a general understanding of how miRNAs function, their biogenesis and translational repression functions remain to be elucidated. Considering that circulating miRNAs have previously been reported as promising biomarkers for various pathologic conditions (Divakaran *et al*., 2008), the analysis of their expression profiles could provide information on their regulation, function and role in different disease states, including cancer and CVD (Esquela-Kerscher *&* Slack, 2014). Various observations have indicated that miRNA expression profiles are altered in different disease states, implying that miRNAs may be involved in their development and progression (Goren *et al*., 2012; Li *et al*., 2014). Despite our limited understanding of these molecules, basic expression profiling is proving to be clinically relevant to diagnosis, development and ultimate consequence.

### 3.6.1. Plasma miRNA 208a expression is time-and treatment-dependent in the context of DOX-induced cardiotoxicity

MiR-208a is one of the most critical heart-specific miRNAs playing a crucial role in heart failure, and has been considered to be a plausible biomarker of myocardial injuries. During pathophysiological conditions, miR-208a induces cardiac remodelling, expression of hypertrophy pathway components and arrhythmias (Ji *et al*., 2009). Therefore, this study speculated that this miRNA may possibly leak into circulation from damaged cells and, in so doing, serve as a biomarker for distinguishing the injured cell type. As demonstrated in **Figure 3.11**, miR-208a was barely detectable following four weeks of treatment in the different treatment groups. However after eight weeks of treatment, this study observed a decreased expression of this miRNA in other treatment groups (Tumour: 0.00 ± 0.00%, $p < 0.001$; DOX: 45.79 ± 8.54%, $p < 0.01$; DOX and Tumour: 49.69 ± 8.26%, $p < 0.01$) when compared to the vehicle (control) (100.00 ± 5.17%). Since this study was unable to detect the presence of this miRNA in the tumour group after eight weeks, and only in

the DOX group and DOX and Tumour group, the observed expression in the combination group suggests that the detection of this miRNA was influenced by DOX treatment, albeit being significantly lower that the vehicle (control). Not only do these results demonstrate that the expression of this miRNA increases with time, the treatment regimen also had a major impact on the expression profile of this particular miRNA.

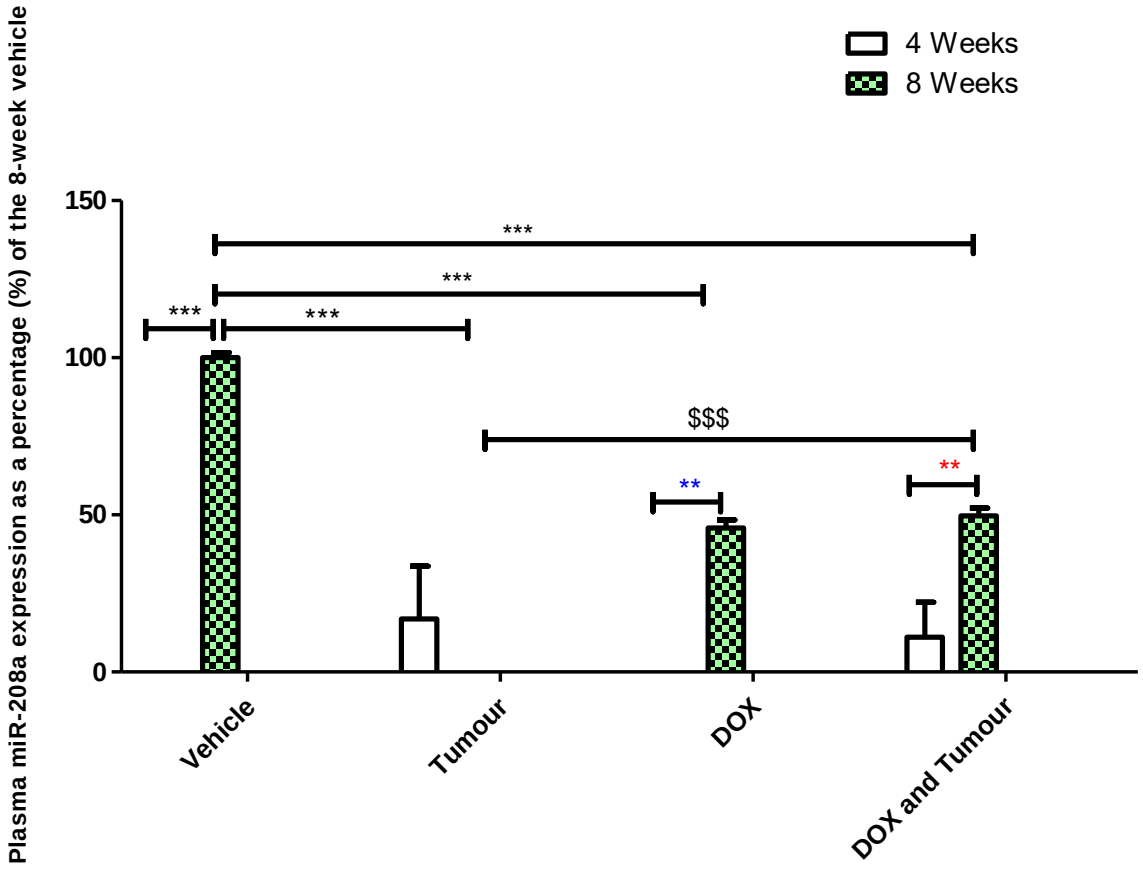


**Figure 3.11: Percentage expression of miR-208a following four and eight weeks of treatment.** Female Sprague-Dawley rats were randomly divided into four groups, and subjected to various treatment protocols over the course of four and eight weeks. Animals inoculated with LA7 cells exhibited mammary gland tumours and animals in the DOX groups were treated with 2.5 mg/kg DOX for four and eight weeks (cumulative dose: 10 and 20 mg/kg, respectively). Percentage expression of plasma miR-208a normalized to that of the exogenous control, cel-miR-39 was evaluated. Normalized plasma miR-208a ΔCq values as a percentage of 8-week vehicle mean ΔCq are represented as mean ± SEM (n = 3 - 5), *** p<0.001 vs 4-week vehicle control, ***p<0.001 vs 8-week vehicle control, **p<0.01 vs 4-week DOX, $^{\$\$\$}$p<0.001, **p<0.01 vs 4-week DOX and Tumour. Abbreviations: **DOX** – Doxorubicin.

### 3.6.2. DOX-induced cardiotoxicity does not induce a time dependent expression of plasma miR-133-a and miR-133b

MiR-133 was originally described in mice and its homologs have since been identified in several other species. In the human genome, miR-133 genes include miR-133a-1, miR-133a-2, and miR-133b found on chromosomes 18, 20, and 6, respectively. Primarily expressed in the heart (Li *et al*., 2018), miR-133 is indispensable for cardiac remodelling in response to different types of stressors as it functions to regulate the development of cardiac fibrosis and cardiac hypertrophy. Within the context of DOX-induced cardiotoxicity, this study discovered no significant changes in the expression profiles of either miR-133a (**Figure 3.12a**) or miR-133b (**Figure 3.12b**) following eight weeks of treatment. Interestingly, we observed a considerable increase in plasma miR-133a after four weeks in the combination group (137.20 ± 18.22%, $p < 0.01$) when compared to the DOX-treatment group (60.23 ± 6.27%). This study inferred from this that the combination of DOX and the tumours in an early model of chronic cardiotoxicity induced an increased expression of miR-133a.

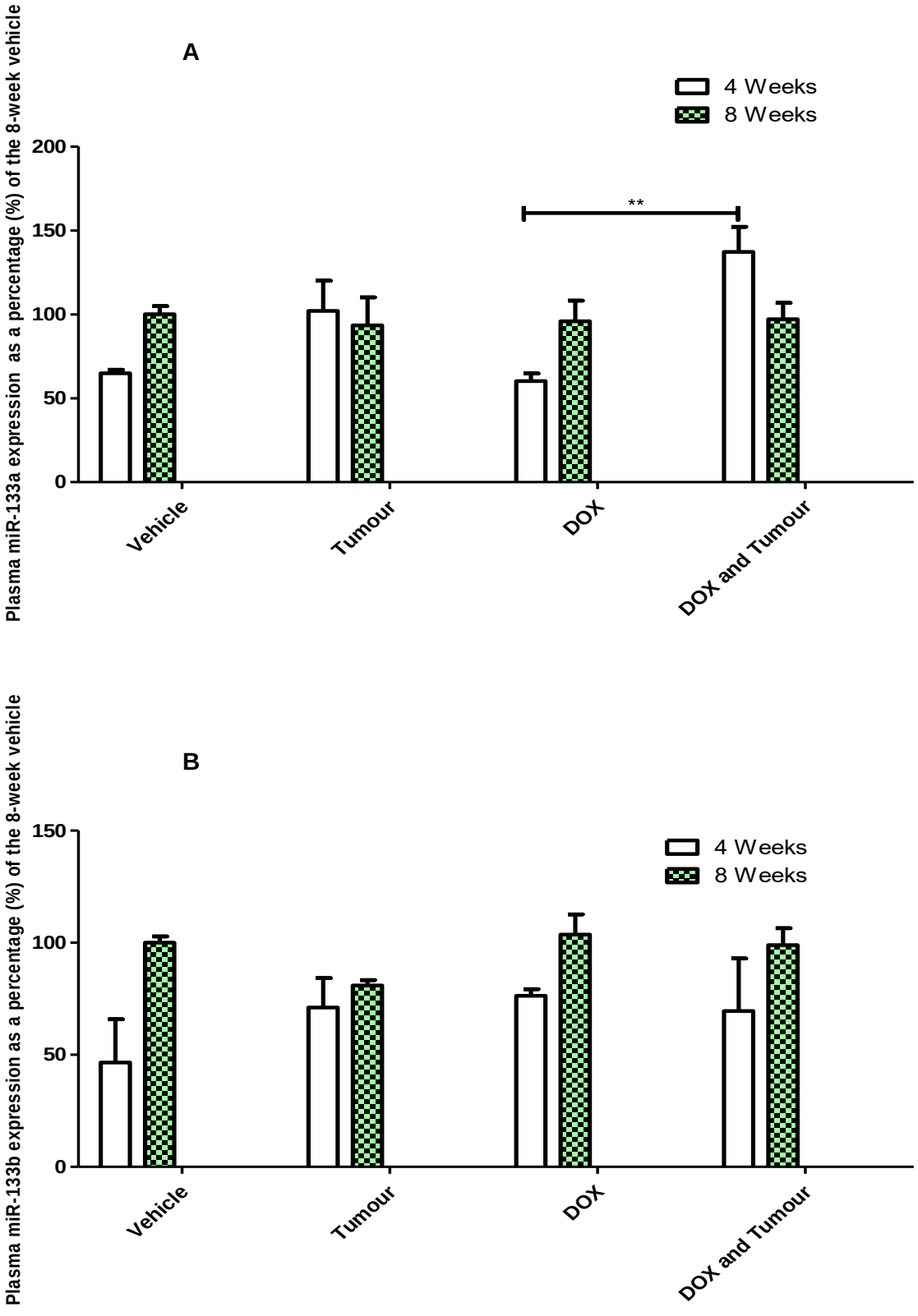


**Figure 3.12: Percentage expression of miR-133 following four and eight weeks of treatment.** Female Sprague-Dawley rats were randomly divided into four groups, and subjected to various treatment protocols over the course of four and eight weeks. Animals inoculated with LA7 cells exhibited mammary gland tumours and animals in the DOX groups were treated with 2.5 mg/kg DOX

for four and eight weeks (cumulative dose: 10 and 20 mg/kg, respectively). Percentage expression of plasma miR-133a (A) and miR-133b (B) normalized to that of the exogenous control, cel-miR-39 was evaluated. Normalized plasma miR-133a (A) and miR-133b (B) ΔCq values as a percentage of 8-week vehicle mean ΔCq are represented as mean ± SEM (n = 3 - 5), **p<0.01 vs DOX and Tumour. Abbreviations: **DOX** – Doxorubicin.

### 3.6.3. miR-29b expression within the context of DOX-induced cardiotoxicity

Reported to be down-regulated in the myocardium as a result of acute DOX treatment (Jing *et al*., 2018), this study identified miR-29b to have strong potential for playing a key role within this context. This miRNA has not only been reported to be present in the pericardial fluid, in fact miR-29b-3p was observed to be present in all body fluids (Kuosmanen *et al*., 2015). qPCR profiling revealed that treatment duration significantly influenced the expression of miR-29b (**Figure 3.13)**.

Analysis of plasma miRNA expression revealed significantly elevated miR-29b expression across the 8-week treatment protocol (vehicle: 100.00 ± 3.82%, $p < 0.001$; Tumour: 111.30 ± 6.64%, $p < 0.01$; DOX: 106.70 ± 6.96%, $p < 0.05$; and DOX and tumour: 121.80 ± 5.46%, $p < 0.001$) groups compared to their respective 4-week groups (vehicle: 36.30 ± 14.53%; Tumour: 64.15 ± 6.54%; DOX: 69.58 ± 1.42%; and DOX and tumour: 46.03 ± 13.82%). This study observed no changes when we compared all the treatment groups after four weeks against one another; however, after eight weeks, the only significant change observed was when the combination group (121.80 ± 31.36%, $p < 0.05$) was compared to the vehicle (control) (100.00 ± 3.82%) as presented in **Figure 3.13**.

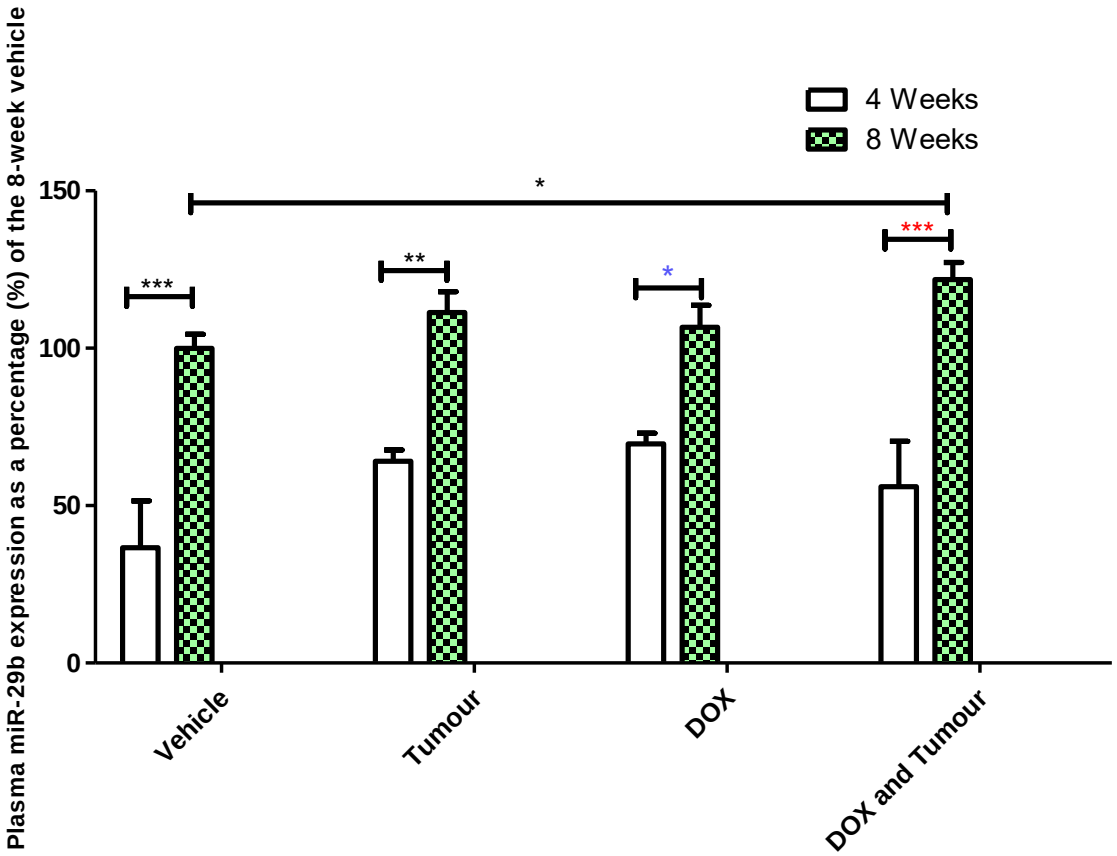


**Figure 3.13: Percentage expression of miR-29b following four and eight weeks of treatment**

Female Sprague-Dawley rats were randomly divided into four groups, and subjected to various treatment protocols over the course of four and eight weeks. Animals inoculated with LA7 cells exhibited mammary gland tumours and animals in the DOX groups were treated with 2.5 mg/kg DOX for four and eight weeks (cumulative dose: 10 and 20 mg/kg, respectively). Percentage expression of plasma miR-29b normalized to that of the exogenous control, cel-miR-39 was evaluated. Normalized plasma miR-29b ΔCq values as a percentage of 8-week vehicle mean ΔCq are represented as mean ± SEM (n = 3 - 5), *p<0.05, ***p<0.001 vs 8-week vehicle control, **p<0.01 vs 8-week tumour group, *p<0.05 vs 8-week DOX, ***p<0.001 vs 8-week DOX and tumour. Abbreviations: **DOX** – Doxorubicin.

## 3.7. Isolation of Mitochondrial and Cytosolic Fractions

Mitochondria are critical to cardiac function (Martinou & Youle, 2011). Within this context, dysfunctional mitochondria contribute to oxidative stress and the activation of apoptosis. This study aimed to differentiate between protein expression within the mitochondria, as well as the cytosol to elucidate the organelle-specific expression of critical proteins associated with oxidative stress and apoptosis within the context. To

confirm our molecular fractionation process, mitochondrial and cytosolic specific markers were probed for *via* western blotting. The study was able to confirm sufficient fractionation of the cytosolic samples by evaluating expression of cytosolic house-keeping protein Glyceraldehyde 3-phosphate dehydrogenase (GAPDH) (Kaarbø *et al*., 2003), which was expressed substantially more in the cytosolic samples compared to the mitochondrial sample.

In accordance with the above, the study also confirmed sufficient fractionation of the mitochondrial samples by evaluating the expression of mitochondrial house-keeping protein TOMM20 (Translocase of Outer Mitochondrial Membrane 20) as utilized in Morciano *et al*., (2016). Considerable expression of this marker was observed in the mitochondrial samples, while no expression could be detected in the cytosolic samples (**Figure 3.14**).

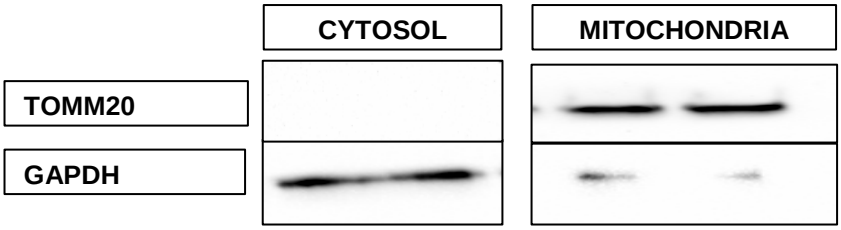


**Figure 3.14: Tissue fractionation confirmation**

Confirmation of tissue fractionation was achieved through protein determination of TOMM20 and GAPDH, utilized as markers for mitochondria and the cytosol, respectively. (n = 3), Abbreviations: **TOMM** – Translocase of Outer Mitochondrial Membrane, **GAPDH** – Glyceraldehyde 3-Phosphate Dehydrogenase.

## 3.8. Protein Expression in Isolated Mitochondrial Samples

### 3.8.1. SOD2

Naturally occurring antioxidants possess a critical role in the regulation of homeostasis, maintenance of ROS levels, and prevention of oxidative stress. Along with catalase and glutathione peroxidase, superoxide dismutase (SOD) forms the trident of physiologically available antioxidant enzymes in mammalian cells. The multiple isoforms of SOD have been established to be differentially localized and

target specific organelles. These forms include the Copper/Zinc SOD (CuZnSOD) and the Manganese SOD (MnSOD). In this study, MnSOD (described as SOD2 from this point) was identified as a critical role player and indicator of oxidative stress capacity within the context. This is due to SOD2's localization within the mitochondrial matrix (Daosukho *et al*., 2005). This characteristic is especially important since mitochondria are the primary source of ROS in mammalian cells (Boveris, 1977; Daosukho *et al*., 2005).

As a measure of mitochondrial anti-oxidant capacity, SOD2 expression was determined. Western blotting of isolated mitochondrial samples from the 4-week groups demonstrated no significant differences in SOD2 expression between the treatment groups compared to the vehicle control. However, a slight trend towards upregulation could be observed in the DOX-treated group (**Figure 3.15A**). In the 8-week groups, SOD2 expression was significantly upregulated in the DOX group (147.60 ± 16.82%, $p < 0.05$) compared to the vehicle control group (100.00 ± 1.05%). The DOX-treated animals also demonstrated significantly upregulated SOD2 expression compared to the DOX-treated tumour bearing animals (79.55 ± 6.24%, $p < 0.01$) and the untreated tumour group (89.69 ± 13.21%, $p<0.001$)(**Figure 3.15B**).

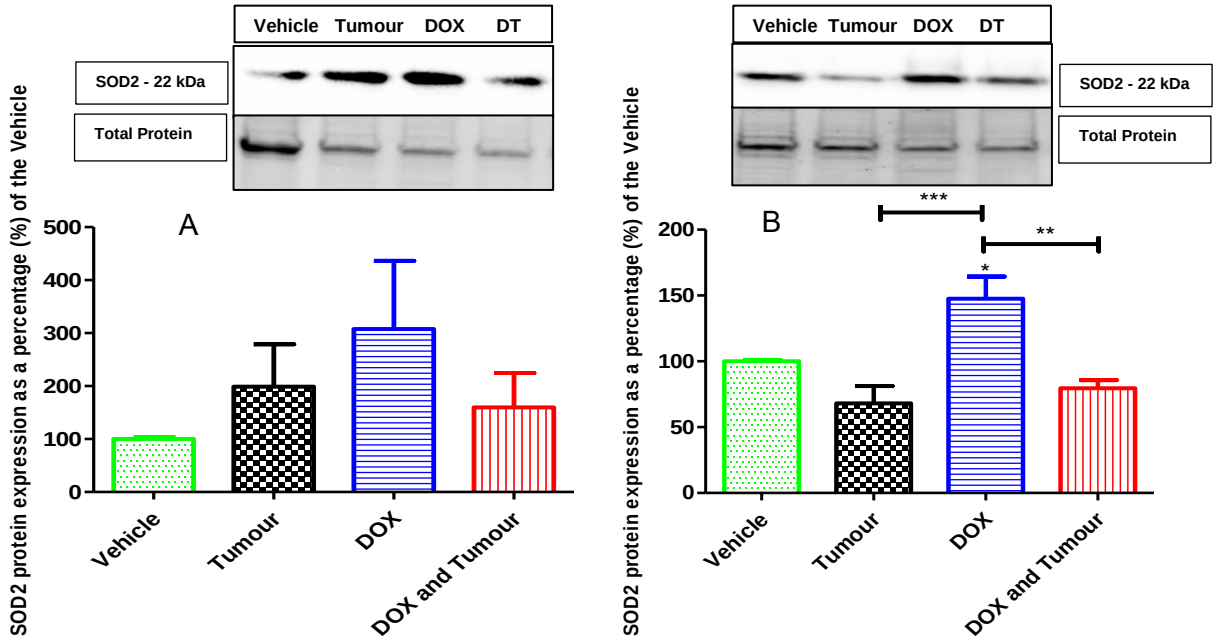


**Figure 3.15: Protein expression of SOD2 within the mitochondrial component following four (A) and eight (B) weeks of treatment.**

Female Sprague-Dawley rats were randomly divided into four groups, and subjected to various treatment protocols over the course of four and eight weeks. Animals inoculated with LA7 cells exhibited mammary gland tumours and animals in the DOX groups were treated with 2.5 mg/kg DOX for four (**A**) and eight (**B**) weeks (cumulative dose: 10 and 20 mg/kg). Protein expression was evaluated in cardiac tissue samples via western blotting. Data was normalized to total protein and results are presented as mean ± SEM (n = 3 - 5), *p<0.05 vs vehicle control, **p<0.01 vs DOX and Tumour, *** p<0.001 vs Tumour. Abbreviations: **DOX** – Doxorubicin, **DT** – DOX and Tumour **SOD** – Superoxide Dismutase.

### 3.8.2. DRP1

Mitochondrial homeostasis is essential for cellular survival. Maintenance of this important process is achieved through intricately interconnected and well-balanced feed-back loops achieved by the various proteins involved (Hom & Sheu, 2009). The major processes involved in mitochondrial homeostasis are mitochondrial fusion, fission and mitophagy. These intricately connected processes are managed carefully, and have both their advantages and disadvantages. It is generally accepted that healthy mitochondrial networks lean towards mitochondrial fusion, while stressed mitochondria demonstrate higher fission levels (Yue *et al*., 2014). Dynamin-related protein 1 (DRP1) is recruited to the mitochondria where it mediates mitochondrial fission (Park *et al*., 2014).DRP1 expression was subsequently assessed within the cytosolic and mitochondrial components of the frozen cardiac samples. Western blotting revealed more conspicuous DRP1 presence in the cytosolic lysates.

This study observed no significant changes in DRP1 expression levels within the mitochondria between the 4-week and 8-week groups post western blotting of isolated mitochondrial samples **Table 3.2**.

**Table 3.2: Protein expression of DRP1 within the mitochondrial component following four and eight weeks of treatment.**

| | Vehicle (control) | Tumour | DOX | DOX and Tumour |
|---|---|---|---|---|
| **Mitochondrial DRP1 expression as a % of the vehicle control at 4 weeks (n = 3-5)** | | | | |
| | 100.00 ± 6.73% | 155.00 ± 47.03% | 128.70 ± 43.61% | 135.20 ± 30.66% |
| **Mitochondrial DRP1 expression as a % of the vehicle control at 8 weeks (n = 5)** | | | | |
| | 100.00 ± 2.47% | 145.90 ± 35.16% | 123.50 ± 27.01% | 73.39 ± 18.44% |

Whilst no significant differences were observed in DRP1 expression at four weeks, DRP1 was significantly upregulated by eight weeks in the cytosol of the DOX-treated tumour bearing animals (186.50 ± 12.29%), compared to the other groups (vehicle controls: 100.00 ± 2.47%, $p < 0.01$; DOX: 114.40 ± 20.10%, $p < 0.05$; Tumour: 78.50 ± 16.85%, $p < 0.001$) (**Figure 3.16B**).

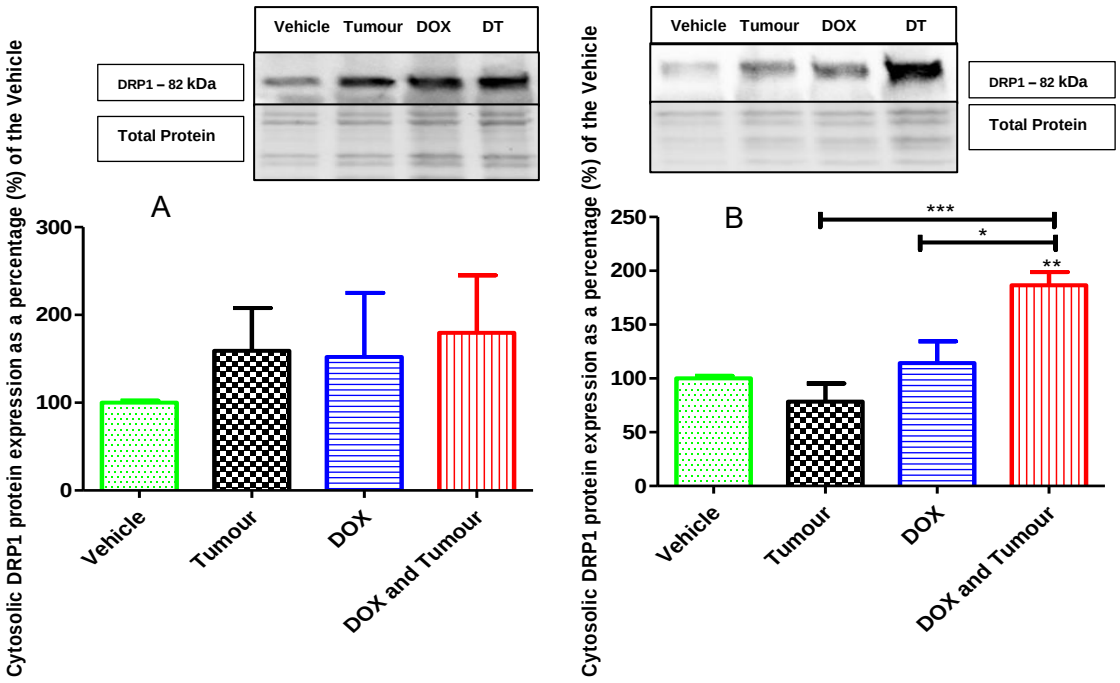


**Figure 3.16: Protein expression of DRP1 within the cytosolic component following four (A) and eight (B) weeks of treatment.**

Female Sprague-Dawley rats were randomly divided into four groups, and subjected to various treatment protocols over the course of four and eight weeks. Animals inoculated with LA7 cells exhibited mammary gland tumours and animals in the DOX groups were treated with 2.5 mg/kg DOX for four (**A**) and eight (**B**) weeks (cumulative dose: 10 and 20 mg/kg). Protein expression was evaluated in cardiac tissue samples via western blotting. Data was normalized to total protein and results are presented as mean ± SEM (n = 3 - 5), *p<0.05 vs DOX, **p<0.01 vs Vehicle control ***p<0.001 vs Tumour. Abbreviations: **DOX** – Doxorubicin, **DT** – DOX and Tumour **DRP1** – Dynamin Related Protein 1.

## 3.9. Cytosolic Protein expression

### 3.9.1. Apoptosis

#### 3.9.1.1. Caspases

Apoptosis is a critical factor in the aetiology of cardiotoxicity. It's been identified as the determining factor responsible for the permanent nature of chronic cardiotoxicity (Minotti, 2004). Caspases are integral components of the apoptosis machinery, where activator caspases - through proteolytic cleavage - activate effector caspases, which subsequently execute apoptotic degradation of structural and regulatory proteins (Suzuki *et al*., 2001).

As a measure of cellular apoptotic state, expression of the effector caspases-7 and -3 as well as their cleaved components were evaluated. It is established that the effector caspases-3 and -7 execute downstream cell death mechanisms. As structurally similar proteins (Lakhani *et al*., 2006), they demonstrate a degree of functional compensation in their operation (Walsh *et al*., 2008). Knock-outs of caspase-7 have been reported to prevent the lethality induced by intraperitoneal injections of lipopolysaccharides (Lamkanfi *et al* ., 2010). These molecules contribute to the production of tumour necrosis factor alpha (TNF-α) (Saini *et al*., 2005), and augment the lethal effect of DOX (Hassan *et al*., 2008) This study proceeded to investigate the expression of caspase-7 as a measure of apoptosis since it is reported to be activated during apoptosis and under inflammatory conditions (Lamkanfi & Kanneganti, 2010).

While trends were observed in the four week groups, there were no statistically significant changes to report. At eight weeks, the combination group was the only group to demonstrate significantly upregulated expression of caspase-7 (1048.00 ± 79.35%) vs the vehicle controls (100.00 ± 4.16%, $p < 0.001$) and the tumour (515.70 ± 115.30%, $p < 0.05$) (**Figure 3.17B**).

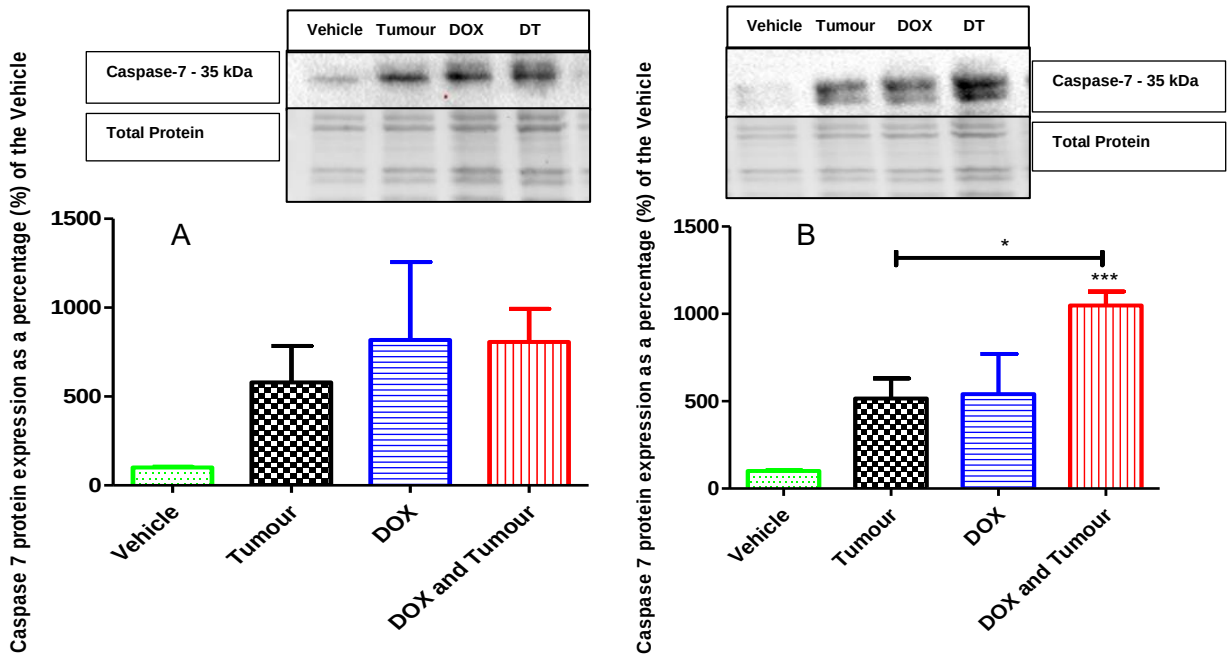


**Figure 3.17: Protein expression of Caspase-7 within the cytosolic component following four (A) and eight (B) weeks of treatment.**

Female Sprague-Dawley rats were randomly divided into four groups, and subjected to various treatment protocols over the course of four and eight weeks. Animals inoculated with LA7 cells exhibited mammary gland tumours and animals in the DOX groups were treated with 2.5 mg/kg DOX for four (**A**) and eight (**B**) weeks (cumulative dose: 10 and 20 mg/kg). Protein expression was evaluated in cardiac tissue samples via western blotting. Data was normalized to total protein and results are presented as mean ± SEM (n = 3 - 5), *p<0.05 vs Tumour, ***p<0.001 vs Vehicle Control. Abbreviations: **DOX** – Doxorubicin, **DT** – DOX and Tumour.

#### 3.9.1.2. Caspase Activation

Activator caspases, such as caspase 9, execute the proteolytic cleavage and activation of effector caspases such as caspase-7 and -3 (Suzuki *et al*., 2001). Cleaved Caspase-7 and -3 are by-products of caspase cleavage, and is indicative of the activation levels of this caspase. Increased levels of cleaved caspases indicate an accelerated activation of the caspase cascade and consequently a more pro-apoptotic cellular state (Chan *et al*., 2005).

At the four week time-point (**Figure 3.18A**), cleaved caspase-7 levels were demonstrated to be significantly upregulated in the DOX-treated animals (494.90 ± 90.75%, $p < 0.05$) compared to the vehicle controls (100.00 ± 3.40%).

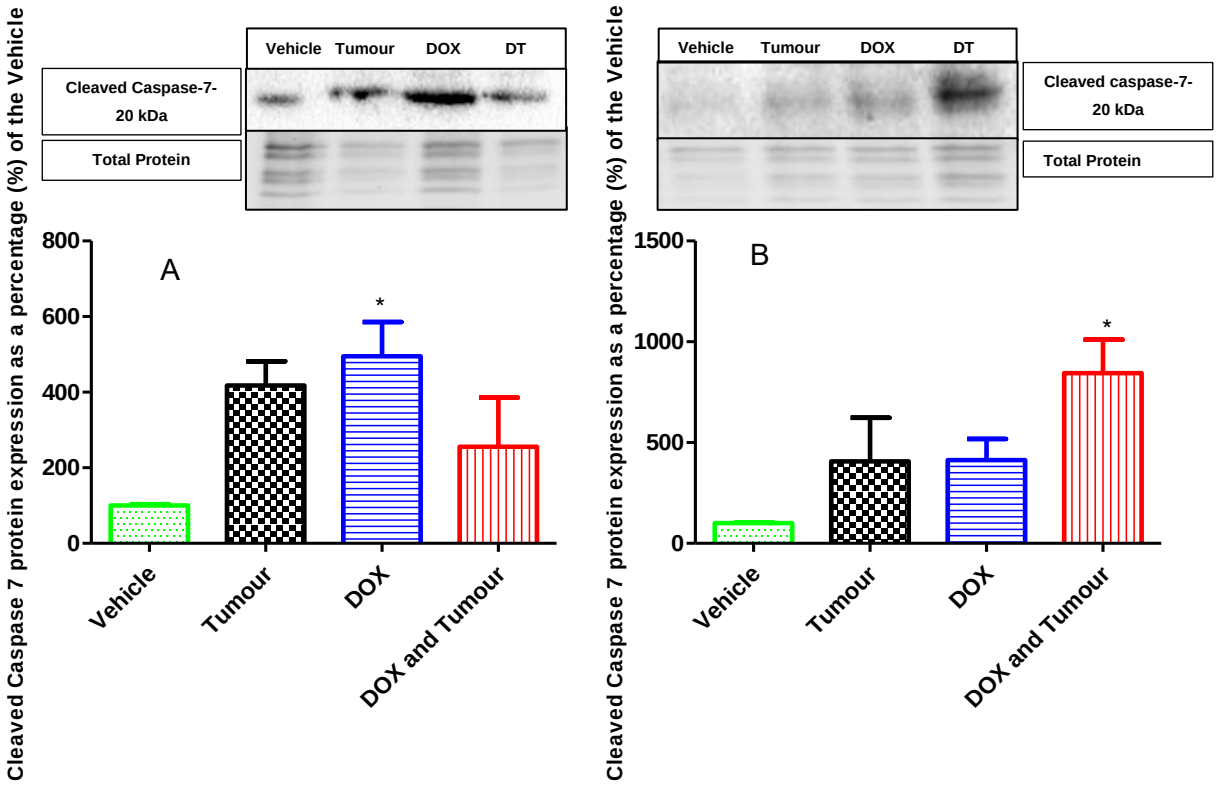


**Figure 3.18: Protein expression of Cleaved Caspase-7 within the cytosolic component following four (A) and eight (B) weeks of treatment.**

Female Sprague-Dawley rats were randomly divided into four groups, and subjected to various treatment protocols over the course of four and eight weeks. Animals inoculated with LA7 cells exhibited mammary gland tumours and animals in the DOX groups were treated with 2.5 mg/kg DOX for four (**A**) and eight (**B**) weeks (cumulative dose: 10 and 20 mg/kg). Protein expression was evaluated in cardiac tissue samples via western blotting. Data was normalized to total protein and results are presented as mean ± SEM (n = 3 - 5), *p<0.05 vs Vehicle Control. Abbreviations: **DOX** – Doxorubicin, **DT** – DOX and Tumour.

Intriguingly, by the eight week time-point, cleaved caspase-7 expression was only significantly upregulated in DOX-treated tumour-bearing animals (844.10 ± 166.21%, $p < 0.05$) compared to the vehicle controls (100.00 ± 3.76%) **(Figure 3.18B)**.

Caspase-3 and -7 activation leads to downstream cleavage of poly(ADP)ribose polymerase (PARP) which depletes ATP in order to repair damaged DNA; a process which results in cell lysis and death (Jing *et al*., 2018). Caspase-3, PARP and their

cleaved fragments were also assessed and results are presented in APPENDIX A: SUPPLEMENTARY RESULTS, pg. 113, where the only protein significantly upregulated was caspase-3 in the DOX (165.1 ± 18.82%) and the combination (169.1 ± 8.77%) groups compared to the vehicle controls (100.0 ± 2.67%) at 4 weeks.

### 3.9.2. Myosin Light Chain (Cardiac isoform)

Myosin light chain-2 (MLC-2) exists as three (3) isoforms. These isoforms are the skeletal fast-twitch isoform (MLC-2f), the cardiac atrial isoform (MLC-2a) and the cardiac ventricular and slow-twitch isoform (MLC-2v). Of these three, the cardiac ventricular isoform (MLC-2v) is most relevant to this context. This isoform is regulatory in nature and is a critical component of the contractile machinery in cardiac muscle (Haase *et al*., 2002; Bunney *et al*., 2017).

In the four week groups, MLC-2v expression was significantly upregulated in the DOX-treated tumour bearing animals (624.10 ± 100.40%, $p < 0.001$) compared to the vehicle controls (100.00 ± 2.27%), the tumour group (183.10 ± 21.29%) and the DOX group (162.60 ± 53.07%) (**Figure 3.19A**).

Similar patterns were observed in the 8-week model, where DOX-treated tumour-bearing animals demonstrated significantly upregulated MLC-2v protein expression (406.90± 47.18%, $p < 0.01$) compared to the vehicle (100.00 ± 3.12%), Tumour (144.30 ± 52.87%) and the DOX group (131.30 ± 44.26%) (**Figure 3.19B).**

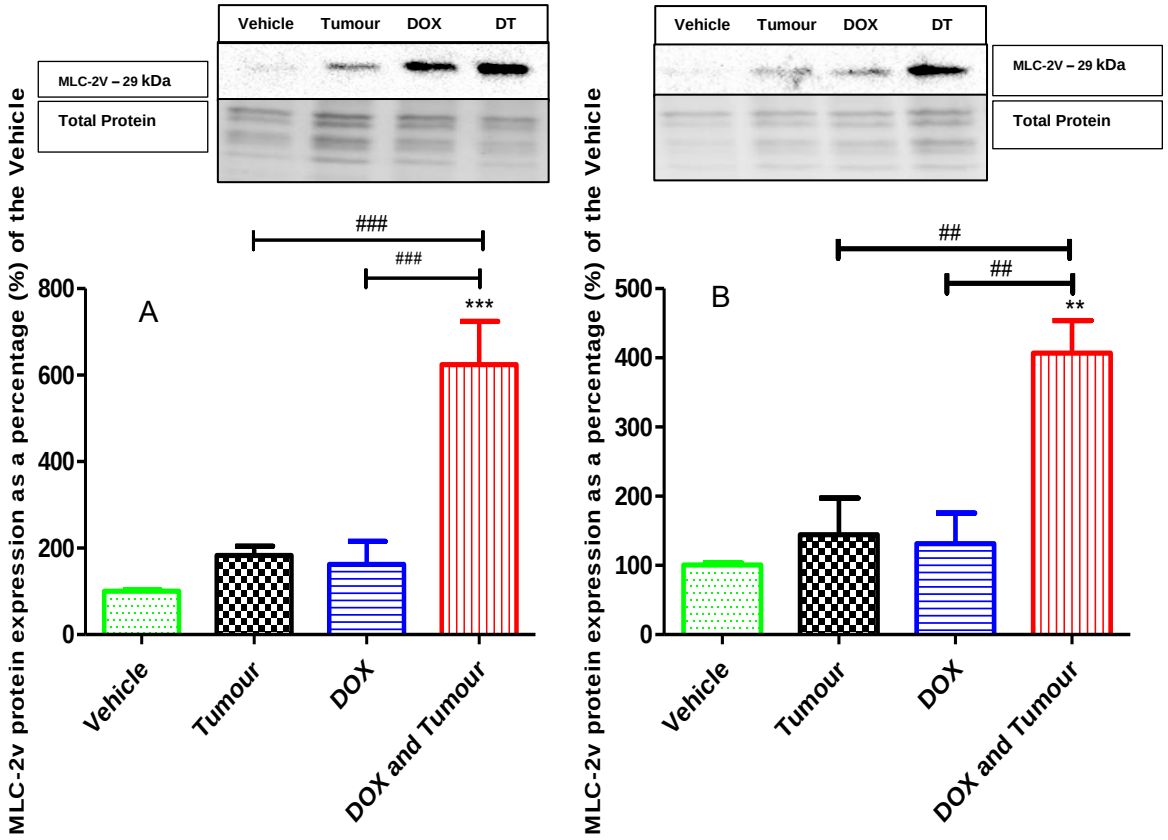


**Figure 3.19: Protein expression of MLC-2v within the cytosolic component following four (A) and eight (B) weeks of treatment.**

Female Sprague-Dawley rats were randomly divided into four groups, and subjected to various treatment protocols over the course of four and eight weeks. Animals inoculated with LA7 cells exhibited mammary gland tumours and animals in the DOX groups were treated with 2.5 mg/kg DOX for four (**A**) and eight (**B**) weeks (cumulative dose: 10 and 20 mg/kg). Protein expression was evaluated in cardiac tissue samples via western blotting. Data was normalized to total protein and results are presented as mean ± SEM (n = 3 - 5). (**A**) ***p<0.001 vs Vehicle control, ###p<0.001 vs DOX and Tumour. (**B**) **p<0.01 vs Vehicle control, ##p<0.01 vs DOX and Tumour. Abbreviations: **DOX** – Doxorubicin, **DT** – DOX and Tumour, **MLC-2v** - Myosin light chain 2.

### 3.9.3. RhoA

Ras homolog family member A (RhoA) is a protein which is important for normal embryogenesis and is generally highly upregulated during early heart development (KaarbØ *et al*., 2003). It is targeted by miR-133a in the process of cardiac remodelling (Care *et al*., 2007; Villar *et al*., 2011).This study observed an increase in RhoA in the combination group (119.20 ± 7.74%, $p < 0.05$) compared to the tumour group (67.39 ± 10.38%) at four weeks. By eight weeks, RhoA was significantly upregulated in the combination group (335.10 ± 49.98%) compared to the DOX

(164.6 ± 26.44%, p < 0.05), Tumour (149.50 ± 21.54%, p < 0.01) and Vehicle control groups (100.00 ± 4.16%, p < 0.001)

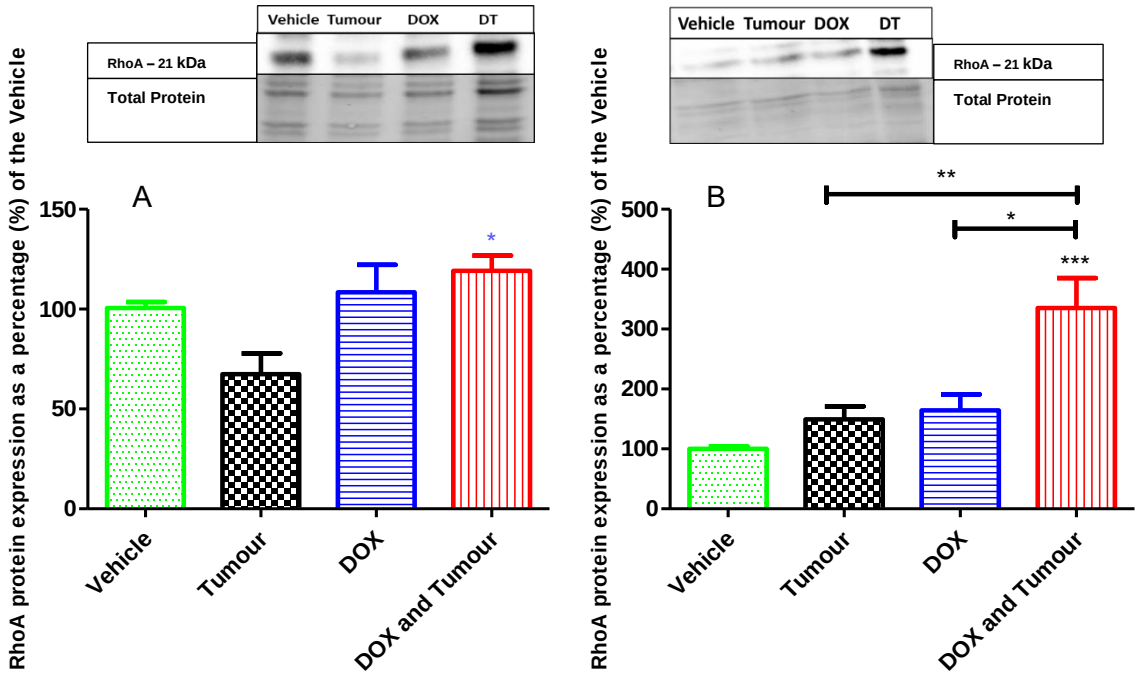


**Figure 3.20: Protein expression of RhoA within the cytosolic component following four (A) and eight (B) weeks of treatment.**

Female Sprague-Dawley rats were randomly divided into four groups, and subjected to various treatment protocols over the course of four and eight weeks. Animals inoculated with LA7 cells exhibited mammary gland tumours and animals in the DOX groups were treated with 2.5 mg/kg DOX for four (**A**) and eight (**B**) weeks (cumulative dose: 10 and 20 mg/kg). Protein expression was evaluated in cardiac tissue samples via western blotting. Data was normalized to total protein and results are presented as mean ± SEM (n = 3 - 5). (**A**) *p<0.05 vs Tumour, (**B**) ***p<0.001 vs Vehicle control, **p<0.01 vs Tumour, *p<0.05 vs DOX. Abbreviations: **DOX** – Doxorubicin, **DT** – DOX and Tumour, **RhoA** – Ras homolog family member A.

# Chapter 4. DISCUSSION

Although significant strides have been undertaken in the management and treatment of cancer, progress to date has been overwhelmed by a number of significant obstacles. Numerous complications and side-effects of the major treatment strategies have been encountered (Hortobagyi, 1997). Of these, complications contributing towards the development of CVDs, including HF are the most relevant, owing to their significant impact towards the morbidity and mortality of cancer survivors (Ky *et al.,* 2013). Intense research towards the elucidation of the contributing mechanisms behind such complications revealed that chemotherapeutic regimens, particularly anthracyclines utilized in the management of breast cancers, presented with cardiotoxic characteristics (Minotti *et al.*, 1999). As such, the concept of anthracycline-induced cardiotoxicity was born. With the persistent nature of these cardiotoxic effects, investigations aimed at understanding the underlying mechanisms identified a number of pathways believed to be involved in the initiation and progression of this pathology. Numerous studies have demonstrated that prolonged oxidative stress, apoptosis and mitochondrial dysfunction are most evidentt in this scenario (Minotti, 2004; Simunek *et* al., 2009; Sishi *et al*., 2013a; Xu *et al*., 2005). Taking these into consideration, the development of numerous intervention and management strategies were embarked upon within the field of cardio-oncology, to limited benefit. Anti-oxidant-based adjuvant therapies have, to a large extent, failed in the clinical setting (Van Dalen *et al*., 2005; D'Andrea, 2005). Other strategies have been beset with complications including the development of secondary malignancies (Choi *et al*., 2010; Lipshultz *et al*., 2010).

It is in light of this that this study embarked on a multi-pronged approach aimed at both identifying early markers of myocardial damage in an effort to gain an overview of the mechanisms which govern cardiotoxicity, and testing the model of chronic cardiotoxicity to determine if previously utilized approaches have been characterized by fundamental flaws.

## 4.1. LA7 epithelial tumour cell model successfully induced mammary tumours

One of the major challenges often encountered in oncological research is the replication of tumours in pre-clinical experimental models. Methods such as the utilization of immuno-deficient mice, for transplantation and xenograft inductions, have proven to not only be expensive but inconvenient and complicated to execute as well (Kim *et al*., 2006). Other approaches, such as the use of carcinogens, are complex, dangerous and time-consuming (Salami & Karami, 2003). In contrast, the challenge with models of cardiotoxicity, include the inconsistency of dosing regimens that are clinically relevant, as well as the difficulty to simulate cardiotoxicity *in vitro* or *in vivo* due to the classification of cardiotoxicity. For example, early anthracycline-induced cardiotoxicity takes place while a patient is under treatment for cancer (Simunek *et al*., 2009). In other words, the cancer is still present. However, chronic anthracycline-induced cardiotoxicity can take place long after a patient has completed treatment and is in remission (Curigliano *et al*., 2012). The advantage of having cancer present in such a model is that the potential effects that cancer, independent of treatment, may have on the heart is also taken into consideration. This important aspect has remained neglected in this field of research.

Considering that chronic anthracycline-induced cardiotoxicity is the most detrimental, the tumour-bearing experimental model utilized in this study was developed with reference to previously executed models (Abbasalipourkabir *et al*., 2010; Govender, 2017). Both studies utilized the LA7 mammary epithelial tumour cell line to achieve mammary tumours in Sprague-Dawley rats; however the time in which the tumours became palpable took seven to ten days. The present study adapted the cell culture conditions (APPENDIX B: CELL CULTURE, pg. 121) and inoculation technique (APPENDIX C: TUMOUR INNOCULATION, pg.125); in a manner that enabled this study to achieve palpable tumours within two (2) days post-inoculation (**Figure 3.1**). Peak tumour volumes in untreated animals were ±2500 $mm^3$ by the second week, which was also considerably higher than the aforementioned models. In addition to these, tumours persisted for an extended period of time than was reported by Govender (2017). It is noteworthy that the tumours induced in this study were not maintained for the duration of the treatment. The reasons for this have not been

completely elucidated; however, literature indicates that tumours in animal models could regress due to immune activation (Baldwin, 1955) or restoration of p53 function (Ventura *et al*., 2007). Either of these reasons could be responsible for the regression observed within these LA7 cell-derived tumours, which has also been reported in literature (Rani *et al*., 2014). This study had a few considerations to take into account in the development of the present model:

I. Chronic cardiotoxicity primarily develops during or post-recovery from tumours.
II. Animals are a precious resource, and the possible risk of death or excessive discomfort due to the tumours needed to be mitigated.

For these reasons, the present study needed to find a compromise that sufficiently replicated the necessary conditions, whilst mitigating the above-listed obstacles. The tumour model utilized was most compatible to the study since it ensured that the tumours were not present by the end of the study; and as the animals could recover independent of treatment, the risk of inadvertent loss of animal life due to sickness or for humane reasons was mitigated.

DOX was used as the chemotherapeutic agent of choice in this study as it is considered the most potent of all anthracyclines and is used as a first-line treatment strategy for breast cancer patients (Ky *et al*., 2014). To induce early and late chronic cardiotoxicity, which could manifest during therapy or up to months or years after chemotherapy has been completed, clinically relevant low doses (2.5 mg/kg = ± 60 - 75 kg/m$^2$) were used over a four- and eight-week period, which is in contrast to other studies utilizing supra-physiological doses over an acute period (Nigris *et al*., 2008; Ichikawa *et al.,* 2014), but in agreement with similar chronic models of DOX cardiotoxicity (Xiang *et al*., 2009; Desai *et al*., 2013; Zhu *et al*., 2017) (

**Table 4.**1).

**Table 4.1. Various approaches utilized in literature to simulate DOX-induced cardiotoxicity.**

| Study | Model | Treatment | Duration |
|---|---|---|---|
| **Kang *et al* ., 1996** | Acute, Both, Mice | 20 mg/kg (once-off) | 4 days |

| | | | |
|---|---|---|---|
| **Nigris *et al*., 2008** | Acute, Male, Rats | 18 mg/kg (daily) | 12 days |
| **Zordoky *et al*., 2011** | Acute, Male, Rats | 15 mg/kg (once-off) | 6, 24 hrs |
| **Sauter *et al*., 2011** | Acute, Male, Mice | 75 mg/m$^2$ (once-off) | 16 hrs |
| **Sishi *et al*., 2013a** | Acute, Female, Mice | 20 mg/kg (split into 2 injections in 3 days) | 45 days (15 days after treatment started) |
| **Ichikawa *et al*., 2014** | Acute, Male, Mice | 30 mg/kg, 24 mg/kg (3, 4 injections) | 5, 10 days |
| **Cheung *et al*., 2015** | Acute, Female, Mice | 8 mg/kg (weekly) | 4 weeks |
| **Xiang *et al*., 2009** | Chronic, Male, rats | 2.5 mg/kg (weekly) | 6 weeks |
| **Desai *et al*., 2013** | Chronic, Male, Mice | 3 mg/kg (weekly) | 4,6,8,10,12 and 14 weeks |
| **Desai *et al*., 2014** | Chronic, Male, Mice | 3 mg/kg (weekly) | 2,3,4,6 and 8 weeks |
| **Zhu *et al.,* 2017** | Chronic, Male, Rats | 2 mg/kg (bi-weekly) | 4, 8 weeks |

This study was able to confirm cardiac damage indicated by increased expression of plasma cTNT within the combination group and reduced total CK-MB expression within tissue (**Figure 3.10**). It should be noted that whilst this model utilizes a chronic treatment schedule, the early time point selected for this study (4 weeks) has been reported to be sufficient for studies on early biomarkers of chronic cardiotoxicity (Desai *et* al., 2013; Desai *et al.,* 2014). Although both cancer and cardiotoxicity share the characteristics of inflammation and oxidative stress, a burden of all diseases of life-style, minimal side effects with regards to weight and well-being of the animals was observed (**Figure 1.1**). Therefore, we believe that all considerations were taken in account to develop an appropriate experimental model with reasonable limitations to fulfil our hypothesis, aims and objectives set out for this study.

## 4.2. Tumour presence exerts effects unaccounted for in current models of cardiotoxicity.

Current models utilized to study the aetiology of cardiotoxicity are designed upon the premise that its deleterious side-effects are induced specifically by chemotherapeutic interventions undertaken, independent of tumours being treated. It is common knowledge that cachexia is a regularly occurring adverse effect induced by the

presence of cancer. It is defined as a “multifactorial syndrome characterized by an ongoing loss of skeletal muscle mass that cannot be fully reversed by conventional nutritional support and leads to progressive functional impairment” (Fearon *et al*., 2011). It is a characteristic widely observed in patients of pancreatic or gastric cancers (Tisdale, 2009). Its molecular mechanisms of action have been reported to include numerous pathways including systemic inflammation, side-effects due to chemotherapeutic treatment, miRNAs and exosomal transport of miRNAs (Argiles *et al*., 2019).

With the above in mind, it was expected that the typical weight loss associated with cancer cachexia would be observed. However, this was not the case, as instead, DOX treatment significantly limited the weight gained after four weeks and eight weeks of treatment (**Figure 3.4**, **Figure 3.6**). In support of our results, Kihara *et al*., (2016) demonstrated similar observations in a model investigating the protective effects of Ghrelin in acute DOX-induced cardiotoxicity. Interestingly, the tumour-bearing animals consistently demonstrated increase in weight gain superior to the other groups as observed in **Figure 3.6**, whilst the tumour-bearing animals treated with DOX exhibited significantly elevated weight gain per week compared to the non-tumour bearing animals subjected to DOX treatment. These results indicated that although DOX negatively affects weight gain, the presence of the mammary tumour paradoxically improved this effect in these animals. At surface level, this result is contradictory, as there is a reasonable expectation that the cachexia associated with cancer would compound the reduction in weight gain experienced in the DOX-treated animals. However, literature has reported that patients diagnosed with breast cancers, sarcomas and acute non-lymphocytic leukaemia present with a lower frequency of weight loss (Tisdale, 2009). In fact, research from as early as the late 1990’s revealed that in cases of breast cancer, weight gain rather than weight loss is the more frequently observed side effect (Demark-Wahnefried *et al*., 1997; Rock *et al*., 1999; Kroenke *et al*., 2005).

Whilst numerous reasons for this observation have been speculated; the more concrete postulations have involved the treatment regimens utilized (Demark-Wahnefried *et al.*, 1997; Kroenke *et al*., 2005). However, the most reasonable explanation does not involve these treatment regimens, but the disease itself. As such, Demark-Wahnefried *et al*., (1997) inferred that weight gain results in

psychological effects that are influenced by different factors. These factors include a shift in metabolic status due to fatigue and reduced physical activity as a result of the cancer (Rock *et al*., 1999; Kroenke *et al*., 2005). Whilst the resulting psychological effects in the animals can only be confirmed with a purpose-designed model, the weight gained in the tumour-bearing animals was likely due to fatigue and reduced physical activity. This finding presents a significant oversight to current preclinical models of cancer, as it reveals that whereas current models report a reduction in weight gain and weight loss due to DOX treatment, a more accurate representation would involve less severe effects on animal weight due to weight gain induced by the presence of a mammary tumour.

## 4.3. Plausible mechanism through which tumour presence influences Cardiac homeostasis

As previously mentioned, the field of cardio-oncology has largely focused on the toxic effects of chemotherapeutic interventions. The present study postulated that the presence of a tumour may possibly influence the molecular mechanisms and the pathology resulting from the interaction between DOX and the myocardium. While our results appear to support this hypothesis, due to differential expression of critical proteins in the DOX control versus the tumour-bearing DOX treated animals (**Sections 3.8 & 3.9**), the mechanism through which the presence of a tumour may affect the myocardium and its interactions with cardiotoxic interventions remains unclear. Studies have established that cancer cells specifically possess the ability to induce the migration of monocytes to tumour sites to form tumour-associated macrophages (TAMs). This process is facilitated by monocyte chemo-attractant proteins such as chemokine ligand (CCL)-2 and CCL5 expressed by breast tumour cells. These TAMs subsequently secrete cytokines, such as tumour necrosis factor alpha (TNF-α) (Sirotkovic-skerlev *et al*., 2006), a 26 kDa protein that possesses a soluble 17 kDa fragment which is regarded as an endogenous regulator of inflammation (Bradham *et al*., 2002). Demonstrated to promote breast cancer cell migration and the development of mammary tumours (Wolczyk *et al*., 2016; Cai *et al*., 2017); TNF-α is reported to be the most important mediator of cardiovascular diseases because of its association with myocardial remodelling and the induction of

cardiac depression due to the promotion of apoptosis in cardiomyocytes (Bradham *et al*., 2002; Saini *et al*., 2005).

Considering that female rats were utilized in this study, the role of estrogen in this context cannot be ignored, since TNF-α has been demonstrated to influence local estrogen biosynthesis. Recently, Kamel *et al*., (2012) showed that an altered rate and pattern of estrogen metabolites regulates critical genes and enzymes that govern estrogen metabolism. It is common knowledge that estrogen is cardioprotective (Subbiah, 2002), and as such, the relationship between TNF-α and breast cancer cells, needs to be better understood. Considering that TNF-α-linked estrogen metabolism can directly influence the myocardium via inflammation, and DOX has been linked with increased expression of inflammatory markers, specifically including TNF-α in both serum (Sauter *et al*., 2011) and the liver (Zordoky *et al*., 2011); this could be the missing link connecting the presence of mammary gland tumours to cardiac dysfunction within the context of DOX-induced cardiotoxicity. This is because an already compromised heart would be more susceptible to damage induced by DOX.

## 4.4. Targeting MiRNAs

As endogenous regulators of gene expression, miRNAs have been proven to be critical regulators of the majority of physiological processes (Li *et al*., 2014). Though little is known about the expression patterns of these small RNA molecules with regards to the cardiotoxic assault of DOX on the myocardium within the current context, various miRNAs have been demonstrated to be present in endothelial cells, cardiac exosomes and the pericardial fluid. Only a handful of these have been identified as markers of HF (Kuosmanen *et al*., 2015). Since some of these tissue-specific miRNAs can be detected in plasma due to their packaging in exosomes, endogenous miRNAs have been demonstrated to be especially stable in this biological fluid compared to exogenous miRNAs (Mitchell *et al*., 2008; Coenan-Stass *et al*., 2019). As a result of these characteristics, detection of these small RNA molecules makes them very plausible biomarkers of damage, unlike previously established molecules

## 4.5. miR-208a and miR-133a have the potential to serve as markers for the activation of the foetal genes governing cardiac hypertrophy

Regarded as one of the hallmark characteristics of cardiomyopathy, the development of cardiac hypertrophy is usually compensatory in its initial stages, however, it becomes pathological over time. Cardiac remodelling is primarily regarded as a protective response to the reduction of contractile efficacy due to acute or sustained stress (Mckinsey *et al*., 2005). During foetal development, cardiac growth is characterized by cardiomyocyte proliferation; however, cardiac hypertrophy induced by toxic insults is also induced by the reactivation of similar foetal cardiac genes. In this case, cardiac hypertrophy is characterized by an increase in cardiomyocyte size without the proliferation (Dorn II, 2011). It is accompanied by ventricular wall thickening, serial assembly of the sarcomere and myocyte apoptosis (Mckinsey *et al*., 2005). Van Rooij *et al*., (2006) reported that prolonged cardiac hypertrophy may possibly serve as a predictor for HF and sudden death. The compensatory mechanisms that govern this process become detrimental in the long run, and thus contribute to the development of HF (Cheung *et al*., 2015).

Left ventricular hypertrophy is a commonly reported side effect in patients that have previously been treated with DOX. Not only has this been described in early literature when DOX side effects were initially discovered (Bristow *et al*., 1978), more recent literature attests to the fact that left ventricular hypertrophy is a clinically relevant event that takes place during cardiotoxicity and the progression towards heart failure (Curigliano *et al*., 2012; Zordoky *et al*., 2010; Angsutararux *et al*., 2015).

Our analysis of the ratio between cardiac mass and body mass revealed no significant differences between the different groups at both time points (**Table 3.1**), suggesting that no hypertrophy took place as a result of the different treatment regimens. This study thus further investigated the molecular mechanisms associated with cardiac hypertrophy. At the molecular level, the genes that are associated with regulation of cardiac hypertrophy include ventricular myosin light chain-2 (MLC-2v), alpha-myosin heavy chain (α-MHC) and atrial natriuretic peptide (ANP) (Karagiannis *et al*., 2010). MLC-2v functions are mainly regulatory in nature, and its

phosphorylation by the cardiac myosin light chain kinase has been demonstrated to be crucial for heart function (Chang *et al*., 2016). Selective loss of MLC-2v phosphorylation results in contractile dysfunction, ventricular hypertrophy, necrosis and fibrosis (Ding *et al.,* 2010; Bunney *et al*., 2017).

It was observed in this study that tumour-bearing animals treated with DOX presented with significantly elevated levels of MLC-2v within the myocardial tissue at both time points evaluated (**Figure 3.19A**, **Figure 3.19B**). These results demonstrate that from as early as four weeks, DOX stimulates adverse molecular events within cardiac tissue in the presence of a tumour. Similar observations have been reported by others (Karagiannis *et al*., 2010), where DOX induced a dose-dependent increase in MLC-2v in differentiated H9C2 cardiomyocytes, albeit within the acute setting. Interestingly, in our model of cardiotoxicity, DOX treatment alone was not sufficient to induce significant upregulation of this protein as these alterations were only established in the groups that had tumours and were treated with DOX.

While the physical appearance and the weight of the myocardium indicated the absence of cardiac hypertrophy, this result was insufficient to confirm cardiac hypertrophy. Since the upregulation of MCL-2v has been demonstrated to be a specific feature of other cardiomyopathies (Haase *et al*., 2002), it becomes likely that the upregulation of this protein as demonstrated in our model is significant to this context. We thus postulate that MLC-2v upregulation observed in the DOX-treated tumour bearing animals is indicative of the activation of foetal cardiac genes responsible for the induction of the cardiac hypertrophic pathways.

Interestingly, literature has indicated that both miR-208a and miR-133a have been associated with cardiac hypertrophy induction. Our results revealed considerable downregulation of miR-208a after eight weeks of treatment (**Figure 3.11**), in contrast to the upregulation of miR-133a after four weeks in the DOX -treated tumour bearing group (**Figure 3.12A**). Mutant miR-208a animals are reportedly more resistant to cardiac hypertrophy due to the inhibition of cardiac myosin proteins, particularly the inhibition of beta-myosin heavy chain (β-MHC) (Van Rooij *et al*., 2007).It was therefore concluded that miR-208a is essential for β-MHC upregulation and downstream cardiac remodelling.

Specific miRNAs can be selected for export from cells. These miRNAs are typically packed into cell-derived vesicles, and exported from the cell into circulation, where they retain their stability due to the simultaneous release of RNA-binding proteins which protect them from degradation (Wang *et* al., 2010). The relationship between circulating and organ-specific miRNA expression levels has puzzled scientists. However, Pigati *et al*. (2010) noted that within cells, there is a differential relationship between the release and retention of miRNA. The aforementioned study observed that depending on physiological conditions, specific miRNAs are released more abundantly than they are retained within cells; giving meaning to observations made by Sempere *et al,* who in 2007, observed low expression of miR-451 in mammary epithelia accompanied by enriched expression of the same miRNA interstitially. Since we observed reduced expression of miR-208a within the plasma of the DOX-treated animals, we postulate that the myocardium of these animals have a higher propensity towards hypertrophy due to likely increased retention of this miRNA within this organ. This increase in myocardial miR-208a was also reported in a review by Ruggeri *et al*., (2018).

Higher expression levels of miR-208a within the plasma of the vehicle groups indicate that under normal conditions, this miRNA is constitutively exported into plasma. Reduced miR-208a release into plasma may be a compensatory response of the stressed heart; and as such this makes this miRNA a plausible marker of cardiac hypertrophy during chronic DOX-induced cardiotoxicity. Its potential as a marker of cardiotoxic damage is debatable, considering the undetectable levels of this miRNA after four weeks of treatment. A comparison between baseline miRNA levels obtained prior to the commencement of treatment and subsequent fluctuations of miR-208a levels within plasma post treatment, could be indicative of a propensity towards cardiac hypertrophy, since Ji *et al*., (2009) determined that miR-208a is almost exclusively produced in the heart and could leak out of cardiomyocytes, into circulating blood.

As previously mentioned, the present study demonstrated an increase in the expression profile of miR-133a within the plasma of DOX-treated tumour bearing animals only after four weeks (**Figure 3.12**). In a study by Care *et al*., (2007), an inverse relationship between miR-133 and myocardial hypertrophy was established. The over-expression of this miRNA was established to inhibit an increase in

cardiomyocyte size, by targeting the protein RhoA. A protein abundantly expressed during early cardiac development (Kaarbø *et al*., 2003), it is also a known inducer of hypertrophic growth factors such as angiotensin II via its downstream target Rho kinase (RhoK) (Shimokawa & Takeshita, 2005; Chau *et al*., 2011). In contrast, others have provided evidence that in patients suffering from acute myocardial infarction, an increased tissue expression of miR-133a is observed (Devaux *et al*., 2015). Since miR-133a in this study was detected in the plasma, we propose that there is less retention of this miRNA in the heart. This then suggests that the release of miR-133a into the plasma is indicative of myocardial damage and the potential stimulation of hypertrophic growth factors *via* RhoA; which this study demonstrated to be upregulated in the combination groups (**Figure 3.20**). This study observed no significant differences in miR-133b expression between the groups. Whilst similar to miR-133a, miR-133b is not a cardiac specific miRNA, and this is the likely reason for the lack of observable differences in its expression.

## 4.6. miR-29b could serve as a late marker for DOX-cardiotoxicity induced myocardial fibrosis

Myocardial fibrosis, characterized by excessive deposition of collagen fibres, has been associated with a plethora of CVDs (Picano *et al*., 2011). This accumulation of fibrotic tissue disrupts normal morphology, leading to increased mechanical stiffness, culminating in contractile dysfunction (Kuosmanen *et al*., 2015). Within the current context, this study demonstrated augmented fibrosis as a result of DOX treatment **(Figure 3.9**). These results are consistent with the observations reported by Renu *et al.* in 2018.

Moreover, miR-208a and miR-29b have been associated with the development and maintenance of fibrosis. On the one hand, Van Rooij *et al*., (2007) reported that the genetic deletion of miR-208a resulted in reduced cardiac hypertrophy and fibrosis. On the other hand, Divakaran & Mann, (2008) stated that the dynamic regulation of miR-29b contributes to the development and progression of fibrosis. The latter study also observed that the downregulation of miR-29b caused increased collagen deposition. In agreement with these observations, studies by Small and colleagues

(2010) indicated that miR-29b possesses a high propensity to target genes involved in fibrosis such as collagen, fibrillins and elastin. With regards to the results obtained in this study, we demonstrated that the elevated expression profile of miR-29b was time-dependent and treatment-dependent (**Figure 3.13**). Our finding that miR-29b was upregulated in the plasma of DOX-treated tumour bearing animals after eight weeks suggests that this miRNA is released from the myocardium during a cardiotoxic insult, and this export is mediated via exosomal transport into circulation (Mitchell *et al*., 2008). The export into circulation indicates reduced retention of miR-29b within the myocardium, which agrees with Jing *et al*., (2018), who established that miR-29b which is perceived as cardioprotective in the cardiovascular context, is downregulated within an acute setting of DOX–induced cardiotoxicity. This would explain the highly significant increase in fibrosis observed in the DOX-treated tumour groups following eight weeks of treatment (**Figure 3.8**).

## 4.7. miR-29b demonstrates potential as a marker for DOX-cardiotoxicity induced apoptosis

Along with fibrosis, myocardial apoptosis is regarded as a downstream consequence of DOX-induced cardiomyopathy, notwithstanding the contribution of other cell death modes such as necrosis and autophagy (Renu *et al*., 2018). Arguably the most influential cell death mechanism within this context, a very apt description of the integral role apoptosis plays within this context had been excellently conveyed in the review by Renu *et al*., (2018) (**Figure 4.1**) along with many others who have demonstrated apoptotic influence during DOX-induced cardiotoxicity (Minotti *et al*., 1999; Minotti, 2004; Suter & Ewer, 2013; Green & Leeuwenburgh, 2002). It should be noted that this study attempted to simulate the chronic form of cardiotoxicity which is associated with myocardial apoptosis. The acute form of this pathology has been associated with myocardial dysfunction, hence is considered to be reversible (Volkova & Russel, 2011).

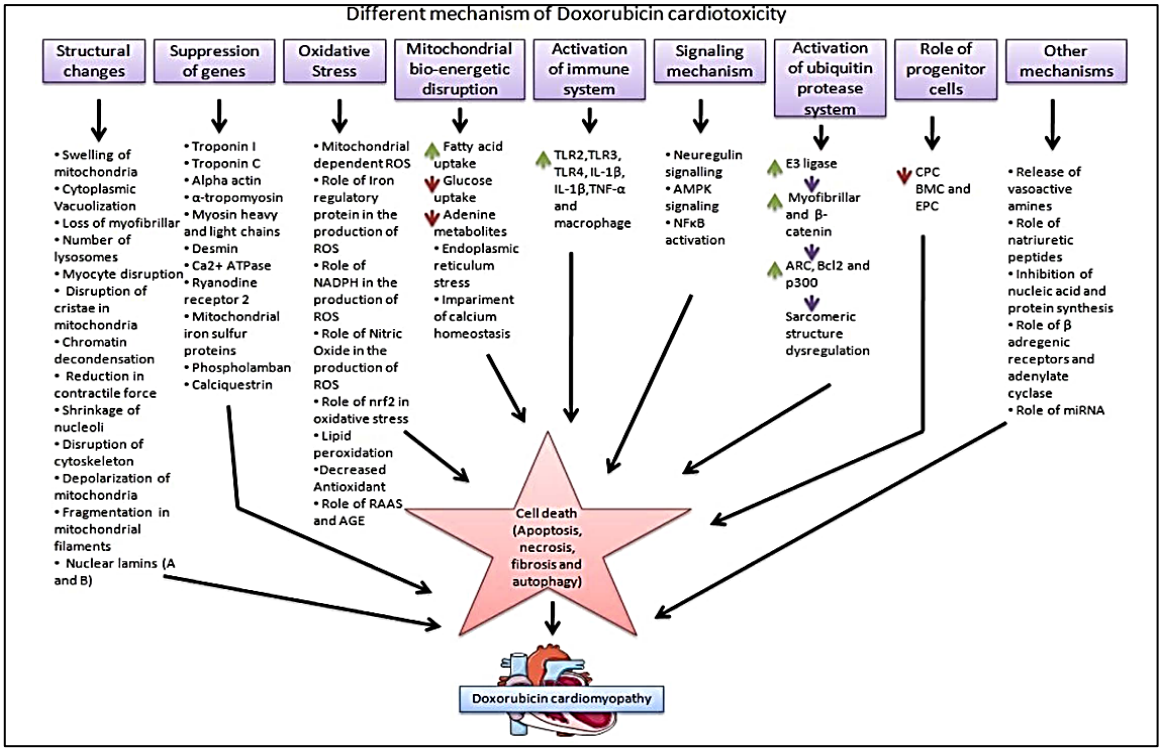


**Figure 4.1: Diagram demonstrating the various mechanisms of DOX-induced cardiotoxicity that culminates in apoptosis induction (Renu *et al*., 2018).**

It has since been proposed that inhibition of apoptotic events could be an effective approach in preventing DOX-induced cardiotoxicity (Jing *et al*., 2018). As such, exploring the relationship between miRNA expression and their role in apoptosis induction within this context of chronic DOX-induced cardiotoxicity was of utmost importance. The implication of the SOD2 upregulation observed by the present study in the DOX-only treated animals after eight weeks (**Figure 3.15**) is a compensatory reaction, providing an enhanced capacity to manage ROS-induced damage. Considering that this upregulation was not replicated in the DOX-treated tumour-bearing animals, it is evident that the animals in this group remained vulnerable to oxidative stress and downstream apoptosis. Our experimental approach demonstrated elevated levels of caspase-7; an effector caspase within the apoptotic cascade (**Figure 3.17B**), along with its cleaved form (**Figure 3.18B**) after eight weeks of treatment in DOX-treated tumour-bearing animals. Considering that neither DOX-treatment alone nor the presence of a tumour alone induced changes in total caspase-7, it was interesting to observe a substantial increase in cleaved caspase-7 in the DOX and Tumour group following eight weeks of treatment.

The novelty of this finding has to be emphasised, as numerous studies have demonstrated increased apoptosis within acute models of cardiotoxicity (Green & Leeuwenburgh, 2002; Arola *et al*., 2000). This study demonstrated that DOX alone may not necessarily be sufficient to induce significant activation of apoptotic pathways within the chronic context.

In an effort to strengthen the results of the current study, we investigated the protein expression of Dynamin-related protein 1 (DRP1) in the cytosolic and mitochondrial fractions, considering that upon mitochondrial membrane depolarization, DRP1 is recruited to the mitochondrial membrane to induce mitochondrial fission (Smirnova *et al*., 1998; Cleland & Youle 2017), which ultimately results in intrinsic apoptosis induction via cytochrome c leakage. DRP1 protein expression remained unchanged in the mitochondrial component of the myocardial tissue across all groups (**Table 3.2**), the cytosolic fraction presented with substantially elevated expression levels of this protein in the DOX-treated tumour-bearing animals after eight weeks (**Figure 3.16**). During apoptosis, cytosolic DRP1 and pro-apoptotic Bax translocate to the outer mitochondrial membrane, where DRP1 co-localizes with the mitochondrial fission factor (MFF) to induce mitochondrial fission (Frank *et al*., 2001; Morciano *et al*., 2016; Marin-Gracia *et al*., 2013). While regulated levels of DRP1 and mitochondrial fission are important for mitochondrial and cellular homeostasis, in this context, its role would be pro-apoptotic and hence deleterious. Our finding of significantly increased cytosolic DRP1 levels in DOX-treated tumour-bearing animals indicates an upregulation of DRP1 transcription. This is likely as a result of the initiation of the mitochondrial apoptotic pathway, which results in cytochrome c leakage, subsequent activation of activator caspases and effector caspases such as caspase-7 (Suzuki *et al*., 2001).

miR-29b has previously been demonstrated to inhibit DOX-induced apoptosis within the acute context (Jing *et al*., 2018). Its role in preventing this mode of cell death has made this miRNA an attractive target for our study within the context. Considering that this study observed an increase in plasma miR-29b levels in the DOX-treated tumour-bearing animals after eight weeks (**Figure 3.13)**, with an increase in apoptosis induction (**Figure 3.18B**), it initially seems to contrast the results obtained by Jing *et al.,* (2018). Upon further scrutiny however, it was observed that the aforementioned study upregulated miR-29b levels within cardiomyocytes, while the present study

demonstrated its increased expression within plasma. Considering this increase occurred within the same group and time point as was demonstrated to express elevated apoptotic markers, it becomes plausible that miR-29b levels in plasma become elevated either due to one of two reasons: (i) miR-29b release into circulation from the myocardium is context dependent, resulting in lower miR-29b expression within the myocardium; and (ii) miR-29b is increased in circulation as a compensatory reaction to the elevated apoptotic state within the hearts of DOX-treated tumour-bearing subjects. These motivations however can only be justified by an investigation into miR-29b expression within the myocardium within a similar context. Another notable observation was that plasma miR-29b levels increased in the eight-week groups compared to their four-week counterparts. Whilst this could be an artefact induced by the longer storage time for the plasma obtained from the four-week animals, this reasoning is unlikely due to the well-established stability of miRNAs within plasma (Coenan-Stass *et al*., 2019). A more likely reason could be the increased transport out of the myocardium due to ageing, indicating less protection against the natural upregulation of apoptosis within cardiomyocytes associated with ageing (Boon *et al*., 2013; Seeger & Boon, 2016; Xu *et al*., 2013). This could also be responsible for the observation that miR-29b was also released into the plasma of the control animals (**Figure 3.13**). Within the clinical setting, this detection could result in false positive diagnosis, and as such further research into identifying threshold values for the expression of miR-29b determined through a comparison against baseline expression levels within plasma would provide a more suitable method for utilizing this miRNA as a marker for chronic cardiotoxicity.

All these taken into consideration, it becomes evident that miR-29b indeed possesses the potential to be a viable circulating marker for chronic DOX-induced cardiotoxicity. However, its potential as an early marker remains limited.

# Chapter 5. CONCLUSION

Chronic DOX-induced cardiotoxicity is a multi-factorial problem that not only contributes to CVD morbidity and mortality; it also limits chemotherapeutic interventions in oncological settings. As literature has demonstrated, current approaches have focused on acute models of cardiotoxicity, as well as on the oxidative stress theory. These approaches have utilized pre-clinical models which do not take the possible influences of tumour presence into account. Considering the mixed results and often failure of these approaches in the clinical setting, this study intended to unravel this milieu with a novel and overarching approach.

The pre-clinical experimental model utilized in this study identified and implemented principal changes to the models currently being utilized. This study employed an *in vivo* model that attempted to simulate early and late chronic DOX-induced cardiotoxicity in the presence of breast cancer. As a result of this model, we investigated the expression profile of different miRNAs present within plasma for their potential to serve as biomarkers of DOX-induced cardiotoxicity. These relatively novel molecules are acclaimed for their profound influence in the regulation of various physiological and pathological mechanisms, particularly those implicated in the aetiology of DOX-induced cardiotoxicity. This study sought to determine whether these miRNAs are indeed complicit within this context; and if they could be utilized as minimally invasive biomarkers for this condition. The present study also sought to determine if the presence of a tumour within this context presents as a significant confounding factor for previously established models of the disease.

Novel to the context, this study demonstrated that the presence of the tumour attenuated the weight loss associated with DOX-treatment. Tumour presence, in combination with DOX therapy, was also associated with an increase in the expression of apoptotic markers, fibrosis and the expression of foetal cardiac genes implicated in the aetiology of myocardial hypertrophy. Taking these into consideration, it becomes evident that incorporating a tumour model is critical to implementing accurately representative experimental models of chronic DOX-induced cardiotoxicity. miR-29b, miR-208a and miR-133a showed potential as markers of symptoms associated with chronic DOX-induced cardiotoxicity. Of these

miRNAs, miR-208a and miR-133a remain the only miRNAs within this study with potential as early markers for cardiotoxicity as depicted in **Figure 5.1**.

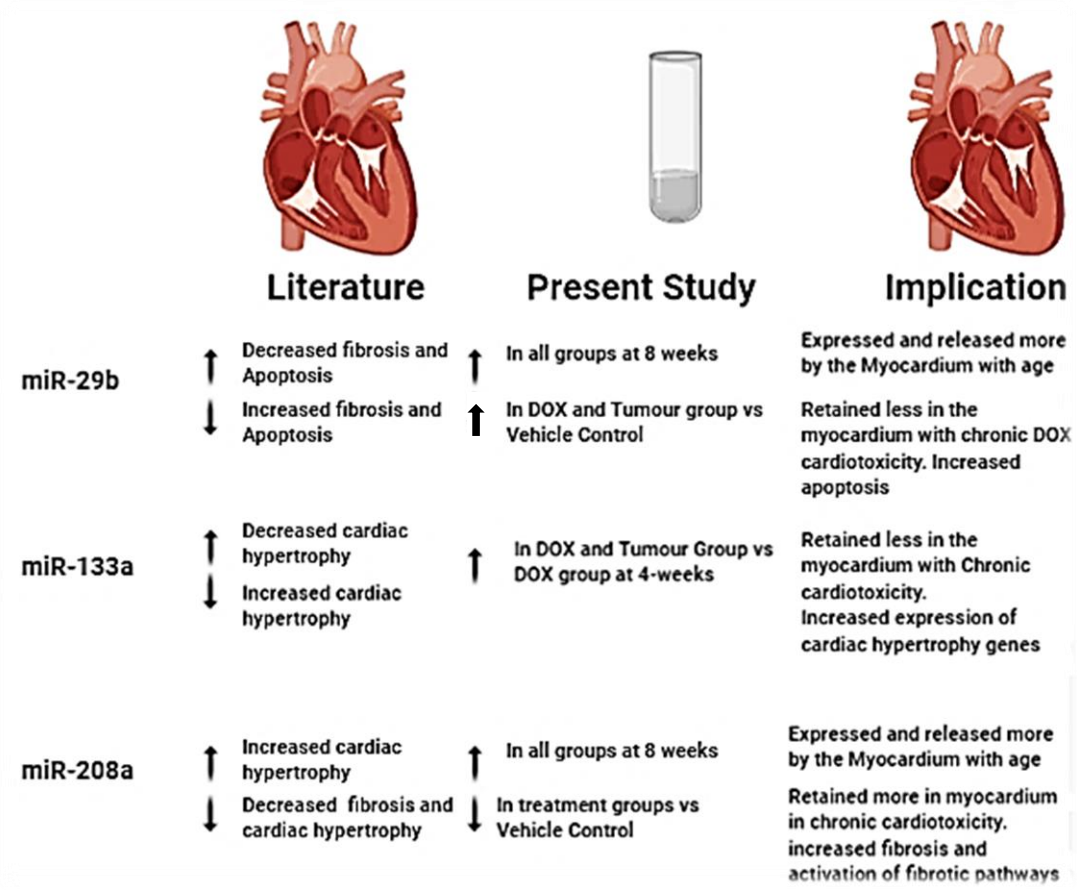


**Figure 5.1: Graphic summary of the conclusions reached by this study.**

All things considered, this study achieved its main aims and objectives and answered its research question; however, it would have been desirable to assess a wider array of miRNAs. A proteomic scale analysis of plasma miRNA was considered, however the very complicated nature of this proteomic analysis as well as the study being limited by financial constraints hindered this option.

It is a really complex task to accurately replicate the features of chronic cardiotoxicity within an animal model due to the complexities of the disease. Apart from increasing the number of animals utilized for the study, the study had to contend with incorporating a tumour model which would last long enough to be significant, without risking the loss of animals. Similarities between acute models and early onset chronic models also presented with a challenge that needed to be navigated. For the future, we recommend an investigation into a wider array of miRNAs, as well as a

comparison between plasma, tissue and exosomal miRNA expression within the context. We observed consistently aberrant liver morphology amongst the DOX-treated animals (*APPENDIX A: SUPPLEMENTARY RESULTS*, pg.113; **Figure 7.3**, **Figure 7.4**). The animals within these groups presented with fused hepatic lobes, devoid of the characteristic deep fissures between the lobes of rat livers (Kogure *et al*., 1999; Vdoviaková *et al*., 2016). As such, an in-depth histological and morphological analysis into the observed maladaptation would be appropriate for a study on DOX-induced hepatotoxicity.

# Chapter 6. REFERENCES


1. Abbasalipourkabir, R., Dehghan, A., Salehzadeh, A., Shamsabadi, F., Abdullah, R., 2010. Induction of mammary gland tumor in female Sprague-Dawley rats with LA7 cells. *African J. Biotechnol*. 9, 4491–4498.
2. Ai, J., Zhang, R., Li, Y., Pu, J., Lu, Y., Jiao, J., Li, K., Yu, B., Li, Zhuqin, Wang, R., Wang, L., Li, Q., Wang, N., Shan, H., Li, Zhongyu, Yang, B., 2010. Circulating microRNA-1 as a potential novel biomarker for acute myocardial infarction. *Biochem. Biophys. Res. Commun*. 391, 73–77.
3. Albini, A., Pennesi, G., Donatelli, F., Cammarota, R., De Flora, S., Noonan, D.M., 2010. Cardiotoxicity of anticancer drugs: The need for cardio-oncology and cardio-oncological prevention. *J. Natl. Cancer Inst*. 102, 14–25.
4. Alturkistani, H.A., Tashkandi, F.M., Mohammedsaleh, Z.M., 2015. Histological Stains: A Literature Review and Case Study. *Glob. J. Health Sci*. 8, 72-79.
5. Angsutararux, P., Luanpitpong, S., Issaragrisil, S., 2015. Chemotherapy-Induced Cardiotoxicity: Overview of the Roles of Oxidative Stress. *Oxid. Med. Cell. Longev*. 2015, 1–13.
6. Argiles, J.M., Lopez-Soriano, F.J., Busquets, S., 2019. Mediators of cachexia in cancer patients. *Nutrition* 66, 11–15.
7. Arola, O.J., Saraste, A., Pulkki, K., Kallajoki, M., Parvinen, M., Voipio-Pulkki, L.M., 2000. Acute doxorubicin cardiotoxicity involves cardiomyocyte apoptosis. *Cancer Res*. 60, 1789–1792.
8. Bachur, N.R., Gordon, S.L., Gee, M. V, 1978. A General Mechanism for Microsomal Activation of Quinone Anticancer Agents to Free Radicals. *Cancer Res*. 38, 1745–1750.
9. Baldwin, R.W., 1955. Immunity to aiethylcholanthrene-induced tumours in inbred rats following atrophy and regression, of the implanted tumours. *Br. J. Cancer*. 9, 652–657.
10. Barbour, J.A., Turner, N., 2014. Mitochondrial stress signaling promotes cellular adaptations. *Int. J. Cell Biol*. 2014, 1-13.
11. Barrett-Lee, P.J., Dixon, J.M., Farrell, C., Jones, a, Leonard, R., Murray, N., Palmieri, C., Plummer, C.J., Stanley, a, Verrill, M.W., 2009. Expert opinion on the use of anthracyclines in patients with advanced breast cancer at cardiac

risk. *Ann. Oncol*. 20, 816–827.

12. Bartel, D.P., 2004. MicroRNAs : Genomics, Biogenesis, Mechanism, and Function. *Cell* 116, 281–297.
13. Bernard, Y., Ribeiro, N., Thuaud, F., Terkeri, G., Dirr, R., Boulberdaa, M., Nebigil, C.G., Desaubry, L., 2011. Flavaglines alleviate doxorubicin cardiotoxicity: Implication of Hsp27. *PLoS One* 6, 1–9.
14. Berthiaume, J.M., Wallace, K.B., 2007. Adriamycin-induced oxidative mitochondrial cardiotoxicity. *Cell Biol. Toxicol*. 23, 15–25.
15. Biologycorner. 2020. Rat - Circulatory. [ONLINE] Available at: https://www.biologycorner.com/worksheets/rat_circulatory.html. [Accessed 12 February 2020].
16. Boon, R.A., Iekushi, K., Lechner, S., Seeger, T., Fischer, A., Heydt, S., Kaluza, D., Tréguer, K., Carmona,G., Bonauer, A., Horrevoets, A.J.G., Didier, N., Girmatsion, Z., Biliczki, P., Ehrlich, J.R., Katus,H.A., Müller, O.J., Potente, M., Zeiher, A.M., Hermeking, H., Dimmeler, S., 2013. MicroRNA-34a regulates cardiac ageing and function. *Nature* 495, 107–110
17. Boveris, A., 1977. Mitochondrial Production of Superoxide Radical and Hydrogen Peroxide, in: Reivich, M., Coburn, R., Lahiri, S., Chance, B. (Eds.), *Tissue Hypoxia and Ischemia*. Springer US, Boston, MA, pp. 67–82.
18. Bradham, W.S., Bozkurt, B., Gunasinghe, H., Mann, D., Spinale, F.G., 2002. Tumor necrosis factor-alpha and myocardial remodeling in progression of heart failure : a current perspective. *Cardiovasc*. *Res*. 53, 822–830.
19. Bray, F., Ren, J., Masuyer, E., Ferlay, J., 2013. Global estimates of cancer prevalence for 27 sites in the adult population in 2008. *Int. J. Cancer* 132, 1133–1145.
20. Bristow, M.R., Thompson, P.D., Martin, R.P., Mason, J.W., Billingham, M.E., Harrison, D.C., 1978. Early anthracycline cardiotoxicity. *Am. J. Med*. 65, 823–832.
21. Bunney, P. E., Zink, A. N., Holm, A. A., Billington, C. J., & Kotz, C.M., 2017. Functions of Myosin Light Chain-2 (MYL2) In Cardiac Muscle and Disease. *Physiol. Behav*. 176, 139–148.
22. Bustin, S.A., Benes, V., Garson, J.A., Hellemans, J., Huggett, J., Kubista, M., Mueller, R., Nolan, T., Pfaffl, M.W., Shipley, G.L., Vandesompele, J., Wittwer, C.T., 2009. The MIQE guidelines: Minimum information for publication of

quantitative real-time PCR experiments. *Clin. Chem*. 55, 611–622.

23. Cai, X., Cao, C., Li, J., Chen, F., Zhang, S., Liu, B., Zhang, X., Ye, L., 2017. Inflammatory factor TNF- α promotes the growth of breast cancer via the positive feedback loop of TNFR1/NF-κB (and/or p38)/p-STAT3/HBXIP/TNFR1. *Oncotarget* 8, 58338–58352.
24. Calin, G.A., Sevignani, C., Dumitru, C.D., Hyslop, T., Noch, E., Yendamuri, S., Shimizu, M., Rattan, S., Bullrich, F., Negrini, M., Croce, C.M., 2004. Human microRNA genes are frequently located at fragile sites and genomic regions involved in cancers. *PNAS* 101, 2999–3004.
25. Callow, A.D., 2006. Cardiovascular disease 2005 - the global picture. *Vascul. Pharmacol*. 45, 302–307.
26. Cao, F., Maguire, M.L., McAndrew, D.J., Lake, H.A., Neubauer, S., Zervou, S., Schneider, J.E., Lygate, C.A., 2020. Overexpression of mitochondrial creatine kinase preserves cardiac energetics without ameliorating murine chronic heart failure. *Basic Res. Cardiol*. 115, 1-11.
27. Care, A., Catalucci, D., Felicetti, F., Addario, A., Gallo, P., Bang, M., Segnalini, P., Gu, Y., Dalton, N.D., Elia, L., Latronico, M.V.G., Høydal, M., Autore, C., Russo, M.A., Ii, G.W.D., Ellingsen, Ø., Ruiz-lozano, P., Peterson, K.L., Croce, C.M., Peschle, C., Condorelli, G., 2007. MicroRNA-133 controls cardiac hypertrophy. *Nat. Med*. 13, 613–618.
28. Carlsson, G., Gullberg, B., Hafström, L., 1983. Estimation of liver tumor volume using different formulas-An experimental study in rats. *J. Cancer Res. Clin. Oncol*. 105, 20–23. doi:10.1007/BF00391826
29. Chan, J.A., Krichevsky, A.M., Kosik, K.S., 2005. MicroRNA-21 Is an Antiapoptotic Factor in Human Glioblastoma Cells. *Cancer Res*. 65, 6029–6033.
30. Chandran, K., Aggarwal, D., Migrino, R.Q., Joseph, J., McAllister, D., Konorev, E.A., Antholine, W.E., Zielonka, J., Srinivasan, S., Avadhani, N.G., Kalyanaraman, B., 2009. Doxorubicin inactivates myocardial cytochrome c oxidase in rats: Cardioprotection by Mito-Q. *Biophys. J*. 96, 1388–1398.
31. Chang, A.N., Mahajan, P., Knapp, S., Barton, H., Sweeney, H.L., Kamm, K.E., Stull, J.T., 2016. Cardiac myosin light chain is phosphorylated by $Ca^{2+}$/calmodulin-dependent and -independent kinase activities. *Proc. Natl. Acad. Sci. U. S. A*. 113, E3824–E3833.

32. Chau, V.Q., Salloum, F.N., Hoke, N.N., Abbate, A., Kukreja, R.C., 2011. Mitigation of the progression of heart failure with sildenafil involves inhibition of RhoA/Rho-kinase pathway. *Am. J. Physiol. Circ. Physiol*. 300, H2272–H2279.

33. Chen, J., Murchison, E.P., Tang, R., Callis, T.E., Tatsuguchi, M., Deng, Z., Rojas, M., Hammond, S.M., Schneider, M.D., Selzman, C.H., Meissner, G., Patterson, C., Hannon, G.J., Wang, D., 2008. Targeted deletion of Dicer in the heart leads to dilated cardiomyopathy and heart failure. *PNAS* 105, 2111–2116.

34. Cheung, K.G., Cole, L.K., Xiang, B., Chen, K., Ma, X., Myal, Y., Hatch, G.M., Tong, Q., Dolinsky, V.W., 2015. Sirtuin-3 (SIRT3) Protein Attenuates Doxorubicin-induced Oxidative Stress and Improves Mitochondrial Respiration in H9C2 Cardiomyocytes. *J. Biol. Chem*. 290, 10981–10993.

35. Choi, H.S., Park, E.S., Kang, H.J., Shin, H.Y., Noh, C. Il, Yun, Y.S., Ahn, H.S., Choi, J.Y., 2010. Dexrazoxane for preventing anthracycline cardiotoxicity in children with solid tumors. *J. Korean Med*. Sci. 25, 1336–1342.

36. Cleland, M.M., Youle, R.J., 2017. Mitochondrial Dynamics and Apoptosis. *Mitochondrial Dynamics and Neurodegeneration*. 2011, 109-138.

37. Coenen-Stass, A.M.L., Pauwels, M.J., Hanson, B., Martin Perez, C., Conceição, M., Wood, M.J.A., Mäger, I., Roberts, T.C., 2019. Extracellular microRNAs exhibit sequence-dependent stability and cellular release kinetics. *RNA Biol*. 16, 1–11.

38. Curigliano, G., Suter, T.M., Plataniotis, G., de Azambuja, E., Sandri, M.T., Criscitiello, C., Goldhirsch, A., Cipolla, C., Roila, F., 2012. Cardiovascular toxicity induced by chemotherapy , targeted agents and radiotherapy : ESMO Clinical Practice Guidelines. *Ann. Oncol*. 23, vii155–vii166.

39. D'Andrea, G.M., 2005. Use of antioxidants during chemotherapy and radiotherapy should be avoided. *Ca-A Cancer J. Clin*. 55, 319–321.

40. Daosukho, C., Ittarat, W., Lin, S.M., Sawyer, D.B., Kiningham, K., Lien, Y.C., St. Clair, D.K., 2005. Induction of manganese superoxide dismutase (MnSOD) mediates cardioprotective effect of tamoxifen (TAM). J*. Mol. Cell. Cardiol*. 39, 792–803.

41. Demark-Wahnefried, W., Rimer, B.K., Winer, E.P., 1997. Weight gain in women diagnosed with breast cancer. *J. Am. Diet. Assoc*. 97, 519–526.

42. Derynck, R., Akhurst, R.J., Balmain, A., 2001. TGF- β signaling in tumor suppression and cancer progression. *Nat. Genet*. 29, 111–129.

43. Desai, V.G., Herman, E.H., Moland, C.L., Branham, W.S., Lewis, S.M., Davis, K.J., George, N.I., Lee, T., Kerr, S., Fuscoe, J.C., 2013. Development of doxorubicin-induced chronic cardiotoxicity in the B6C3F1 mouse model. *Toxicol. Appl. Pharmacol*. 266, 109–121.

44. Desai, V.G., Kwekel, J.C., Vijay, V., Moland, C.L., Herman, E.H., Lee, T., Han, T., Lewis, S.M., Davis, K.J., Muskhelishvili, L., Kerr, S., Fuscoe, J.C., 2014. Early biomarkers of doxorubicin-induced heart injury in a mouse model. *Toxicol. Appl. Pharmacol*. 281, 221-229.

45. Devaux, Y., Mueller, M., Haaf, P., Goretti, E., Twerenbold, R., Zangrando, J., Vausort, M., Reichlin, T., Wildi, K., Moehring, B., Wagner, D.R., Mueller, C., 2015. Diagnostic and prognostic value of circulating microRNAs in patients with acute chest pain. *J. Intern. Med*. 277, 260–271.

46. Ding, P., Huang, J., Battiprolu, P.K., Hill, J.A., Kamm, K.E., Stull, J.T., 2010. Cardiac myosin light chain kinase is necessary for myosin regulatory light chain phosphorylation and cardiac performance in vivo. *J. Biol. Chem*. 285, 40819–40829.

47. Divakaran, V., Mann, D.L., 2008. The Emerging Role of MicroRNAs in Cardiac Remodeling and Heart Failure Biology of MicroRNAs. *Circ. Res*. 103, 1072–1083.

48. Dogru, A., Cabuk, D., Sahin, T., Dolasik, I., Temiz, S., Uygun, K., 2013. Evaluation of cardiotoxicity via speckle-tracking echocardiography in patients treated with anthracyclines. *Onkologie* 36, 712–716.

49. Dorn II, G.W., 2011. MicroRNAs in cardiac disease. *Transl. Res*. 157, 226–235.

50. Esquela-kerscher, A., Slack, F., 2014. Oncomirs- microRNAs with a role in cancer. *Cancer* 6, 259–269.

51. Fearon, K., Strasser, F., Anker, S.D., Bosaeus, I., Bruera, E., Fainsinger, R.L., Jatoi, A., Loprinzi, C., Macdonald, N., Mantovani, G., Davis, M., Muscaritoli, M., Ottery, F., Radbruch, L., Ravasco, P., Walsh, D., Wilcock, A., Kaasa, S., Baracos, V.E., 2011. Definition and classification of cancer cachexia : an international consensus. *Lancet Oncol*. 12, 489–495.

52. Frank, S., Gaume, B., Bergmann-Leitner, E.S., Leitner, W.W., Robert, E.G.,

Catez, F., Smith, C.L., Youle, R.J., 2001. The Role of Dynamin-Related Protein 1, a Mediator of Mitochondrial Fission, in Apoptosis. *Dev. Cell* 1, 515–525.

53. Friedman, M.A., Bozdech, M.J., Rider, A.K., Bilingham, M.E., 1978. Doxorubicin Cardiotoxicity : Serial Endomyocardial Biopsies and Systolic Time Intervals. *JAMA* 240, 1603–1606.
54. Fukuda, A., Wang, S.C., Morris, J.P., Folias, A.E., Liou, A., Kim, G.E., Akira, S., Boucher, K.M., Firpo, M.A., Mulvihill, S.J., Hebrok, M., 2011. Stat3 and MMP7 Contribute to Pancreatic Ductal Adenocarcinoma Initiation and Progression. *Cancer Cell* 19, 441–455.
55. Gaziano, T.A., 2007. Reducing The Growing Burden Of Cardiovascular Disease In The Developing World. *Health Aff*. 26, 13–24.
56. Gharanei, M., Hussain, A., Janneh, O., Maddock, H., 2013. Attenuation of Doxorubicin-Induced Cardiotoxicity by mdivi-1: A Mitochondrial Division/Mitophagy Inhibitor. *PLoS One* 8, 1–15.
57. Ginsburg, O.M., 2013. Breast and cervical cancer control in low-and middle-income countries : Human rights meet sound health policy. *J. Cancer Policy* 1, e35–e41.
58. Goren, Y., Kushnir, M., Zafrir, B., Tabak, S., Lewis, B.S., Amir, O., 2012. Serum levels of microRNAs in patients with heart failure. *Eur. J. Heart Fail*. 14, 147–157.
59. Govender, J., Loos, B., Marais, E., Engelbrecht, A.M., 2014. Mitochondrial catastrophe during doxorubicin-induced cardiotoxicity: A review of the protective role of melatonin. *J. Pineal Res*. 57, 367–380.
60. Govender, Y.J., 2017. *Mitochondrial catastrophe during doxorubicin-induced cardiotoxicity : An evaluation of the protective role of melatonin*. (Unpublished doctoral thesis). Stellenbosch University, Stellenbosch, Western Cape, South Africa.
61. Green, P.S., Leeuwenburgh, C., 2002. Mitochondrial dysfunction is an early indicator of doxorubicin-induced apoptosis. *Biochem. Biophys. Acta - Mol. Basis Dis*. 1588, 94–101.
62. Grivennikov, S.I., Greten, F.R., Karin, M., 2010. Immunity , Inflammation , and Cancer. *Cell* 140, 883–899.
63. Gutkind, J.S., Petricoin, E., Bichsel, V.E., Worth, J.M., Prabhu, V. V, Liotta,

L.A., Munson, P.J., Iii, E.F.P., Krizman, D.B., 2001. Proteomic profiling of the cancer microenvironment by antibody arrays. *Proteomics* 1, 1271–1278.

64. Haase, D., Lehmann, M.H., Körner, M.M., Körfer, R., Sigusch, H.H., Figulla, H.R., 2002. Identification and validation of selective upregulation of ventricular myosin light chain type 2 mRNA in idiopathic dilated cardiomyopathy. *Eur. J. Heart Fail*. 4, 23–31.
65. Harikrishnan, S., Leeder, S., Huffman, M., Panniyammakal, J., Prabhakran, D., 2014. A race against time : The Challenge of Cardiovascular Diseases in Developing economies. *Centre for Chronic Disease Control, New Delhi, India*. (Book).
66. Hassan, F., Morikawa, A., Islam, S., Tumurkhuu, G., Dagvadorj, J., Koide, N., Naiki, Y., Mori, I., Yoshida, T., Yokochi, T., 2008. Lipopolysaccharide augments the in vivo lethal action of doxorubicin against mice via hepatic damage. *Clin. Exp. Immunol*. 151, 334–340.
67. Heron, M., 2015. National Vital Statistics Reports Deaths : Leading Causes for 2012. Natl. Vital Stat. *Reports* 64, 1–93.
68. Hom, J., Sheu, S.S., 2009. Morphological dynamics of mitochondria - A special emphasis on cardiac muscle cells. *J. Mol. Cell. Cardiol*. 46, 811–820.
69. Hornier, M.J., Ries, L.A.G., Krapcho, M., 2009. SEER Cancer Statistics Review 1975-2006, Bethseda MD: National Cancer Institute. (Report)
70. Hortobagyi, G.N., 1997. Anthracyclines in the Treatment of Cancer: An Overview. *Drugs* 54, 1–7.
71. Hwang, H.-W., Wentzel, E.A., Mendell, J.T., 2007. A Hexanucleotide Element Directs MicroRNA Nuclear Import. *Science* 315, 97–100.
72. Ibrahim, M.M., Damasceno, A., 2012. Hypertension in developing countries. *Lancet* 380, 611–619.
73. Ichikawa, Y., Ghanefar, M., Bayeva, M., Wu, R., Khechaduri, A., Prasad, S.V.N., Mutharasan, R.K., Naik, T.J., Ardehali, H., 2014. Cardiotoxicity of doxorubicin is mediated through mitochondrial iron accumulation. *J. Clin. Invest*. 124, 617–630.
74. Immer, F.F., Stocker, F., Seiler, A.M., Pfammatter, J.P., Bachmann, D., Printzen, G., Carrel, T., 1999. Troponin-I for prediction of early postoperative course after pediatric cardiac surgery. *J. Am. Coll. Cardiol*. 33, 1718-1723.
75. Ji, X., Takahashi, R., Hirokawa, G., Fukushima, Y., Iwai, N., 2009. Plasma

miR-208 as a Biomarker of Myocardial Injury. *Mol. Diagnostics Genet*. 55, 1944–1949.

76. Jing, X., Yang, J., Jiang, L., Chen, J., Wang, H., 2018. MicroRNA-29b Regulates the Mitochondria-Dependent Apoptotic Pathway by Targeting Bax in Doxorubicin Cardiotoxicity. *Cell. Physiol. Biochem*. 48, 692–704.
77. Junjing, Z., Yan, Z., Baolu, Z., 2010. Scavenging effects of dexrazoxane on free radicals. *J. Clin. Biochem. Nutr*. 47, 238–45.
78. Kaarbø, M., Crane, D.I., Murrell, W.G., 2003. RhoA is highly up-regulated in the process of early heart development of the chick and important for normal embryogenesis. *Dev. Dyn*. 227, 35–47.
79. Kamel, M., Shouman, S., El-merzebany, M., Kilic, G., Veenstra, T., Wagih, M., Diaz-arrastia, C., Patel, D., Salama, S., 2012. Effect of Tumour Necrosis Factor-Alpha on Estrogen Metabolic Pathways in Breast Cancer Cells. *J. Cancer* 3, 310–321.
80. Kang, Y.J., Chen, Y., Epstein, P.N., 1996. Suppression of doxorubicin cardiotoxicity by overexpression of catalase in the heart of transgenic mice. *J. Biol. Chem*. 271, 12610–12616.
81. Karagiannis, T.C., Lin, A.J.E., Ververis, K., Chang, L., Tang, M.M., Okabe, J., El-Osta, A., 2010. Trichostatin A accentuates doxorubicin-induced hypertrophy in cardiac myocytes. *Aging* (Albany. NY). 2, 659–668.
82. Karbowski, M., Youle, R.J., 2011. Regulating mitochondrial outer membrane proteins by ubiquitination and proteasomal degradation. *Curr. Opin. Cell Biol*. 23, 476–482.
83. Kaya, M.G., Ozkan, M., Gunebakmaz, O., Akkaya, H., Kaya, E.G., Akpek, M., Kalay, N., Dikilitas, M., Yarlioglues, M., Karaca, H., Berk, V., Ardic, I., Ergin, A., Lam, Y.Y., 2013. Protective effects of nebivolol against anthracycline-induced cardiomyopathy : A randomized control study. *Int. J. Cardiol*. 167, 2306–2310.
84. Kiernan, J.A., 1995. Sirius Red for Collagen Staining Protocol. 1-2, (Report).
85. Kihara, M., Kaiya, H., Win, Z.P., Kitajima, Y., Nishikawa, M., 2016. Protective Effect of Dietary Ghrelin-Containing Salmon Stomach Extract on Mortality and Cardiotoxicity in Doxorubicin-Induced Mouse Model of Heart Failure. *J. Food Sci*. 81, H2858–H2865.
86. Kim, A.S., Johnston, S.C., 2011. Global Variation in the Relative Burden of

Stroke and Ischemic Heart Disease. *Circulation* 124, 314–323.

87. Kim, SA., Kim, HW., Kim, DK., Kim, SG., Park, JC., Kang, DW., Kim, SW., Ahn, SG., Yoon, JH., 2006. Rapid induction of malignant tumor in Sprague-Dawley rats by injection of RK3E-ras cells. *Cancer Lett*. 235: 53-59.
88. Kim, M.S., Ramakrishna, S., Lim, K.H., Kim, J.H., Baek, K.H., 2011. Protein stability of mitochondrial superoxide dismutase SOD2 is regulated by USP36. *J. Cell. Biochem*. 112, 498–508.
89. Kingham, T.P., Alatise, O.I., Vanderpuye, V., Casper, C., Abantanga, F.A., Kamara, T.B., Olopade, O.I., Habeebu, M., Abdulkareem, F.B., Denny, L., 2013. Treatment of cancer in sub-Saharan Africa. *Lancet Oncol*. 14, e158–e167.
90. Kissin, I., Morgan, P.L., Smith, L.R., 1983. Comparison of Isoflurane and Halothane Safety Margins in Rats. *Anesthesiology* 58, 556–561.
91. Kogure, K., Ishizaki, M., Nemoto, M., Kuwano, H., Makuuchi, M., 1999. A comparative study of the anatomy of rat and human livers. J. Hepatobiliary. *Pancreat. Surg*. 6, 171–175.
92. Kostenko, S., Moens, U., 2009. Heat shock protein 27 phosphorylation : Kinases , phosphatases , functions and pathology. *Cell. Mol. Life Sci*. 66, 3289–3307.
93. Kroenke, C.H., Chen, W.Y., Rosner, B., Holmes, M.D., 2005. Weight , Weight Gain, and Survival After Breast Cancer Diagnosis. *J. Clin. Oncol*. 23, 1370–1378.
94. Kroh, E.M., Parkin, R.K., Mitchell, P.S., Tewari, M., 2010. Analysis of circulating microRNA biomarkers in plasma and serum using quantitative reverse transcription-PCR (qRT-OCR). *Methods* 50, 1–9.
95. Kuosmanen, S.M., Hartikainen, J., Hippeläinen, M., Kokki, H., Levonen, A.L., Tavi, P., 2015. MicroRNA profiling of pericardial fluid samples from patients with heart failure. *PLoS One* 10, 1–23.
96. Ky, B., Putt, M., Sawaya, H., French, B., Januzzi, J.L., Sebag, I.A., Plana, J.C., Cohen, V., Banchs, J., Carver, J.R., Wiegers, S.E., Martin, R.P., Picard, M.H., Gerszten, R.E., Halpern, E.F., Passeri, J., Kuter, I., Scherrer-Crosbie, M., 2014. Early increases in multiple biomarkers predict subsequent cardiotoxicity in patients with breast cancer treated with doxorubicin, taxanes, and trastuzumab. *J. Am. Coll. Cardiol*. 63, 809–816.

97. Ky, B., Vejpongsa, P., Yeh, E.T.H., Force, T., Moslehi, J.J., 2013. Emerging Paradigms in Cardiomyopathies Associated With Cancer Therapies. *Circ. Res*. 113, 754–764.

98. Lamkanfi, M., Kanneganti, T.D., 2010. Caspase-7: A protease involved in apoptosis and inflammation. *Int. J. Biochem. Cell Biol*. 42, 21–24.

99. Lakhani, S.A., Masud, A., Kuida, K., Porter, G.A., Booth, C.J., Mehal, W.Z., Inayat, I., Flavell, R.A., 2006. Caspases 3 and 7: Key mediators of mitochondrial events of apoptosis. *Science* 311, 847–851.

100. Laslett, L.J., Alagona, P., Clark, B.A., Drozda, J.P., Saldivar, F., Wilson, S.R., Poe, C., Hart, M., 2012. The Worldwide Environment of Cardiovascular Disease : Prevalence , Diagnosis , Therapy , and Policy Issues A Report From the American College of Cardiology. *J. Am. Coll. Cardiol*. 60, S1–S49.

101. Lee, Y., Jeong, S., Karbowski, M., Smith, C.L., Youle, R.J., 2004. Roles of the Mammalian Mitochondrial Fission and Fusion Mediators Fis1, Drp1, and Opa1 in Apoptosis. *Mol. Biol. Cell* 15, 5001–5011.

102. Leeder, S., Raymond, S., Greenberg, H., Liu, H. and Esson, K., 2004. A race against time: the challenge of cardiovascular disease in developing economies. *New York, Trustees of Columbia University*. (Book)

103. Lesina, M., Kurkowski, M.U., Ludes, K., Rose-John, S., Treiber, M., Klöppel, G., Yoshimura, A., Reindl, W., Sipos, B., Akira, S., Schmid, R.M., Algül, H., 2011. Stat3/Socs3 Activation by IL-6 Transsignaling Promotes Progression of Pancreatic Intraepithelial Neoplasia and Development of Pancreatic Cancer. *Cancer Cell* 19, 456–469.

104. Li, C., Pei, F., Zhu, X., Duan, D.D., Zeng, C., 2012. Circulating microRNAs as novel and sensitive biomarkers of acute myocardial Infarction. *Clin. Biochem*. 45, 727–732.

105. Li, J., Li, Yuzhen, Jiao, J., Wang, J., Li, Yanrui, Qin, D., Li, P., 2014. Mitofusin 1 is Negatively Regulated by miR-140 in Cardiomyocyte Apoptosis. *Mol. Cell. Biol*. 34, 1788–1799.

106. Li, N., Grivennikov, S.I., Karin, M., 2011. Previews The Unholy Trinity : Inflammation, Cytokines, and STAT3 Shape The Cancer Microenvironment. *Cancer Cell* 19, 429–431.

107. Li, N., Zhou, H., Tang, Q., 2018. miR-133: A suppressor of cardiac remodeling? *Front. Pharmacol*. 9. 1-19.

108. Lipshultz, S.E., Scully, R.E., Lipsitz, S.R., Sallan, S.E., Silverman, L.B., Miller, T.L., Barry, E. V., Asselin, B.L., Athale, U., Clavell, L.A., Larsen, E., Moghrabi, A., Samson, Y., Michon, B., Schorin, M.A., Cohen, H.J., Neuberg, D.S., Orav, E.J., Colan, S.D., 2010. Assessment of dexrazoxane as a cardioprotectant in doxorubicin-treated children with high-risk acute lymphoblastic leukaemia: Long-term follow-up of a prospective, randomised, multicentre trial. *Lancet Oncol*. 11, 950–961.

109. Liu, J., Mao, W., Ding, B., Liang, C., 2008. ERKs/p53 signal transduction pathway is involved in doxorubicin-induced apoptosis in H9c2 cells and cardiomyocytes. *Am. J. Physiol. Heart Circ. Physiol*. 295, H1956–H1965.

110. Lovett, J.A.C., Durcan, P.J., Myburgh, K.H., 2018. Investigation of circulating extracellular vesicle microRNA following two consecutive bouts of muscle-damaging exercise. *Front. Physiol*. 9, 1–8.

111. Marin-Gracia, J., Akhmedov, A.T., Moe, G.W., 2013. Mitochondria in heart failure : the emerging role of mitochondrial dynamics. *Heart Fail. Rev*. 18, 439–456.

112. Martinou, J.C., Youle, R.J., 2011. Mitochondria in Apoptosis: Bcl-2 Family Members and Mitochondrial Dynamics. *Dev. Cell* 21, 92–101.

113. Mckinsey, T.A., Olson, E.N., Mckinsey, T.A., Olson, E.N., 2005. Toward transcriptional therapies for the failing heart : chemical screens to modulate genes. *J. Clin. Invest*. 115, 538–546.

114. Merriam-Webster, 2005. "intercalate." *Merriam-Webster.com*, https://www.merriam-webster.com/dictionary/intercalate. (Dictionary) Accessed 24 Dec, 2020.

115. Minotti, G., 2004. Anthracyclines: Molecular Advances and Pharmacologic Developments in Antitumor Activity and Cardiotoxicity. *Pharmacol. Rev*. 56, 185–229.

116. Minotti, G., Cairo, G., Monti, E., 1999. Role of iron in anthracycline cardiotoxicity: new tunes for an old song? *FASEB J*. 13, 199–212.

117. Mitchell, P.S., Parkin, R.K., Kroh, E.M., Fritz, B.R., Wyman, S.K., Pogosova-agadjanyan, E.L., Peterson, A., Noteboom, J., Briant, K.C.O., Allen, A., Lin, D.W., Urban, N., Drescher, C.W., Knudsen, B.S., Stirewalt, D.L., Gentleman, R., Vessella, R.L., Nelson, P.S., Martin, D.B., Tewari, M., 2008. Circulating microRNAs as stable blood-based markers for cancer detection. *PNAS* 105,

10513–10518.

118. Mizutani, H., Tada-Oikawa, S., Hiraku, Y., Kojima, M., Kawanishi, S., 2005. Mechanism of apoptosis induced by doxorubicin through the generation of hydrogen peroxide. *Life Sci*. 76, 1439–1453.

119. Montaigne, D., Hurt, C., Neviere, R., 2012. Mitochondria death/survival signaling pathways in cardiotoxicity induced by anthracyclines and anticancer-targeted therapies. *Biochem. Res. Int*. 2012, 1–12.

120. Morciano, G., Giorgi, C., Balestra, D., Marchi, S., Perrone, D., 2016. Mcl-1 involvement in mitochondrial dynamics is associated with apoptotic cell death. *Mol. Biol. Cell* 27, 20–34.

121. Moulin, M., Piquereau, J., Mateo, P., Fortin, D., Rucker-Martin, C., Gressette, M., Lefebvre, F., Gresikova, M., Solgadi, A., Veksler, V., Garnier, A., Ventura-Clapier, R., 2015. Sexual dimorphism of doxorubicin-mediated cardiotoxicity potential role of energy metabolism remodeling. *Circ. Hear. Fail*. 8, 98–108.

122. Mozaffarian, D., Benjamin, E.J., Go, A.S., Arnett, D.K., Blaha, M.J., Cushman, M., Das, S.R., de Ferranti, S., Després, J.-P., Fullerton, H.J., Howard, V.J., Huffman, M.D., Isasi, C.R., Jiménez, M.C., Judd, S.E., Kissela, B.M., Lichtman, J.H., Lisabeth, L.D., Liu, S., Mackey, R.H., Magid, D.J., McGuire, D.K., Mohler, E.R., Moy, C.S., Muntner, P., Mussolino, M.E., Nasir, K., Neumar, R.W., Nichol, G., Palaniappan, L., Pandey, D.K., Reeves, M.J., Rodriguez, C.J., Rosamond, W., Sorlie, P.D., Stein, J., Towfighi, A., Turan, T.N., Virani, S.S., Woo, D., Yeh, R.W., Turner, M.B., 2015. Heart Disease and Stroke Statistics—2016 Update. *Circulation* 131, 431–441.

123. Myers, C.E., Mcguire, W.P., Liss, R.H., Ifrim, I., 1977. Adriamycin : The Role of Lipid Peroxidation in Cardiac Toxicity and Tumor Response. *Science* (80). 197, 165–167.

124. Neves, A.L., Henriques-Coelho, T., Leite-Moreira, A., Areias, J.C., 2016. Cardiac injury biomarkers in paediatric age: Are we there yet? *Heart Fail.Rev.* 21,771-781.

125. Nigris, F. De, Rienzo, M., Schiano, C., Fiorito, C., Casamassimi, A., Napoli, C., 2008. Prominent cardioprotective effects of third generation beta blocker nebivolol against anthracycline-induced cardiotoxicity using the model of isolated perfused rat heart. *Eur. J. Cancer* 44, 334–340.

126. Oliveira-Carvalho, V., Carvalho, V.O., Bocchi, E.A., 2012. The Emerging Role

of miR-208a in the Heart. *DNA Cell Biol*. 32, 8–12.

127. Park, Y., Nguyen, O.T.K., Kang, H., Cho, H., 2014. MARCH5-mediated quality control on acetylated Mfn1 facilitates mitochondrial homeostasis and cell survival. *Cell Death Dis*. 5, e1172-12.

128. Patane, S., 2014. Cardiotoxicity: Cisplatin and long-term cancer survivors. *Int. J. Cardiol*. 175, 201–202.

129. Payne, D.L., Nohria, A., 2017. Prevention of Chemotherapy Induced Cardiomyopathy. *Curr. Heart Fail*. *Rep*. 14, 398–403.

130. Perk, J., De Backer, G., Gohlke, H., Graham, I., Reiner, Ž., Verschuren, M., Albus, C., Benlian, P., Boysen, G., Cifkova, R., Deaton, C., Ebrahim, S., Fisher, M., Germano, G., Hobbs, R., Hoes, A., Karadeniz, S., Mezzani, A., Prescott, E., Ryden, L., Scherer, M., Syvänne, M., Scholte Op Reimer, W.J.M., Vrints, C., Wood, D., Zamorano, J.L., Zannad, F., Cooney, M.T., Bax, J., Baumgartner, H., Ceconi, C., Dean, V., Fagard, R., Funck-Brentano, C., Hasdai, D., Kirchhof, P., Knuuti, J., Kolh, P., McDonagh, T., Moulin, C., Popescu, B.A., Sechtem, U., Sirnes, P.A., Tendera, M., Torbicki, A., Vahanian, A., Windecker, S., Aboyans, V., Ezquerra, E.A., Baigent, C., Brotons, C., Burell, G., Ceriello, A., De Sutter, J., Deckers, J., Del Prato, S., Diener, H.C., Fitzsimons, D., Fras, Z., Hambrecht, R., Jankowski, P., Keil, U., Kirby, M., Larsen, M.L., Mancia, G., Manolis, A.J., McMurray, J., Pajak, A., Parkhomenko, A., Rallidis, L., Rigo, F., Rocha, E., Ruilope, L.M., Van Der Velde, E., Vanuzzo, D., Viigimaa, M., Volpe, M., Wiklund, O., Wolpert, C., 2012. European Guidelines on cardiovascular disease prevention in clinical practice (version 2012). *Eur. Heart J*. 33, 1635–1701.

131. Picano, E., Benassi, A., Marzilli, M., Pelosi, G., L'Abbate, A., Lattanzi, F., Landini, L., 2011. In vivo quantitative ultrasonic evaluation of myocardial fibrosis in humans. *Circulation* 81, 58–64.

132. Pigati, L., Yaddanapudi, S.C.S., Iyengar, R., Kim, D.J., Hearn, S.A., Danforth, D., Hastings, M.L., Duelli, D.M., 2010. Selective release of MicroRNA species from normal and malignant mammary epithelial cells. *PLoS One* 5, 1–13.

133. Pinedo, H., Smorenburg, C., 2006. Drugs Affecting Growth of Tumours. *Springer Science & Business Media*. Birkhauser, 1-237. (Book)

134. Rani, M.L., Shreya, R., Dimpal, T., Monjula, R., Kurade, N.P., Meena, K., Sharma, A.K., Tiwari, A.K., 2014. Pathology of LA7 cell induced tumours in

Sprague Dawley rats. *Indian Journal of Veterinary Pathology*. 38, 43-48.

135. Rao, P.K., Toyama, Y., Chiang, H.R., Gupta, S., Bauer, M., Medvid, R., Reinhardt, F., Liao, R., Krieger, M., Jaenisch, R., Lodish, H.F., Blelloch, R., 2009. Loss of Cardiac microRNA-Mediated Regulation Leads to Dilated Cardiomyopathy and Heart Failure. *Circ. Res*. 105, 585–594.

136. Raymond, C.K., Roberts, B.S., Garrett-engele, P., Lim, L.E.E.P., Johnson, J.M., 2005. Simple, quantitative primer-extension PCR assay for direct monitoring of microRNAs and short-interfering RNAs. *RNA* 11, 1737–1744.

137. Ren, X., Wu, J., Wang, X., Sartor, M.A., Qian, J., Jones, K., Nicolaou, P., Pritchard, T.J., Fan, G., 2009. MicroRNA-320 Is Involved in the Regulation of Cardiac Ischemia / Reperfusion Injury by Targeting Heat-Shock Protein 20. *Circulation* 119, 2357–2366.

138. Renu, K., Abilash, V.G., Pichiah, T.P.B., Arunachalam, S., 2018. Molecular mechanism of doxorubicin-induced cardiomyopathy – An update. *Eur. J. Pharmacol*. 818, 241–253.

139. Roberts, T.C., Coenen-Stass, A.M.L., Wood, M.J.A., 2014. Assessment of RT-qPCR normalization strategies for accurate quantification of extracellular microRNAs in murine Serum. *PLoS One* 9, 1–9.

140. Rock, C.L., Flatt, S.W., Newman, V., Caan, B.J., Haan, M.N., Stefanick, M.L., Faerber, S., Pierce, J.P., 1999. Factors associated with weight gain in women after diagnosis of breast cancer. *J. Am. Diet. Assoc*. 99, 1212–1218.

141. Rosa, G.M., Gigli, L., Tagliasacchi, M.I., Di Iorio, C., Carbone, F., 2016. Update on cardiotoxicity of anti-cancer treatments. *Eur. J. Clin. Invest*. 46, 264–284.

142. Roth, G.A., Huffman, M.D., Moran, A.E., Feigin, V., Mensah, G.A., Naghavi, M., Murray, C.J.L., 2015. Global and regional patterns in cardiovascular mortality from 1990 to 2013. *Circulation* 132, 1667–1678.

143. Ruggeri, C., Gioffré, S., Achilli, F., Colombo, G.I., D'Alessandra, Y., 2018. Role of microRNAs in doxorubicin-induced cardiotoxicity: an overview of preclinical models and cancer patients. *Heart Fail. Rev*. 23, 109–122.

144. Saini, H.K., Xu, Y., Zhang, M., Liu, P.P., Kirshenbaum, L.A., Dhalla, N.S., 2005. Role of tumour necrosis factor-alpha and other cytokines in ischemia-reperfusion-induced injury in the heart. *Exp. Clin. Cardiol*. 10, 213–222.

145. Salami, S., Karami-Tehrani, F., 2003. Biochemical studies of apoptosis

induced by tamoxifen in estrogen receptor positive and negative breast cancer cell lines. *Clin. Biochem*. 36, 247–253.

146. Santulli, G., 2013. Epidemiology of Cardiovascular Disease in the 21st Century : Updated Numbers and Updated Facts. *J. Cardiovasc*. *Dis*. 1, 1–2.

147. Sauter, K.A.D., Wood, L.J., Wong, J., Iordanov, M., Magun, B.E., 2011. Doxorubicin and daunorubicin induce processing and release of interleukin-1β through activation of the NLRP3 inflammasome. *Cancer Biol. Ther*. 11, 1008–1016.

148. Seeger, T., Boon, R.A., 2016. MicroRNAs in cardiovascular ageing. *J. Physiol*. 594, 2085–2094.

149. Seidman, A., Hudis, C., Pierri, M.K., Shak, S., Paton, V., Ashby, M., Murphy, M., Stewart, S.J., Keefe, D., 2002. Cardiac dysfunction in the trastuzumab clinical trials experience. *J. Clin. Oncol*. 20, 1215–1221.

150. Sempere, L.F., Christensen, M., Silahtaroglu, A., Bak, M., Heath, C. V., Schwartz, G., Wells, W., Kauppinen, S., Cole, C.N., 2007. Altered microRNA expression confined to specific epithelial cell subpopulations in breast cancer. *Cancer Res*. 67, 11612–11620.

151. Shimokawa, H., Takeshita, A., 2005. Rho-kinase is an important therapeutic target in cardiovascular medicine. *Arterioscler. Thromb. Vasc. Biol*. 25, 1767–1775.

152. Simunek, T., Sterba, M., Popelova, O., Adamcova, M., Hrdina, R., Gersi, V., 2009. Anthracycline-induced cardiotoxicity: Overview of studies examining the roles of oxidative stress and free cellular iron. *Pharmacol. Reports* 61, 154–171.

153. Sirotkovic-skerlev, M., Cacev, T., Kapitanovic, S., 2006. Tumor necrosis factor-α and breast cancer. *Period. Biol*. 108, 541–546.

154. Sishi, B.J.N., Loos, B., van Rooyen, J., Engelbrecht, A.M., 2013a. Doxorubicin induces protein ubiquitination and inhibits proteasome activity during cardiotoxicity. *Toxicology* 309, 23–29.

155. Sishi, B.J.N., Loos, B., Van Rooyen, J., Engelbrecht, A.M., 2013b. Autophagy upregulation promotes survival and attenuates doxorubicin-induced cardiotoxicity. *Biochem. Pharmacol*. 85, 124–134.

156. Small, E.M., Frost, R.J.A., Olson, E.N., 2010. MicroRNAs add a new dimension to cardiovascular disease. *Circulation* 121, 1022–1032.

157. Smirnova, E., Shurland, D.L., Ryazantsev, S.N., Van Der Bliek, A.M., 1998. A human dynamin-related protein controls the distribution of mitochondria. *J. Cell Biol*. 143, 351–358.

158. Smith, S.C., Chen, D., Collins, A., Harold, J.G., Jessup, M., Josephson, S., Logstrup, S., Sacco, R.L., Vardas, P.E., Wood, D.A., Zoghbi, W.A., 2013. Moving from political declaration to action on reducing the global burden of cardiovascular diseases: A statement from the global cardiovascular disease taskforce. *Glob. Heart* 8, 383–386.

159. Sotocinal, S.G., Sorge, R.E., Zaloum, A., Tuttle, A.H., Martin, L.J., Wieskopf, J.S., Mapplebeck, J.C.S., Wei, P., Zhan, S., Zhang, S., McDougall, J.J., King, O.D., Mogil, J.S., 2011. The Rat Grimace Scale: A partially automated method for quantifying pain in the laboratory rat via facial expressions. *Mol. Pain* 7, 1–10.

160. Stephenson, B., 2015. A modified Picro-Sirius Red (PSR) staining procedure with polarization microscopy for identifying collagen in archaeological residues. *J. Archaeol*. *Sci*. 61, 235–243.

161. Steyn, K., Fourie, J., Temple, N., 2006. Chronic Diseases of Lifestyle in South Africa: 1995-2005. *Medical Research Council-Technical Report*. (Report)

162. Su, S., Li, Q., liu, Y., Xiong, C., Li, J., Zhang, R., Niu, Y., Zhao, L., Wang, Y., Guo, H., 2014. Sesamin ameliorates doxorubicin-induced cardiotoxicity: Involvement of Sirt1 and Mn-SOD pathway. *Toxicol. Lett*. 224, 257–263.

163. Subbiah, M.T.R., 2002. Estrogen replacement therapy and cardioprotection : mechanisms and controversies. *Brazilian J. Med. Biol. Res*. 35, 271–276.

164. Suter, T.M., Ewer, M.S., 2013. Cancer drugs and the heart : importance and management. *Eur. Heart J*. 34, 1102–1111.

165. Suzuki, Y., Imai, Y., Nakayama, H., Takahashi, K., Takio, K., Takahashi, R., 2001. A Serine Protease, HtrA2, Is Released from the Mitochondria and Interacts with XIAP, Inducing Cell Death. *Mol. Cell* 8, 613–621.

166. Swain, S.M., Vici, P., 2004. The current and future role of dexrazoxane as a cardioprotectant in anthracycline treatment : expert panel review. *J. Cancer Res. Clin. Oncol*. 130, 1–7.

167. Swain, S.M., Whaley, F.S., Ewer, M.S., 2003. Congestive heart failure in patients treated with doxorubicin: A retrospective analysis of three trials. *Cancer* 97, 2869–2879.

168. Tebbi, C.K., London, W.B., Friedman, D., Villaluna, D., Alarcon, P.A. De Constine, L.S., Mendenhall, N.P., Sposto, R., Chauvenet, A., Schwartz, C.L., 2007. Dexrazoxane-Associated Risk for Acute Myeloid Leukemia / Myelodysplastic Syndrome and Other Secondary Malignancies in Pediatric Hodgkin's Disease. *J. Clin. Oncol*. 25, 493–500.

169. The American Cancer Society., 2018. The Cancer Atlas. [online] Available at https://canceratlas.cancer.org/data/map/. [Accessed 15 April 2020].

170. Thum, T., Galuppo, P., Wolf, C., Fiedler, J., Kneitz, S., Laake, L.W. Van, Doevendans, P.A., Mummery, C.L., Borlak, J., Haverich, A., Gross, C., Engelhardt, S., Ertl, G., Bauersachs, J., 2007. MicroRNAs in the Human Heart A Clue to Fetal Gene Reprogramming in Heart Failure. *Circulation* 116, 258–267.

171. Tijsen, A.J., Creemers, E.E., Moerland, P.D., Windt, L.J. De, Wal, A.C. Van Der, Kok, W.E., Pinto, Y.M., 2010. MiR423-5p As a Circulating Biomarker for Heart Failure. *Circ. Res*. 106, 1035–1039.

172. Tisdale, M.J., 2009. Mechanisms of Cancer Cachexia. *Physiol. Rev*. 89, 381–410.

173. Titford, M., 2005. The long history of hematoxylin. *Biotech. Histochem*. 80, 73–78.

174. Torti, F.M., Bristow, M.M., Lum, B.L., Carter, S.K., Howes, A.E., Aston, D.A., Brown, B.W., Hannigan, J.F., Meyers, F.J., Mitchell, E.P., 1986. Cardiotoxicity of epirubicin and doxorubicin: Assessment by endomyocardial biopsy. *Cancer Res*. 46, 3722–3727.

175. van Dalen, E.C., Caron, H.N., Dickinson, H.O., Kremer, L.C.M., 2008. Cardioprotective interventions for cancer patients receiving anthracyclines. *Cochrane database Syst. Rev*. 2, CD003917.

176. van Dalen, E.C., Caron, H.N., Dickinson, H.O., Kremer, L.C.M., 2005. Cardioprotective interventions for cancer patients receiving anthracyclines. *Cochrane database Syst. Rev*. 1, CD003917.

177. van Rooij, E., Sutherland, L.B., Liu, N., Williams, A.H., Mcanally, J., Gerard, R.D., Richardson, J.A., Olson, E.N., 2006. A signature pattern of stress-responsive microRNAs that can evoke cardiac hypertrophy and heart failure. *PNAS* 103, 18255–18260.

178. van Rooij, E., Sutherland, L.B., Qi, X., Richardson, J.A., Hill, J., Olson, E.N.,

2007. Control of stress-dependent cardiac growth and gene expression by a microRNA. *Science* 316, 575–579.

179. Vasquez-Vivar, J., Martasek, P., Masters, B.S.S., Pritchard, K.J., Kalyanaraman, B., 1997. Endothelial Nitric Oxide Synthase-Dependent Superoxide Generation from Adriamycin. *Biochemistry* 36, 11293–11297.

180. Vdoviaková, K., Petrovová, E., Maloveská, M., Krešáková, L., Teleky, J., Elias, M.Z.J., Petrášová, D., 2016. Surgical anatomy of the gastrointestinal tract and its vasculature in the laboratory rat. *Gastroenterol. Res. Pract*. 2016, 1–11.

181. Vera, J.C., Rivas, C.I., Vela, F. V, Zhang, R.H., Concha, I.I., Golde, D.W., 1995. Resolution of the Facilitated Transport of Dehydroascorbic Acid from Its Intracellular Accumulation as Ascorbic Acid. *J. Biol. Chem*. 270, 23706–23712.

182. Ventura, A., Kirsch, D.G., McLaughlin, M.E., Tuveson, D.A., Grimm, J., Lintault, L., Newman, J., Reczek, E.E., Weissleder, R., Jacks, T., 2007. Restoration of p53 function leads to tumour regression in vivo. *Nature.* 445, 661–665.

183. Villar, A. V., Merino, D., Wenner, M., Llano, M., Cobo, M., Montalvo, C., García, R., Martín-Durán, R., Hurlé, J.M., Hurlé, M.A., Nistal, J.F., 2011. Myocardial gene expression of microRNA-133a and myosin heavy and light chains, in conjunction with clinical parameters, predict regression of left ventricular hypertrophy after valve replacement in patients with aortic stenosis. *Heart,* 97, 1132–1137.

184. Volkova, M., Russell, R., 2011. Anthracycline cardiotoxicity: prevalence, pathogenesis and treatment. *Curr. Cardiol. Rev*. 7, 214–220.

185. Walsh, J.G., Cullen, S.P., Sheridan, C., Lüthi, A.U., Gerner, C., Martin, S.J., 2008. Executioner caspase-3 and caspase-7 are functionally distinct proteases. *PNAS*. 105, 12815–12819.

186. Wang, K., Zhang, S., Weber, J., Baxter, D., Galas, D.J., 2010. Export of microRNAs and microRNA-protective protein by mammalian cells. *Nucleic Acids Res*. 38, 7248–7259.

187. Wentink, M.Q., Räkers, M., Stupart, D.A., Algar, U., Ramesar, R., Goldberg, P.A., 2010. Incidence and histological features of colorectal cancer in the Northern Cape Province, South Africa. *SAJS* 48, 109–113.

188. Wolczyk, D., Zaremba-czogalla, M., Hryniewicz-jankowska, A., Tabola, R., Grabowski, K., Sikorski, A.F., Augoff, K., 2016. TNF-α promotes breast cancer cell migration and enhances the concentration of membrane-associated proteases in lipid rafts. *Cell. Oncol*. 39, 353–363.

189. World Economic Forum., World Health Organization, 2011. From Burden to "Best Buys": Reducing the Economic Impact of Non-communicable Diseases in Low- and Middle-Income Countries. Geneva, Switzerland. 1-12. (Report)

190. World Health Organization, 2010. World Health Statistics 2010. *World Health Statistics* 1, 127-168.

191. Xiang, P., Deng, H.Y., Li, K., Huang, G.-Y., Chen, Y., Tu, L., Ng, P.C., Pong, N.H., Zhao, H., Zhang, L., 2009. Dexrazoxane protects against doxorubicin-induced cardiomyopathy: upregulation of Akt and Erk phosphorylation in a rat model. *Cancer Chemotherapy and Pharmacology* 63, 343–349.

192. Xu, X., Persson, H.L., Richardson, D.R., 2005. Molecular Pharmacology of the Interaction of Anthracyclines with Iron. *Mol. Pharmacol*. 68, 261–271.

193. Xu, X., Persson, H.L., Richardson, D.R., 2005. Molecular Pharmacology of the Interaction ofAnthracyclines with Iron. *Mol. Pharmacol*. 68, 261–271.

194. Xue, M., Jackson, C.J., 2015. Extracellular Matrix Reorganization During Wound Healing and Its Impact on Abnormal Scarring. *Adv. Wound Care* 4, 119–136.

195. Yin, F.C., Spurgeon, H.A., Rakusan, K., Weisfeldt, M.L., Lakatta, E.G., 1982. Use of tibial length to quantify cardiac hypertrophy: application in the ageing rat. *Heart and Circulatory Physiology*. 243(6), H941 - H947.

196. Yu, A.F., Ky, B., 2016. Roadmap for biomarkers of cancer therapy cardiotoxicity. *Heart* 102, 425–430.

197. Yue, W., Chen, Z., Liu, H., Yan, Chen, Chen, M., Feng, D., Yan, Chaojun,Y., Wu, H., Du, L., Wang, Y., Liu, J., Huang, X., Xia, L., Liu, L., Wang, X., Jin, H., Wang, J., Song, Z., Hao, X., Chen, Q., 2014. A small natural molecule promotes mitochondrial fusion through inhibition of the deubiquitinase USP30. *Cell Res.* 24, 482–96.

198. Zhu, J.N., Fu, Y.H., Hu, Z.Q., Li, W.Y., Tang, C.M., Fei, H.W., Yang, H., Lin, Q.X., Gou, D.M., Wu, S.L., Shan, Z.X., 2017. Activation of miR-34a-5p/Sirt1/p66shc pathway contributes to doxorubicin-induced cardiotoxicity. *Sci. Rep*. 7, 1–12.

199. Zordoky, B.N.M., Anwar-Mohamed, A., Aboutabl, M.E., El-Kadi, A.O.S., 2011. Acute doxorubicin toxicity differentially alters cytochrome P450 expression and arachidonic acid metabolism in rat kidney and liver. *Drug Metab. Dispos*. 39, 1440–1450.

200. Zordoky, B.N.M., Anwar-Mohamed, A., Aboutabl, M.E., El-Kadi, A.O.S., 2010. Acute doxorubicin cardiotoxicity alters cardiac cytochrome P450 expression and arachidonic acid metabolism in rats. *Toxicol. Appl. Pharmacol*. 242, 38–46.

# Chapter 7. APPENDIXES

## *APPENDIX A: SUPPLEMENTARY RESULTS*

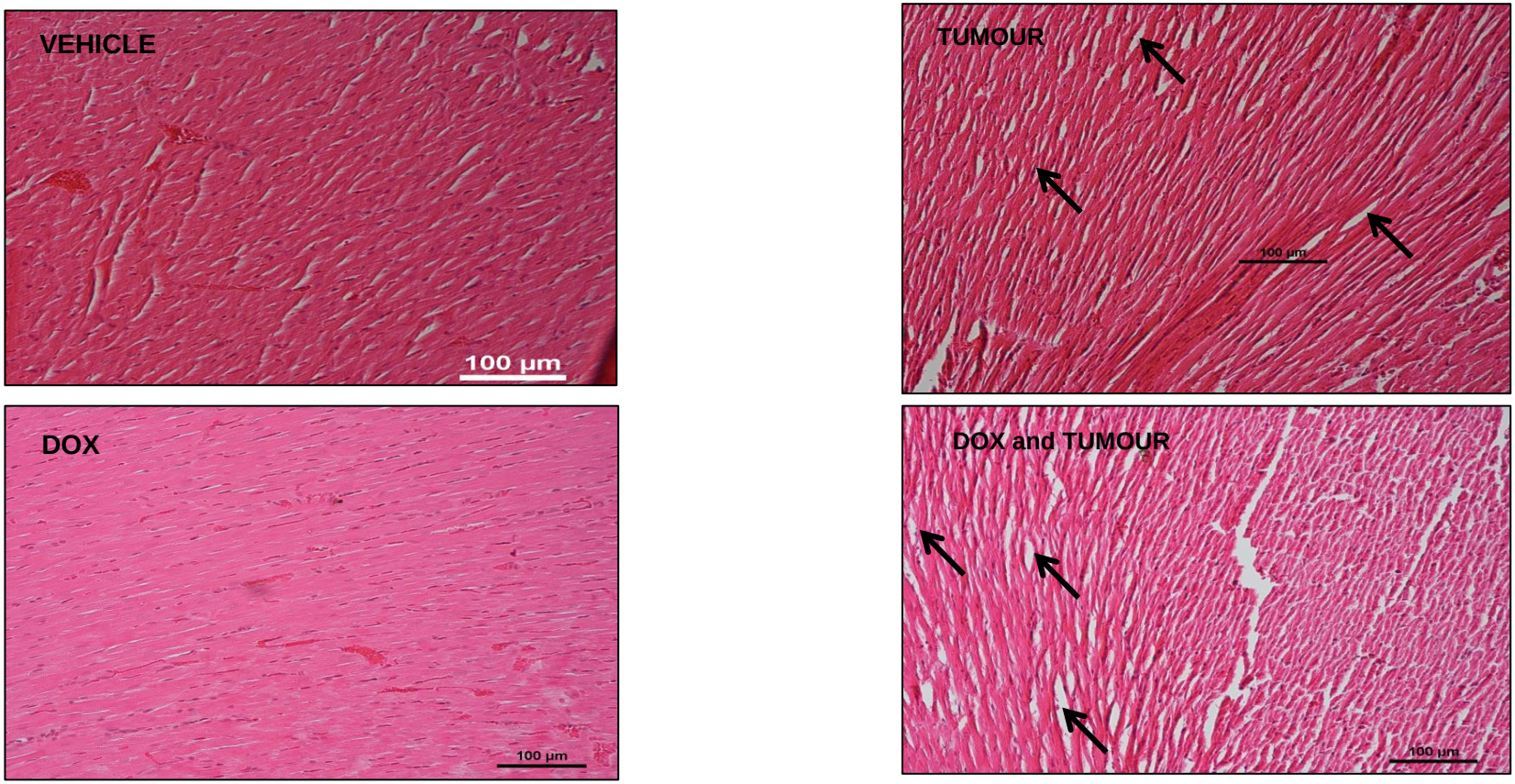


**Figure 7.1: H & E stains demonstrating cardiomyocyte morphology in preserved heart tissue from the 4-week groups.**

Tumour bearing animals exhibited less compact and wavy cardiomyocyte networks, with visible vacuolization and oedema (black arrows).

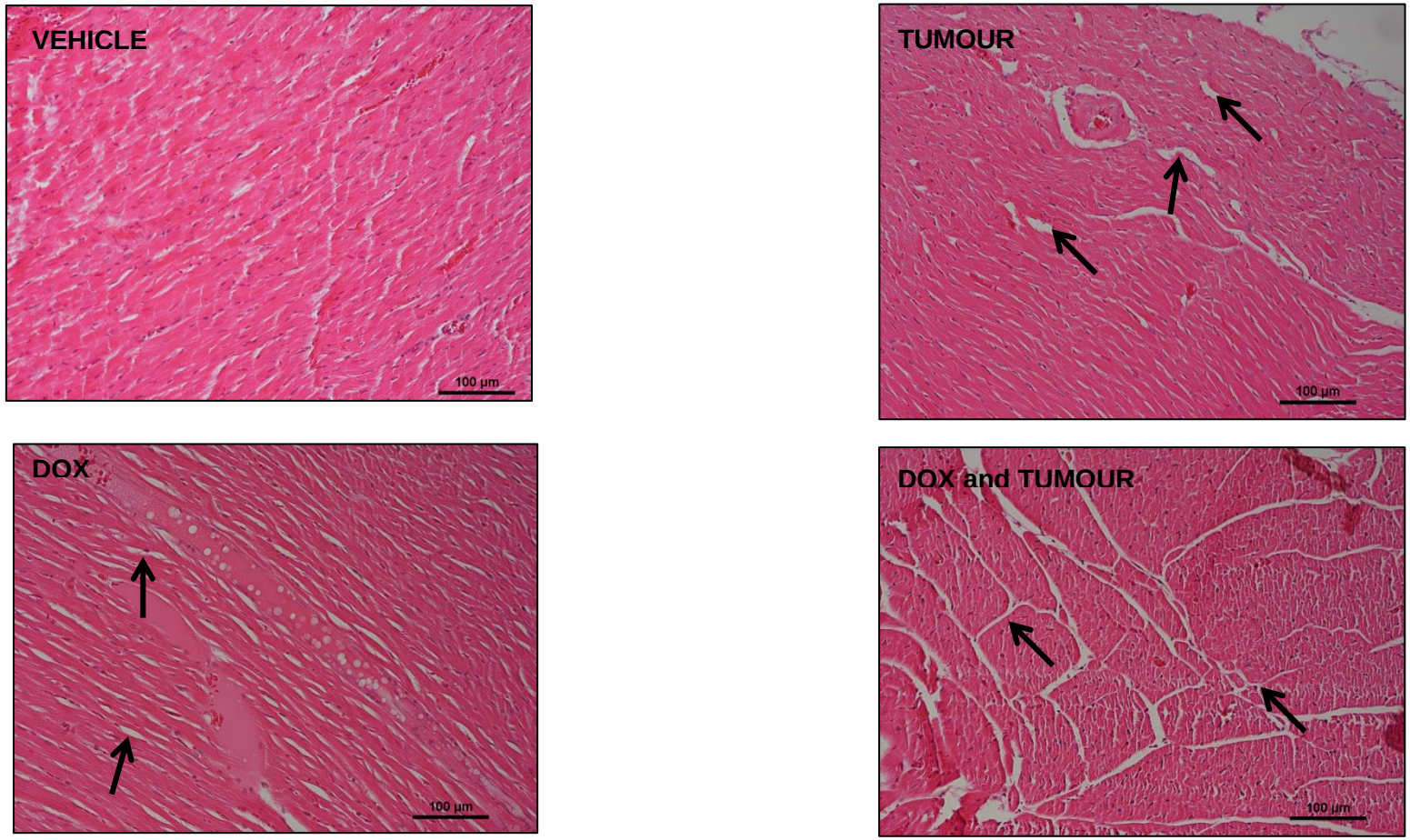


**Figure 7.2: H & E stains demonstrating cardiomyocyte morphology in preserved heart tissue from the eight week groups.**

Tumour bearing animals exhibited less compact cardiomyocyte networks, with vacuolization and oedema visible. After eight weeks of treatment, DOX-treated non-tumour bearing animals also began to exhibited less compact cardiomyocyte networks

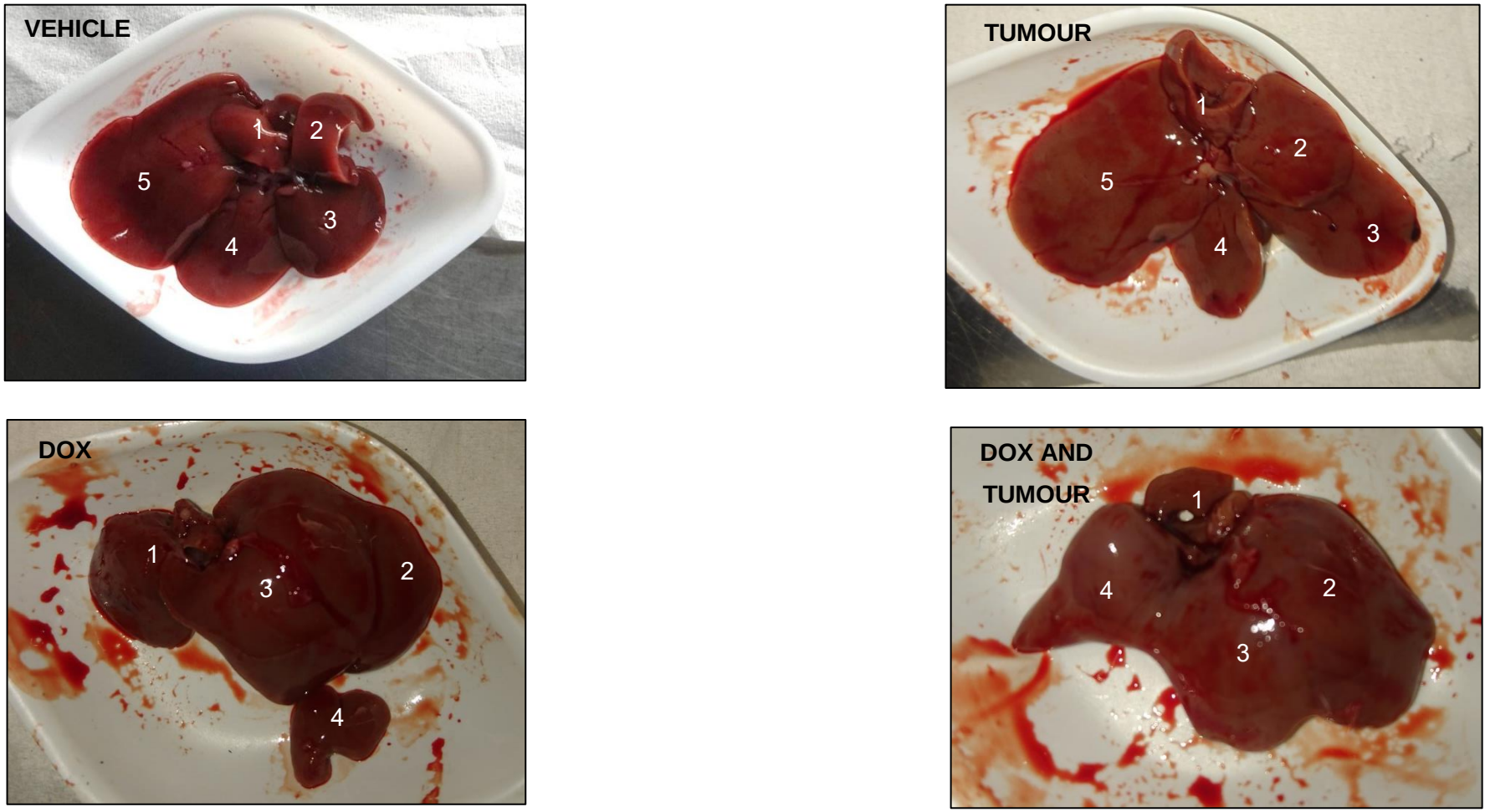


**Figure 7.3: Gross morphology of isolated livers after four weeks of treatment.**

All treatment groups with the exception of the vehicle controls demonstrated aberrant liver morphology characterized by varying levels of lobular fusion and swelling. This effect was more prominent in the DOX-treated animals, since they displayed fewer liver lobes characterized by conical shapes opposed to the flat shaped vehicle controls.

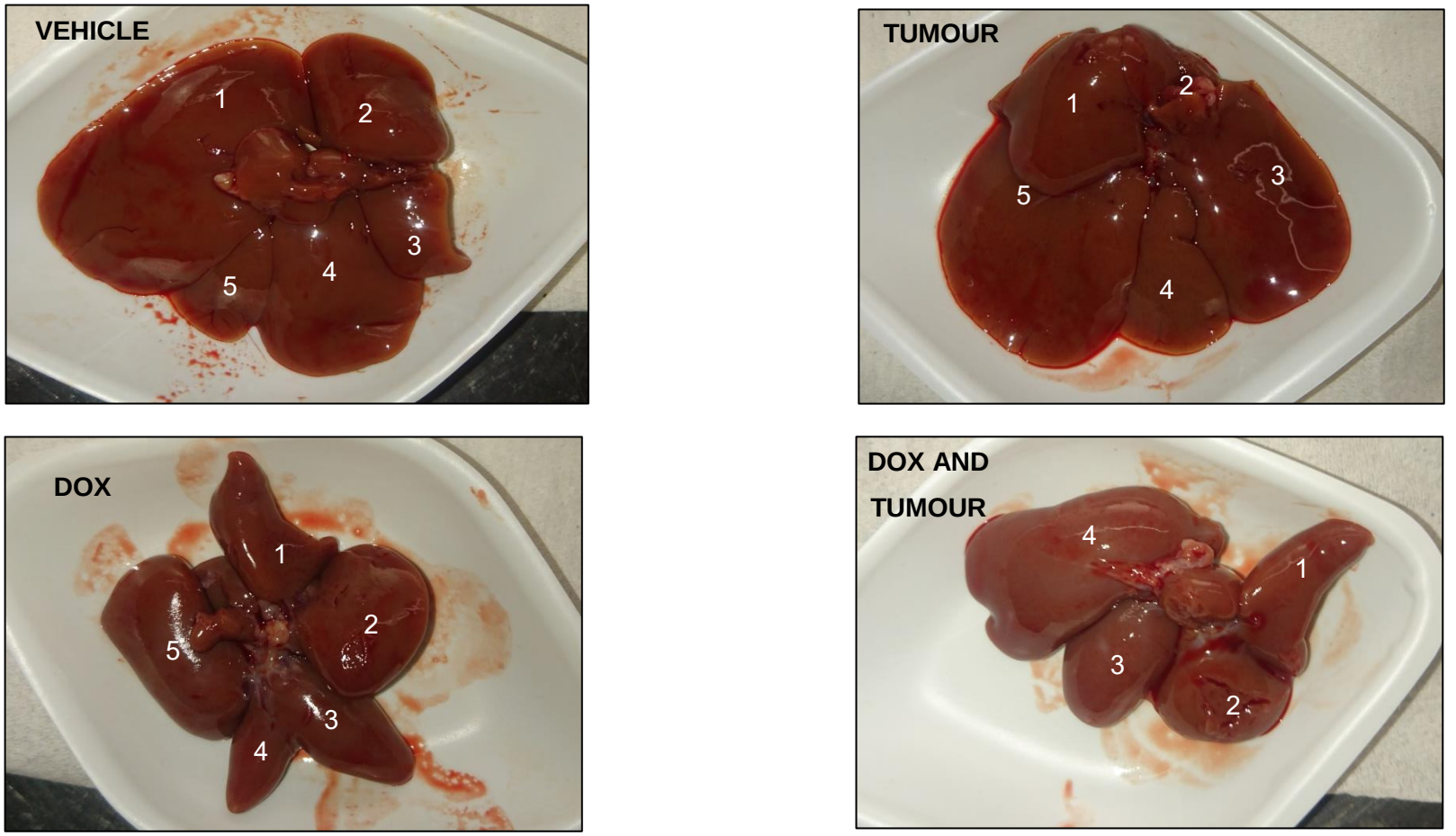


**Figure 7.4: Gross morphology of isolated livers after eight weeks treatment.**

After eight weeks, it was evident that DOX-treated animals' specifically demonstrated aberrant liver morphology characterized by lobular fusion and swelling as well as organ shrinkage. This effect was more prominent in the DOX-treated animals with extensive shrinking, conical shapes and pale coloration.

## Caspase 3

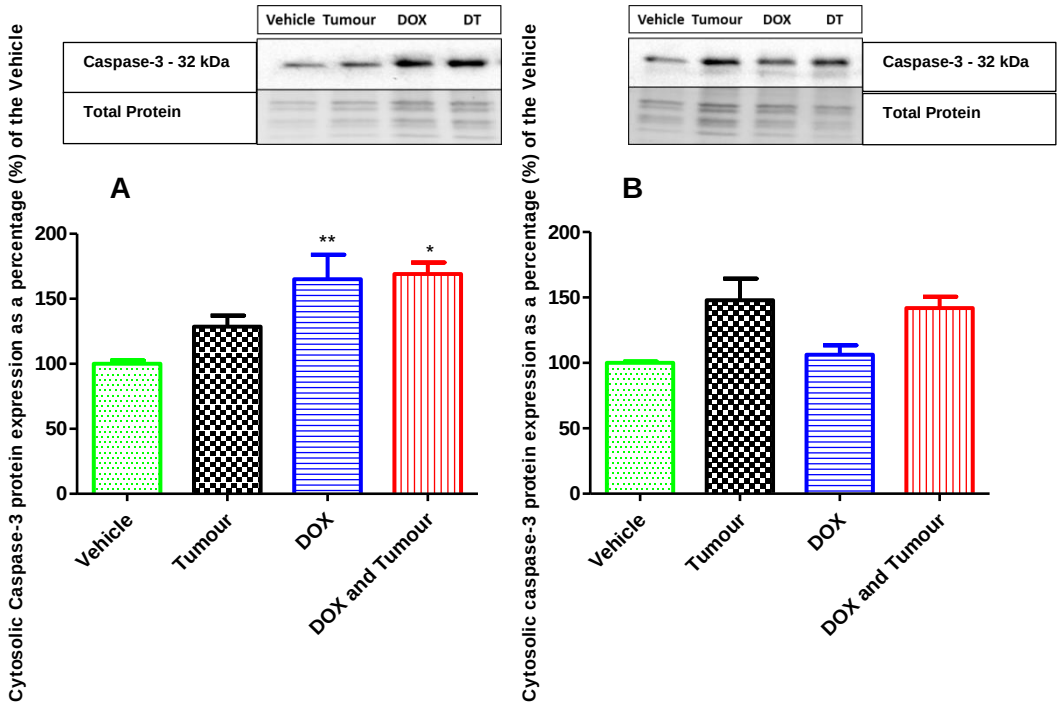


**Figure 7.5: Protein expression of Caspase-3 within the cytosolic component following four (A) and eight (B) weeks of treatment.**

Female Sprague-Dawley rats were randomly divided into four groups, and subjected to various treatment protocols over the course of four and eight weeks. Animals inoculated with LA7 cells exhibited mammary gland tumours and animals in the DOX groups were treated with 2.5 mg/kg DOX for four (**A**) and eight (**B**) weeks (cumulative dose: 10 and 20 mg/kg). Protein expression was evaluated in cardiac tissue samples via western blotting. Data was normalized to total protein and results are presented as mean ± SEM (n = 3 - 5), *p<0.05 vs Vehicle Control, ***p<0.001 vs Vehicle Control. Abbreviations: **DOX** – Doxorubicin, **DT** – DOX and Tumour.

## Cleaved Caspase 3

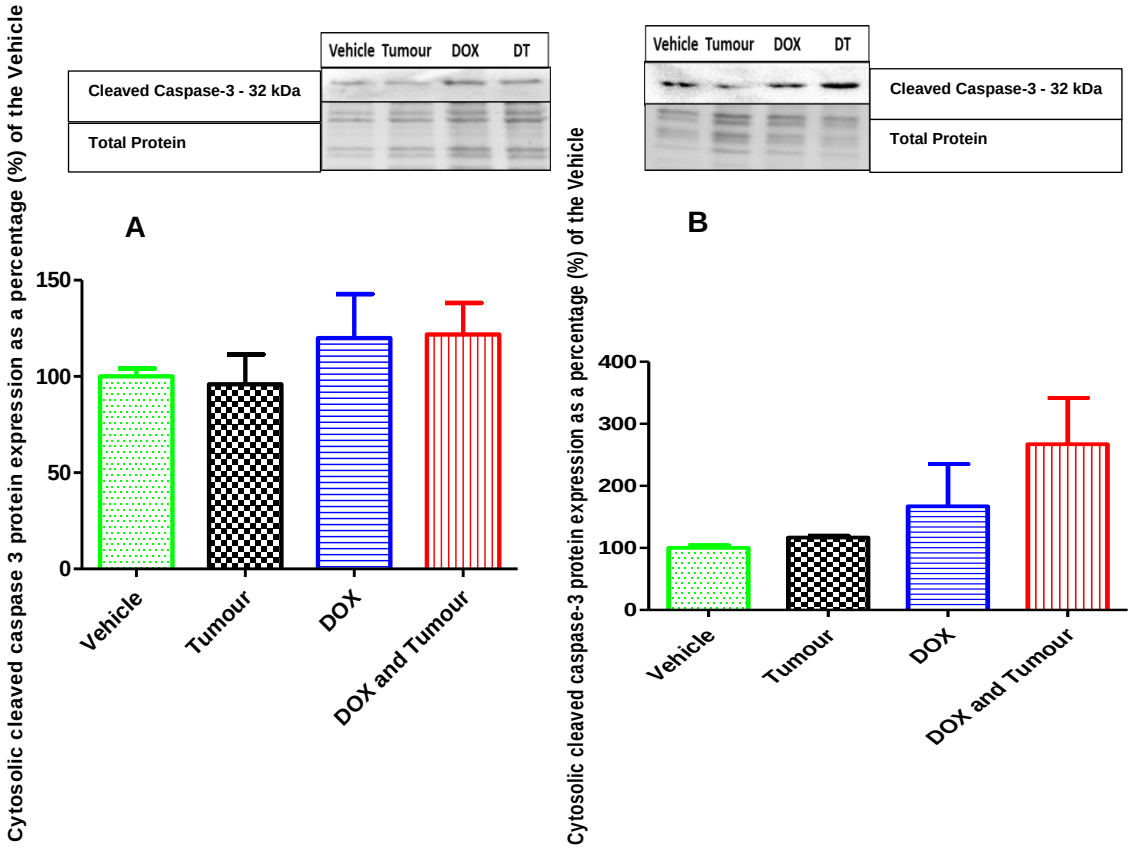


**Figure 7.6: Protein expression of Cleaved Caspase-3 within the cytosolic component following four (A) and eight (B) weeks of treatment.**

Female Sprague-Dawley rats were randomly divided into four groups, and subjected to various treatment protocols over the course of four and eight weeks. Animals inoculated with LA7 cells exhibited mammary gland tumours and animals in the DOX groups were treated with 2.5 mg/kg DOX for four (**A**) and eight (**B**) weeks (cumulative dose: 10 and 20 mg/kg). Protein expression was evaluated in cardiac tissue samples via western blotting. Data was normalized to total protein and results are presented as mean ± SEM (n = 3 - 5). Abbreviations: **DOX** – Doxorubicin, **DT** – DOX and Tumour.

## PARP

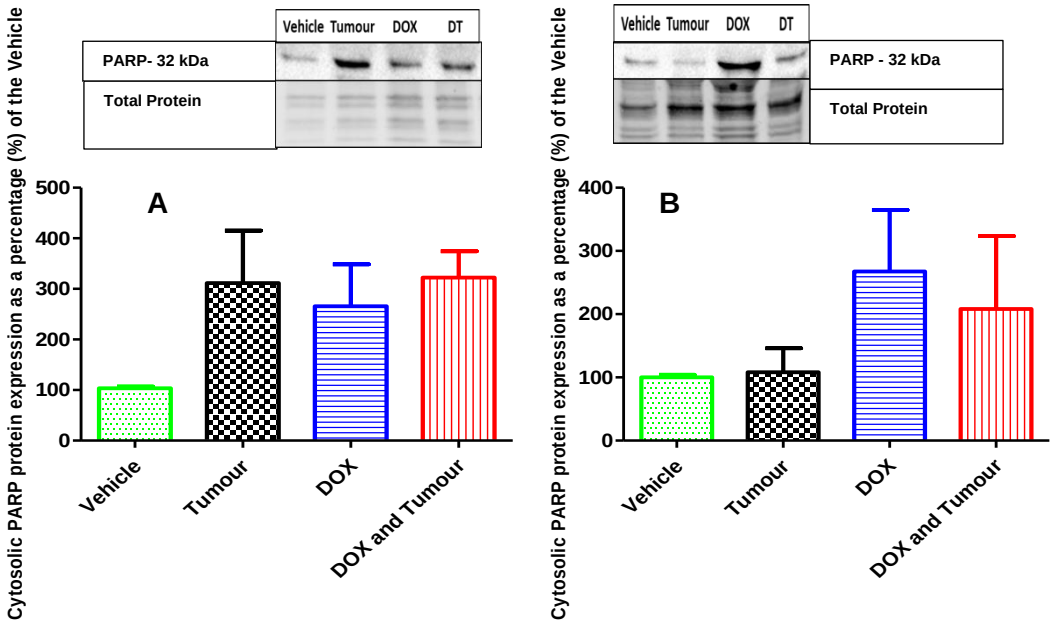


**Figure 7.7: Protein expression of PARP within the cytosolic component following four (A) and eight (B) weeks of treatment**

Female Sprague-Dawley rats were randomly divided into four groups, and subjected to various treatment protocols over the course of four and eight weeks. Animals inoculated with LA7 cells exhibited mammary gland tumours and animals in the DOX groups were treated with 2.5 mg/kg DOX for four (**A**) and eight (**B**) weeks (cumulative dose: 10 and 20 mg/kg). Protein expression was evaluated in cardiac tissue samples via western blotting. Data was normalized to total protein and results are presented as mean ± SEM (n = 3 - 5). Abbreviations: **DOX** – Doxorubicin, **DT** – DOX and Tumour, **PARP** – poly(ADP)ribose polymerase.

## Cleaved PARP

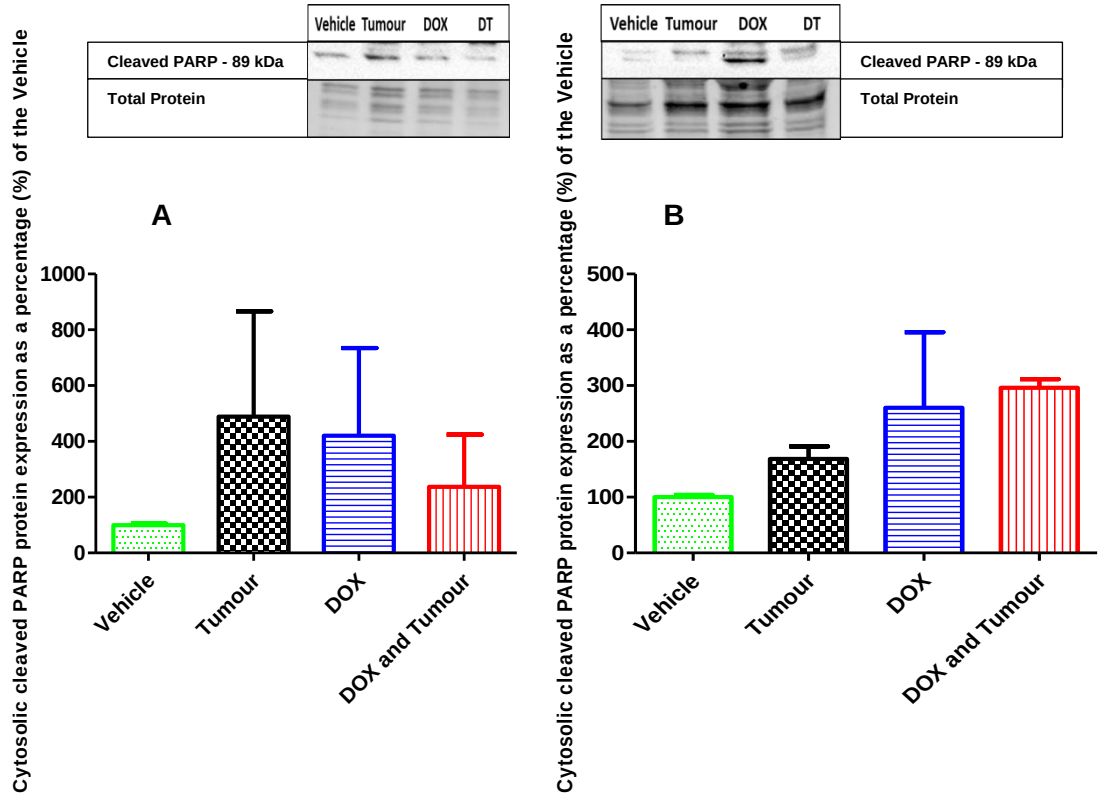


**Figure 7.8: Protein expression of cleaved PARP within the cytosolic component following four (A) and eight (B) weeks of treatment**

Female Sprague-Dawley rats were randomly divided into four groups, and subjected to various treatment protocols over the course of four and eight weeks. Animals inoculated with LA7 cells exhibited mammary gland tumours and animals in the DOX groups were treated with 2.5 mg/kg DOX for four (**A**) and eight (**B**) weeks (cumulative dose: 10 and 20 mg/kg). Protein expression was evaluated in cardiac tissue samples via western blotting. Data was normalized to total protein and results are presented as mean ± SEM (n = 3 - 5). Abbreviations: **DOX** – Doxorubicin, **DT** – DOX and Tumour, **PARP** – poly(ADP)ribose polymerase.

## *APPENDIX B: CELL CULTURE*

A. Cell Culturing

a. Make sure Lab coat is worn, wash hands, wear gloves, and then wash gloved hands.

b. Spray gloved hands with 70% ethanol, spray and wipe down laminar flow hoods, waste beakers, pipettes and all tubes placed in hoods with 70% ethanol.

c. Make up DMEM media

i. Get 500ml DMEM:HAMS F12 with Hepes media bottle and place in shaking incubator for an hour.

ii. Place FBS and antibiotics in bead bath for 15 minutes.

iii. Spray all with 70% ethanol and place in laminar flow hood, spray gloved hands as well.

iv. Extract 55ml of DMEM from its stock bottle using a pipette and put into a labelled tube.

v. Add 50ml of FBS and 5ml of antibiotic to the stock DMEM bottle.

vi. Swirl, shake or tilt gently and pipette into falcon tubes.

vii. Seal falcon tubes with parafilm and place in fridge.

viii. Add appropriate volumes of insulin and hydrocortisone to each falcon tube freshly on day of use.

d. Cell seeding

i. Get an appropriate vile from the liquid nitrogen canisters adhering to safety rules, and thaw at 37ºC.

ii. Add 5ml of growth media to a T25 flask.

iii. Pipette 1ml of the cells into the T25 flask, close cap, and swirl gently in a North-South-East-West manner.

iv. Incubate at 37ºC and 5% $CO_2$ until cells are 80% confluent.

e. Cell growth maintenance

    i. Remove cells from incubator, and examine for confluence and health under microscope.

    ii. If cells aren't confluent but growing and healthy, replace media every couple days and re-incubate, while checking for health and confluence regularly.

    iii. Once cells are about 80% confluent, split cells.

f. Splitting cells

    i. Place growth media, PBS and trypsin in bead bath for about 15 minutes.

    ii. Discard spent growth media, and gently wash with warm sterile PBS.

    iii. Add 4ml of trypsin to T25 and place in 37ºC shaking incubator for approximately 4-5 minutes to detach cells from bottom of flask.

    iv. Check for detachment from 3$^{rd}$ minute, and once detached and loose, add growth media double the amount of trypsin that was added to the flask to neutralize trypsin.

    v. Transfer all flask content to a sterile falcon tube, and centrifuge at 1500 rpm for 3 minutes.

    vi. Carefully remove and dispose of supernatant once cells have formed pellet at the bottom.

    vii. Re-suspend pellet in 2ml growth media for T25 flasks, and 4ml for T75 flasks.

    viii. Count cells if seeding is to be done, or Pipette 1ml each into sterile T75 flasks.

g. Counting cells

    i. After step F-vii above, wipe down hemocytometer with 70% ethanol,

    ii. Moisten hemocytometer surface with a brief breath, then add cover slip.

iii. Gently pipette 20µL of re-suspended cells under the cover slip covering each chamber of the hemocytometer, and avoid bubbles.

iv. Count the number of cells in 3 boxes in a diagonal manner on the top hemocytometer grid under a microscope, and do the same for bottom grid

v.

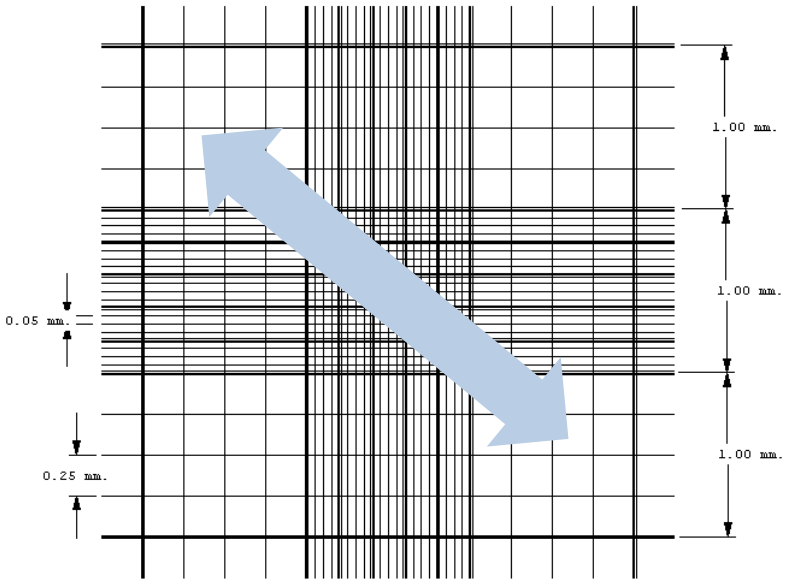


**Figure 7.9**: Hemocytometer grid Adapted from**:** http://www.hausserscientific.com/products/hausser_bright_line.html

vi. Each block is 0.1µL

vii. Calculate average of cells per block

viii. $\frac{Top\ cell\ count + bottom\ cell\ count}{6}$ = number of cells in 0.1µl

$$answer \times 10000 = no\ of\ cells\ in\ 1ml$$

$$no\ of\ cells\ in\ 1ml \times total\ volume\ of\ suspension = number\ of\ cells\ in\ total\ volume$$

$$\frac{number\ of\ cells\ in\ t.vol \leftrightarrow t.volume}{Cells\ to\ be\ seeded \leftrightarrow x\ volume\ ml?}$$

#cells to be seeded determined earlier depending on cell type, number of wells and treatment type.

$$\frac{xml}{1000} = x\ \mu l$$

$$x\mu L \times no\ of\ wells\ (y) = xy\ suspension\ to\ be\ pipetted$$

$$Growth\ media\ to\ be\ used\ with\ drugs\ (ml) \times no\ of\ wells = z\ total\ media\ needed$$

$$z\ total\ media\ needed - xy\ suspension = w\ media\ added\ ml$$

Pipette w ml of media and add xy ml of suspension
pipette into wells, (1 or 2 ml, depending on growth media decided on per well).

ix. Swirl in North-south-east-west manner and incubate.

h. Making up Doxorubicin (DOX) treatment

i. Dox Mr = 579.98 g/mol
total concentration for 4-week and 8-week treatment = 10 mg/Kg and 20 mg/kg = 2.5 mg/kg/week

ii. Dox stock = 4 µg/µL = initial concentration

1. Total Volume to be injected = 200 µL
2. Final Concentration = 2.5 mg/1000 g
3. Animal weight = A; Final mass = X; Final Volume = Y

$$X = \frac{2.5\ mg * A}{1000\ g}$$

$$Y = \frac{X * 1\ \mu L}{4\ \mu g}$$

$$Dissolve\ Y\ in\ 200\ \mu L - Y\ (Hanks\ Salt\ Solution)$$

i. Harvesting cells

i. Get two cooler boxes and fill with ice, work on ice the whole time

ii. Add eppis to represent your experimental groups

iii. Take T175 culture flasks from incubator, and remove media using aspirator.

iv. Add adequate trypsin to flask

v. Neutralize with double the volume of trypsin in media

vi. Aspirate and spin down at 1500 x g for 3 minutes

vii. Remove supernatant and re-suspend the harvested cells in 300 µL Hanks salt solution

viii. Place on ice,

ix. Proceed to inoculation

## *APPENDIX C: TUMOUR INNOCULATION*

I. Carefully aspirate 300 µL LA7:Hanks suspension mixture into syringe and maintain on ice.
II. Retrieve animal to be inoculated and anaesthetize with a low dose of Iso-fluorane.
III. Once reflex response from animal is muted, maintain unconscious animal with a lower dose of Isoflurane.
IV. Clean and disinfect injection site with ethanol.
V. Retrieve syringe and inject carefully into the mammary pad.
    a. Place animal in a supine position on a warm surgical block.
    b. Align syringe in a $10^{o}$ angle against the body and slowly penetrate below the nipple.
    c. Inject at a rate of 60 µL every 30 seconds for a total duration of 5 minutes.
VI. Upon completion of inoculation, carefully remove syringe and shut off anaesthesia supply.
VII. Place animal in clean and warm separate cage and monitor for recovery.

## *APPENDIX D: QUANTITATIVE POLYMERASE CHAIN REACTION*

- **RNA ISOLATION**

Kit used: MiRVana PARIS Total RNA Isolation Kit

**Materials needed:**

- B-mercaptoethanol
- 100% ethanol ACS grade
- Phosphate Buffered Saline
- RNASE-free PCR eppis
- Heating block
- Microcentrifuge

**Procedure**

1. The denaturing solution and the wash solutions were prepared according to manufacturer's instructions
2. Thaw previously frozen plasma samples on ice and transfer 400 µL of each sample into eppis on ice.
3. Add an equal volume of room temperature denaturing solution to the samples and vortex thoroughly. Incubate this mixture on ice for 5 minutes.
4. Subsequently, add a volume of acid-phenol:chloroform equivalent to the volume of the sample-denaturing solution mix to the eppi. Perform this process under a fume hood, and ensure caution as the acid-phenol solution is highly corrosive.
5. Upon addition, vortex thoroughly and centrifuge at 11,000 x g at room temperature for 5 minutes.
6. Upon centrifugation, the samples get separated into a bottom (lower) phase, a middle interphase and an aqueous (upper) phase. Carefully collect 500 µL of the aqueous phase without disturbing the interphase or lower phase and transfer into a new RNASE-free eppi.

7. At this point, 5 µL of the Cel-miR-39 spike-in is introduced into the sample for a final concentration of 5 pM. Vortex to mix.
8. Add 625 µL (1.25x) of 100% ethanol to the aqueous phase and mix thoroughly.
9. Set up the filter cartridge according to the manufacturer's steps and pipette a maximum of 700 µL of sample into the filters.
10. Centrifuge at 10,000 x g for 30 seconds, discard the collected flow-through, and repeat until entire aqueous phase has been passed through filter.
11. Proceed to follow the wash steps according to manufacturer's description.
12. Transfer the filter cartridge into a new collecting tube and elute with 100 µL of preheated elution solution.
13. Centrifuge, collect the eluted sample and store at -80 $^{o}$C.

- **cDNA Synthesis**

***Materials Required***:

- TAQMAN Advanced MicroRNA cDNA Synthesis kit
- RNASE-free Eppis (0.5 ml)
- RNASE-free pipette tips

Protocol

***Poly(A)Tailing Reaction***: Follow the manufacturer's instructions with the following considerations

- Retrieve the 50% PEG 8000 reagent and allow equilibrating to room temperature before use.
- Ensure to allow for errors in pipetting when calculating master mix volumes.
- Place sample mixes in thermal cycler and run according to the manufacturer's instructions.

***Adaptor Ligase Reaction***

- Prepare Adaptor ligase master-mix in 1.5 ml RNASE-free eppis, giving a 10% allowance for pipetting error
- Since the 50% PEG 8000 reagent is quite viscous, pipette slowly over 10 seconds for both the withdrawal and ejection.
- Vortex thoroughly and centrifuge slightly to draw down sample

***Reverse Transcriptase Reaction***

- Follow steps according to manufacturer's instructions, with an allowance for pipetting error.
- Product can be stored at -20 $^{o}$C for up to two months.

***miR Amplification Reaction***

- Perform according to manufacturer's instructions. Store at 20 $^{o}$C for up to two months of proceed to QPCR.

***Quantitative Polymerase Chain Reaction***

- Prepare a 0.1X dilution of TE buffer
  - 1350 µL of RNASE free water
  - 150 µL of TE buffer
- Prepare 1:10 dilution of cDNA template
  - 5 µL of cDNA template
  - 45 µL of TE buffer
- Prepare Taqman fast advanced assay master mix
- Transfer 15 µL of prepared master-mix to the assigned wells of the 96-well assay plate
- Transfer 5 µL of the cDNA template:TE buffer into the assigned wells of the assay plate.
- Proceed to run the qPCR instrument

***qPCR Experiment***

- Add 15 µl of the PCR master-mix which consists of 10 µl of the Taqman advanced master-mix (4444557, Thermofisher Scientific), 1 µl of the hydrolysis probe (A25576, Thermofisher Scientific) and 4 µl of RNASE-free water, onto 5 µl of a 1:10 dilution of the amplified sample in the 96-well microplates.
- Load Microplate onto the StepOnePlus ™ (Applied Biosystems, North Carolina, USA)
- The 40 minute experimental set-up was selected and run.

## *APPENDIX E: MITOCHONDRIAL ISOLATION*

**Mitochondria Isolation kit for Tissue**

**Kit Components (89901)**

Mitochondria Isolation Reagent A, 50 mL

Mitochondria Isolation Reagent B, 500 µL

Mitochondria Isolation Reagent C, 65 mL

Bovine Serum Albumin, 230 mg

**Components provided by user:**

Phosphate Buffered Saline (PBS); Also provided in kit, however we opted to utilize a self-made preparation.

Clean Dounce Homogenizers kept chilled in ice

Centrifuge Eppis

Centrifuge

Protease inhibitors

**Protocol:**

- Wash 80mg Tissue with 2 mL cold PBS twice, discard PBS
- Cut tissue into small pieces utilizing chilled sharp sterilized scissors
- Add 800 µL of prepared reagent A/BSA
- Confirm empirically determined requirement for dounce strokes
- For 80 mg rat cardiac tissue, 16 strokes required
- Perform dounce homogenization on ice (Do not exceed allow tissue exceed 2 minutes in reagent A)
- Add 800 µL reagent C and invert multiple times to mix (do not vortex).

- Centrifuge at 700 g (2900 rpm) for 10mins at 4 $^{o}$C.
- Carefully discard pellet and transfer supernatant to a new 2 ml eppi on ice
- Centrifuge supernatant at 3000 g (5900 rpm) for 15 minutes at 4 $^{o}$C.
- Remove cytosolic supernatant and store at -20 $^{o}$C.
- Add 500 µL of wash buffer to mitochondrial pellet
- Centrifuge at 12000 g (13,300 rpm) for 5 minutes; discard supernatant and store at -20 $^{o}$C.
- For western blotting, resuspend pellet in 200 µL of

## *APPENDIX F: WESTERN BLOTTING*

A. Sample Preparation

a. In a process carried out on ice at all times, retrieve frozen samples and weigh out sufficient tissue.

b. Place tissue in chilled eppi and cut to small pieces with chilled sharp sterile scissors

c. Add sufficient RIPA buffer to sample tissue (≈ 400 µL per 80 mg of cardiac tissue)

d. Homogenize tissue for approximately one minute on ice, or until sufficiently homogenized.

e. Centrifugation

i. Centrifuge at 12 000 x g for 20 minutes.

ii. Allow foam to settle

iii. Retrieve supernatant and discard pellet.

iv. Store at -80 $^{o}$C or proceed to protein concentration step

f. Measure Protein concentration

i. Retrieve and maintain all samples on ice.

ii. Vortex sample eppis and pipette 2 µl of each sample onto Direct Detect ™ Assay-free cards (Merek, DDAC00010-GR)

iii. Measure protein concentration using Direct Detect ™ spectrometer using the RIPA calibration curve, and RIPA buffer as a blank.

iv. Read protein concentration values and determine loading volumes.

g. Make volumes of protein samples in Laemlli's sample buffer.

h. Boil at 95 -100 $^{o}$C for 5 minutes

i. Proceed to running step or store in -80$^{0}$C freezer

B. Preparation of Gels

a. Prepare well combs, back plates, front plates and clean thoroughly with 70% alcohol.

b. Set up front and back plates in Western blot Gel holder.

c. Make resolving gel using TGX Stain-Free ™ FastCast ™ (BIO-RAD) kit according to manufacturer's protocol (APPENDIX J: REAGENT PREPARATION, pg. 142).

d. Briskly fill in plates until green level with Pasteur pipettes

e. Make stacking gel according to BIO-Rad Protocols (APPENDIX J: REAGENT PREPARATION, pg. 142)

f. Add stacking gel till brim, and place combs in, allow setting for about 30 minutes.

C. Loading and running samples

a. Remove combs from set gels, place gels in tank and add 1X running buffer (APPENDIX J: REAGENT PREPARATION, pg. 142) into middle compartment letting it overflow into tank until it levels with the middle compartment.

b. Boil samples for five minutes, load 4 µl BLUeye prestained ladder in the first well.

c. Centrifuge boiled samples for 10 seconds, and then load into appropriate wells.

d. Place lid onto tank ensuring electrodes are oriented correctly,

e. Connect to voltage box and run at 100 V for 10 minutes then 150 V for 30 minutes or until running front runs completely through the gel. Check that there are bubbles while voltage is running.

D. Gel activation

a. Activate fully run gel on the Chemi-Doc system using the Imagelab

b. Remove gel, place in running buffer, then view on chemidoc: using stain free gel application> gel activation> gels used in blotting.

c. 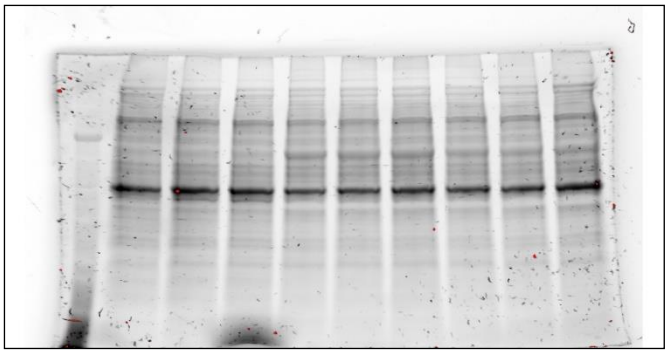

**Figure 7.10: Gel activation Transfer**

Gel activation results displaying protein samples successfully run and separated through acrylamide gel

d. Make up 1X RTA transfer buffer (APPENDIX J: REAGENT PREPARATION, pg. 142)

e. Soak top and bottom transfer stacks in transfer buffer.

f. Soak PVDF membrane in methanol

g. Then soak PVDF membrane in transfer buffer for about 3 minutes for equilibration.

h. Prepare sandwich (bottom stack, PVDF membrane, Gel, and then top stack)

i. Roll out bubbles on each layer to ensure complete contact.

E. Membrane activation

a. Place membrane in ethanol

b. Activate PVDF membrane post transfer using the ChemiDoc, and image-line software. Blots>stain free blot

c. 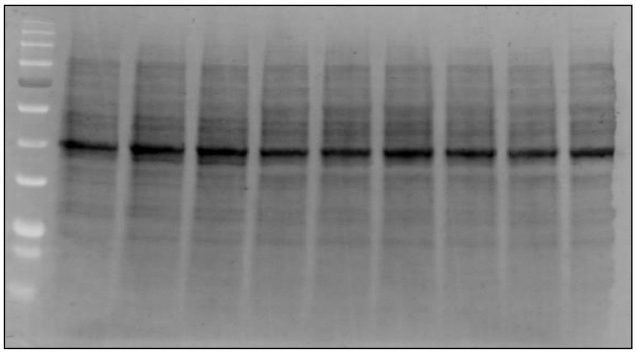

**Figure 7.11: Membrane activation.**

Membrane activation results demonstrating successful transfer of proteins from gel to PVDF membrane. Membrane activation blots for total protein were also utilized as the total protein standard for normalization.

F. Blocking

   a. Block the membrane using 5% milk,

   b. 5ml of milk in 95 ml of TBS tween for an hour on the shaker

G. Antibody binding

   a. Primary Incubation

      i. Wash three times for five minute intervals in TBS-tween, then place in primary antibody

   b. Incubate overnight or for two days at 4$^{o}$ C.

H. Secondary Incubation

   a. Wash in TBS-tween three times for at least five minutes intervals

   b. Incubate in secondary antibody for at least an hour at room temperature

I. visualization

   a. Make up ECL (APPENDIX J: REAGENT PREPARATION, pg. 142), and add approximately 200 - 300 µl to membrane, roll to spread evenly.

   b. Remove excess ECL

   c. Visualize on Chemi-doc ™ spectrophotometer utilizing image-line software

   d. Analyze bands

## *APPENDIX G: HISTOLOGY*

### Fixation:

Tissue samples were fixed in ample amount of diluted formalin (4% formaldehyde) for at least 24 hrs. Formalin a cross-linking fixative attaches to primary amines to form stable cross-links within and between proteins.

(i). Retrieve tissue samples preserved in formalin and dissect with transverse incisions performed in one motion over the cross-section of the left and right ventricles.

(ii). Place cut sections in labelled histological cassettes and placed in 50 % ethanol.

(iii). Transport samples carefully in 50 % ethanol to the automatic tissue processor.

### Automatic Tissue Processing:

**Reagents Required**:

Ethanol (70 %, 90 %, 95 %, 100 %)

Xylene – Sigma

Paraffin wax – Merck (histological melting point 56 °C)

Processing Method

a) Dehydration

a. 70 % ethanol – 1.5 hr

b. 70 % ethanol – 1.5 hr

c. 90 % ethanol – 1.5 hr

d. 95 % ethanol – 1.5 hr

e. 95 % ethanol – 1.5 hr

f. 100 % ethanol – 1.5 hr

g. 100 % ethanol – 2.0 hr

b) Clearing

a. Xylene – 1.5 hr

b. Xylene – 1.5 hr

c) Impregnation

a. Paraffin wax – 2.0 hr

b. Paraffin wax – 2.0 hr

Total processing time = 20 hrs

**Tissue Embedding**

(i). Collect processed tissue from tissue processor

(ii). Move to embedding machine

(iii). Add some melted wax into the appropriate mould

(iv). Place tissue sample in carefully and flat on bottom surface

(v). Place cassette bottom on mould

(vi). Place on cold surface to solidify

(vii). Trim mould once solidified

## *APPENDIX H: MANUAL HEMATOXYLIN AND EOSIN STAINING*

### *Materials Needed:*

**Mayer's Hematoxylin**: is commercially available (Merch Millipore, SAAR2822001LC). This reagent was procured and stored at room temperature. Before staining, a sufficient amount was filtered through Whatman's number 2 filter paper.

**Eosin**: Also commercially available (Leica Biosystems, 3801600E); stock was procured and subsequently diluted (5% in 100% ethanol) to form a working solution utilized in the stains. The stock solution was stored at room temperature.

**Ethanol**: 100% ethanol stored at room temperature was diluted with distilled water to produce working solutions utilized in the various dehydration steps.

**Xylene**: commercially available (Merck, 1086619190). Stock was stored at room temperature and sufficient amount aliquoted for utilization in the clearing steps.

- **Steps**
- Process and section heart tissue into 5 µm sections as explained above
- Carefully mount sectioned tissue onto appropriate slides and allow to air dry on heating block
- Fill the different baths of the Leica Auto stainer XL, with appropriate solutions as described below
- Load slides carefully into the slide slots of the Leica Auto stainer XL's slide holders.
- Utilizing a timer, manually place the slide holder into the first staining bath, and manually transfer to subsequent staining baths, paying meticulous attention to time and step number.

**Table 7.1: Table of detailed steps for H & E staining.**

| Step number | Solution | Time (minutes) |
|---|---|---|
| **1** | Xylene | 5 |
| **2** | Xylene | 5 |
| **3** | Ethanol (99%) | 2 |

| | | |
|---|---|---|
| **4** | Ethanol (99%) | 2 |
| **5** | Ethanol (96%) | 2 |
| **6** | Ethanol (70%) | 2 |
| **7** | Tap water | 2 |
| **8** | Mayer's Hematoxylin | 8 |
| **9** | Running water | 5 |
| **10** | Eosin (0.1%) | 4 |
| **11** | Running water | 1 |
| **12** | Ethanol (70%) | 0.5 |
| **13** | Ethanol (96%) | 0.5 |
| **14** | Ethanol (99%) | 0.5 |
| **15** | Ethanol (99%) | 0.5 |
| **16** | Xylene | 1 |

- Once all steps are completed, mount coverslips onto the slide sections using DPX mounting media. Subsequently allow the slides to air-dry for a period of 48 hrs.

## *APPENDIX I: PICROSIRIUS RED STAIN*

### *Materials Needed:*

**Picro-Sirius Red:** was made up using the following constituents

0.5g of Sirius red (Sigma-Aldrich, 36-554-8)

500 ml of a saturated solution of aqueous picric acid.

*Solid picric was not utilized due to its extremely volatile nature

**Weigert's Haematoxylin:** Commercially available Weigert's hematoxylin was poured and stored at room temperature until use.

**Xylene:** commercially available (Merck, 1086619190). Stock was stored at room temperature and sufficient amount aliquoted for utilization in the clearing steps

**Acidified Water:** was made up using the following reagents

To make up 0.5 % acidified water, add 5 ml of acetic acid to 100 ml distilled water.

### *Steps*

- Dry sectioned slides to be stained on heating blocks
- Fill staining baths with the appropriate staining solutions and label
- Execute the staining procedure according to the following steps

**Table 7.2: Table of detailed steps for Picrosirius Red Staining.**

| Step | Reagent | Duration |
|---|---|---|
| **1** | Xylene | 5 minutes |
| **2** | Xylene | 5 minutes |
| **3** | 99% ethanol | 2 minutes |
| **4** | 99% ethanol | 2 minutes |
| **5** | 96% ethanol | 2 minutes |
| **6** | 70% ethanol | 2 minutes |
| **7** | Tap water | 2 minutes |

| | | |
|---|---|---|
| **8** | Weigert's haematoxylin | 12 minutes |
| **9** | Running tap water | 10 minutes |
| **10** | Picrosirius red | 60 minutes |
| **11** | Acidified water | 2 minutes |
| **12** | Acidified water | 2 minutes |
| **13** | 100% ethanol | 5 dips |
| **14** | 100% ethanol | 5 dips |
| **15** | 100% ethanol | 5 dips |
| **16** | Xylene | 1 minutes |
| **17** | Xylene | 2 minutes |

With all steps being followed, one round of staining should last a duration of ± 110 minutes.

- Upon completion of staining protocol, place slides on absorbent surface to dry for approximately 10 minutes
- Carefully mount coverslips onto slides using dpx mounting media, take care to avoid bubbles.

## *APPENDIX J: REAGENT PREPARATION*

Protocol 1: Growth Medium

Materials needed:

- 500 mL DMEM:F12 1:1 with HEPES
- 50 mL FBS (10%)
- 5 mL Penicillin Streptomycin (PenStrep) solution
- 50 nM hydrocortisone
- 0.005 mg/ml insulin

Preparation

- Thaw all components in the 37 $^{o}$C bead bath.
- Under sterile working conditions, pipette 55 mL of DMEM from the stock bottle
- Add 50 mL filtered FBS and PenStrep and invert gently to mix.
- Aliquot into 50 ml falcon tubes and store at 4 $^{o}$C.
- Add insulin and hydrocortisone freshly before use

Protocol 2: Doxorubicin stock

Materials needed:

- Doxorubicin Hydrochloride (Mg = 579.98 g/mol) at 4mg/mL
- Hanks Salt solution (H8264-500ML, Sigma/MERCK)

Preparation

- Under sterile conditions, dissolve 50 mg Doxorubicin in 12.5 mL of Hanks salt solution
- Store in the dark at 4 $^{o}$C and dilute to 2.5mg/kg/week per animal for treatment

Protocol 3: Mitochondrial isolation

Materials needed:

- Reagent A
- Reagent C
- Wash Buffer
- Bovine serum albumin
- Protease inhibitor cocktail
- NAF
- $Na_3VO_4$
- PMSF

Preparation:

- For 2 samples, add 8.4 mg of BSA to 2.1 mL reagent A
- Dilute 1.1 ml of wash buffer in an equal volume of $dH_2O$

| | Reagent A/BSA (2.1 mL) | Reagent C (2.2 mL) |
|---|---|---|
| PI Cocktail | 88.2 µL | 92.4 µL |
| NAF | 10.5 µL | 11 µL |
| $Na_3VO_4$ | 10.5 µL | 11 µL |
| PMSF | 21 µL | 22 µL |

Protocol 4: Phosphate Buffer Saline (PBS)

Materials needed:

- 16 g NaCl
- 0.4 g KCl
- 2.88 g $Na_2HPO_4$
- 0.48 g $KH_2PO_4$

Preparation:

- Dissolve all components in 1 L of distilled water
- Adjust to 7.4 pH
- Fill up to 2 L with distilled water
- Autoclave

Protocol 5: 95% alcohol

- Dilute 950 mL of 100% ethanol in 50 mL distilled water

Protocol 6: 70% alcohol

- Dilute 700 mL 100% ethanol in 300 mL distilled water

Protocol 7: RIPA Buffer

- Prepare 50 mM Tris-HCL:
    - Add 700 mg Tris to 75 mL distilled water.
    - Add 900 mg NaCl and stir then adjust pH to 7.4.
    - Aliquot and store at 4 $^{o}$C

Protocol 8: RIPA working solution

- To 1 ml of RIPA buffer, add 42 µL of Protease inhibitor cocktail, 5 µL NaF, 5 µL $Na_3VO_4$ and 10 µL Phenylmethylsulponyl Fluoride (PMSF)

Protocol 9: Bovine serum Albumin (BSA)

- To prepare a 2 mg/mL stock of BSA, weigh off 20 mg and mix thoroughly in 10 mL of distilled water.
- Freeze in aliquots of 1 mL

Protocol 10: Laemmli's Sample Buffer (Stock)

- 3.8 mL distilled water
- 1 ML 0.5M Tris-HCL, pH 6.8
- 0.8 mL glycerol

- 1.6 mL 10% (w/v) SDS
- 0.4 – 1.0 mL 0.05% (w/v) Bromophenol blue

For western Blotting, make a working solution by adding 150 µL β-mercaptoethanol to 850 µL Laemmli's stock Solution.

Protocol 11: 10% Sodium dodecyl sulphate (SDS)

- Weigh out 50 g SDS and add 500 mL distilled water

Protocol 12: 10X running buffer

- A 5 L 10X running buffer pack was purchased from Bio-RAD (1610772)
- Buffer make up includes (25 mM Tris, 192 mM glycine, 0.1% SDS).
- Dilution to 1X stabilizes pH at 8.3.
- Dilution to 1X (100 mL of 10X running buffer made up to 1 L with $dH_2O$)

Protocol 13: Transfer buffer (Bio-Rad, 1704272)

- To make up 1 L transfer buffer, dilute 200 mL 5X BIO-RAD Transblot ® Turbo ™ RTA transfer buffer in 200 mL 100% alcohol, and 600 mL $dH_2O$.

Protocol 14: 10X TBS

- Dissolve 24.2 g Tris and 80 g NaCl in 600 mL distilled water
- Adjust pH to 7.6 with HCL
- Fill up to 1L with distilled water
- To make up TBS tween, mix 100 mL 10X TBS in 900 mL distilled water with 1 mL Tween 20.

Protocol 15: 10% Ammonium Persulphate (APS)

- Dissolve 0.5 g APS in 5 mL distilled water.

Protocol 16: Tris pH 8.8

- Dissolve 6.057 g Tris (100 mM) in 400 mL distilled water, mix and adjust pH to 6.7 using HCL.

- Make up final volume to 500 mL with distilled water

Protocol 17: BIO-RAD TGX Stain-free ™ Fastcast ™ Gels.

- To make one 1.00 mm mini Gel using the Bio-Rad 12% stain-free fastcast ™ acrylamide kit;

| | 1.0 mm Bio-Rad Glass plates (n = gels) | |
|---|---|---|
| | Stacker | Resolver |
| Resolver A | - | 3 ml * n |
| Resolver B | - | 3 ml * n |
| Stacker A | 1 ml * n | - |
| Stacker B | 1 ml * n | - |
| Total Volume | 2 ml * n | 6 ml * n |
| TEMED | 2 µl * n | 3 µl * n |
| 10% APS | 10 µl * n | 30 µl * n |

- 

- Stir and dispense the resolving gel first, then the stacking gel, and then insert well combs and allow setting for ± 45 minutes.

Note: add 75 µL TCE to resolving solution if the fast cast gels are not stain-free

Protocol 18: Milk blocking solution

- Weigh out 5 g fat-free instant milk powder and dissolve in 100 ml TBS-tween.
- Alternatively, dissolve 5 ml Fat free milk in 95 ml TBS-tween.

Protocol 19: Primary ($1^{o}$) and secondary ($2^{o}$) Antibody

- Pipette appropriate antibody volume according to recommended or optimized dilution ratios into 5 mL TBS-tween.

**Protocol 20: Clarity ™ Western ECL Substrate, 200 ml (Bio-Rad, 1705060)**

- Mix equal volumes of white and black clarity substrates preferably in the dark.

Protocol 21: Stripping Buffer

- 7.5 g glycine

- 0.5 g SDS
- 5 mL Tween
- Dissolve in ± 300 mL distilled water
- Adjust pH to 2.2
- Fill up to the 500 mL with distilled water

## *APPENDIX K: ETHICS LETTER*

UNIVERSITEIT
STELLENBOSCH
UNIVERSITY

**Protocol Approval**

Date: 15 January 2018

PI Name: Mr Temitope Ogundipe

Protocol #:1701

Title: Identification of Early Markers of Cardiotoxicity Induced by Cancer/Chemotherapy by Targeting MicroRNAs

Dear Temitope Ogundipe ,

The Identification of Early Markers of Cardiotoxicity Induced by Cancer/Chemotherapy by Targeting MicroRNAs , was reviewed on 15 January 2018 by the Research Ethics Committee: Animal Care and Use via committee review procedures and was approved. Please note that this clearance is only valid for a period of twelve months. Ethics clearance of protocols spanning more than one year must be renewed annually through submission of a progress report, up to a maximum of three years.

**Applicants are reminded that they are expected to comply with accepted standards for the use of animals in research and teaching as reflected in the South African National Standards 10386: 2008. The SANS 10386: 2008 document is available on the Division for Research Developments website www.sun.ac.za/research.**

As provided for in the Veterinary and Para-Veterinary Professions Act, 1982. It is the principal investigator's responsibility to ensure that all study participants are registered with or have been authorised by the South African Veterinary Council (SAVC) to perform the procedures on animals, or will be performing the procedures under the direct and continuous supervision of a SAVC-registered veterinary professional or SAVC-registered para-veterinary professional, who are acting within the scope of practice for their profession.

Please remember to use your protocol number 1701 on any documents or correspondence with the REC: ACU concerning your research protocol.

Please note that the REC: ACU has the prerogative and authority to ask further questions, seek additional information, require further modifications or monitor the conduct of your research.

Any event not consistent with routine expected outcomes that results in any unexpected animal welfare issue (death, disease, or prolonged distress) or human health risks (zoonotic disease or exposure, injuries) must be reported to the committee, by creating an Adverse Event submission within the system.

We wish you the best as you conduct your research.

If you have any questions or need further help, please contact the REC: ACU Secretariat at wabeukes@sun.ac.za or 021 808 9003.

Sincerely,

Winston Beukes

REC: ACU Secretariat

Research Ethics Committee: Animal Care and Use

**Figure 7.12: Ethical Approval Letter**

## *APPENDIX L: PERMISSIONS*

**ELSEVIER LICENSE**
**TERMS AND CONDITIONS**

Oct 09, 2019

This Agreement between Mr. Temitope R. Ogundipe ("You") and Elsevier ("Elsevier") consists of your license details and the terms and conditions provided by Elsevier and Copyright Clearance Center.

| | |
|---|---|
| License Number | 4684780670070 |
| License date | Oct 09, 2019 |
| Licensed Content Publisher | Elsevier |
| Licensed Content Publication | The Lancet |
| Licensed Content Title | Hypertension in developing countries |
| Licensed Content Author | M Mohsen Ibrahim,Albertino Damasceno |
| Licensed Content Date | 11–17 August 2012 |
| Licensed Content Volume | 380 |
| Licensed Content Issue | 9841 |
| Licensed Content Pages | 9 |
| Start Page | 611 |
| End Page | 619 |
| Type of Use | reuse in a thesis/dissertation |
| Portion | figures/tables/illustrations |
| Number of figures/tables/illustrations | 1 |
| Format | electronic |
| Are you the author of this Elsevier article? | No |
| Will you be translating? | No |
| Original figure numbers | FIGURE 2 |
| Title of your thesis/dissertation | IDENTIFICATION OF EARLY BIOMARKERS OF CARDIOTOXICITY DUE TO CANCER/CHEMOTHERAPY BY TARGETING MICRO-RNAS |
| Expected completion date | Dec 2019 |
| Estimated size (number of pages) | 140 |
| Requestor Location | Mr. Temitope R. Ogundipe<br>C/O Merriman and Bosman Street,<br>Mike De Vries Building<br>1st floor<br>STELLENBOSCH, WESTERN CAPE 7600<br>South Africa<br>Attn: Mr. Temitope R. Ogundipe |
| Publisher Tax ID | ZA 4110266048 |
| Total | 0,00 USD |
| Terms and Conditions | |

**INTRODUCTION**

1. The publisher for this copyrighted material is Elsevier. By clicking "accept" in connection with completing this licensing transaction, you agree that the following terms and conditions apply to this transaction (along with the Billing and Payment terms and conditions

**Figure 7.13: Permission Letter for Figure 1.1**

**ELSEVIER LICENSE**
**TERMS AND CONDITIONS**

Oct 09, 2019

This Agreement between Mr. Temitope R. Ogundipe ("You") and Elsevier ("Elsevier") consists of your license details and the terms and conditions provided by Elsevier and Copyright Clearance Center.

| | |
|---|---|
| License Number | 4684950347230 |
| License date | Oct 09, 2019 |
| Licensed Content Publisher | Elsevier |
| Licensed Content Publication | Vascular Pharmacology |
| Licensed Content Title | Cardiovascular disease 2005 — the global picture |
| Licensed Content Author | Allan D. Callow |
| Licensed Content Date | Nov 1, 2006 |
| Licensed Content Volume | 45 |
| Licensed Content Issue | 5 |
| Licensed Content Pages | 6 |
| Start Page | 302 |
| End Page | 307 |
| Type of Use | reuse in a thesis/dissertation |
| Intended publisher of new work | other |
| Portion | figures/tables/illustrations |
| Number of figures/tables/illustrations | 1 |
| Format | electronic |
| Are you the author of this Elsevier article? | No |
| Will you be translating? | No |
| Original figure numbers | Table 6 |
| Title of your thesis/dissertation | IDENTIFICATION OF EARLY BIOMARKERS OF CARDIOTOXICITY DUE TO CANCER/CHEMOTHERAPY BY TARGETING MICRO-RNAS |
| Expected completion date | Dec 2019 |
| Estimated size (number of pages) | 140 |
| Requestor Location | Mr. Temitope R. Ogundipe<br>C/O Merriman and Bosman Street,<br>Mike De Vries Building<br>1st floor<br>STELLENBOSCH, WESTERN CAPE 7600<br>South Africa<br>Attn: Mr. Temitope R. Ogundipe |
| Publisher Tax ID | ZA 4110266048 |
| Total | 0.00 USD |
| Terms and Conditions | |

**INTRODUCTION**

**Figure 7.14: Permission Letter for Table 1.1**

**WOLTERS KLUWER HEALTH, INC. LICENSE TERMS AND CONDITIONS**

Oct 09, 2019

This Agreement between Mr. Temitope R. Ogundipe ("You") and Wolters Kluwer Health, Inc. ("Wolters Kluwer Health, Inc.") consists of your license details and the terms and conditions provided by Wolters Kluwer Health, Inc. and Copyright Clearance Center.

| | |
|---|---|
| License Number | 4684951165426 |
| License date | Oct 09, 2019 |
| Licensed Content Publisher | Wolters Kluwer Health, Inc. |
| Licensed Content Publication | Circulation |
| Licensed Content Title | Global Variation in the Relative Burden of Stroke and Ischemic Heart Disease |
| Licensed Content Author | Anthony S. Kim, S. Claiborne Johnston |
| Licensed Content Date | Jul 5, 2011 |
| Licensed Content Volume | 124 |
| Licensed Content Issue | 3 |
| Type of Use | Dissertation/Thesis |
| Requestor type | Individual |
| STM publisher name | |
| Portion | Figures/table/illustration |
| Number of figures/tables/illustrations | 1 |
| Figures/tables/illustrations used | Figure 1 |
| Author of this Wolters Kluwer article | No |
| Title of your thesis / dissertation | IDENTIFICATION OF EARLY BIOMARKERS OF CARDIOTOXICITY DUE TO CANCER/CHEMOTHERAPY BY TARGETING MICRO-RNAS |
| Expected completion date | Dec 2019 |
| Estimated size(pages) | 140 |
| Requestor Location | Mr. Temitope R. Ogundipe<br>C/O Merriman and Bosman Street,<br>Mike De Vries Building<br>1st floor<br>STELLENBOSCH, WESTERN CAPE 7600<br>South Africa<br>Attn: Mr. Temitope R. Ogundipe |
| Publisher Tax ID | 4070265758 |
| Total | 0.00 USD |
| Terms and Conditions | |

**Wolters Kluwer Health Inc. Terms and Conditions**

1. **Duration of License:** Permission is granted for a one time use only. Rights herein do not apply to future reproductions, editions, revisions, or other derivative works. This permission shall be effective as of the date of execution by the parties for the maximum period of 12 months and should be renewed after the term expires.
    i. When content is to be republished in a book or journal the validity of this agreement should be the life of the book edition or journal issue.

**Figure 7.15: Permission Letter for Figure 1.2.**

**SPRINGER NATURE LICENSE**
**TERMS AND CONDITIONS**

Oct 09, 2019

This Agreement between Mr. Temitope R. Ogundipe ("You") and Springer Nature ("Springer Nature") consists of your license details and the terms and conditions provided by Springer Nature and Copyright Clearance Center.

| | |
|---|---|
| License Number | 4685000139783 |
| License date | Oct 09, 2019 |
| Licensed Content Publisher | Springer Nature |
| Licensed Content Publication | Cell Biology and Toxicology |
| Licensed Content Title | Adriamycin-induced oxidative mitochondrial cardiotoxicity |
| Licensed Content Author | J. M. Berthiaume, K. B. Wallace |
| Licensed Content Date | Jan 1, 2006 |
| Licensed Content Volume | 23 |
| Licensed Content Issue | 1 |
| Type of Use | Thesis/Dissertation |
| Requestor type | academic/university or research institute |
| Format | electronic |
| Portion | figures/tables/illustrations |
| Number of figures/tables/illustrations | 1 |
| Will you be translating? | no |
| Circulation/distribution | 30 - 99 |
| Author of this Springer Nature content | no |
| Title | IDENTIFICATION OF EARLY BIOMARKERS OF CARDIOTOXICITY DUE TO CANCER/CHEMOTHERAPY BY TARGETING MICRO-RNAS |
| Institution name | n/a |
| Expected presentation date | Dec 2019 |
| Portions | Figure 1 |
| Requestor Location | Mr. Temitope R. Ogundipe<br>C/O Merriman and Bosman Street,<br>Mike De Vries Building<br>1st floor<br>STELLENBOSCH, WESTERN CAPE 7600<br>South Africa<br>Attn: Mr. Temitope R. Ogundipe |
| Total | 0.00 USD |

Terms and Conditions

**Springer Nature Customer Service Centre GmbH**
**Terms and Conditions**

This agreement sets out the terms and conditions of the licence (the **Licence**) between you and **Springer Nature Customer Service Centre GmbH** (the **Licensor**). By clicking 'accept' and completing the transaction for the material (**Licensed Material**), you also confirm your acceptance of these terms and conditions.

**Figure 7.16: Permission Letter for Figure 1.6.**

**OXFORD UNIVERSITY PRESS LICENSE**
**TERMS AND CONDITIONS**

Oct 09, 2019

This Agreement between Mr. Temitope R. Ogundipe ("You") and Oxford University Press ("Oxford University Press") consists of your license details and the terms and conditions provided by Oxford University Press and Copyright Clearance Center.

| | |
|---|---|
| License Number | 4685000762973 |
| License date | Oct 09, 2019 |
| Licensed content publisher | Oxford University Press |
| Licensed content publication | Annals of Oncology |
| Licensed content title | Expert opinion on the use of anthracyclines in patients with advanced breast cancer at cardiac risk |
| Licensed content author | Barrett-Lee, P. J.; Dixon, J. M. |
| Licensed content date | Jan 19, 2009 |
| Type of Use | Thesis/Dissertation |
| Institution name | |
| Title of your work | IDENTIFICATION OF EARLY BIOMARKERS OF CARDIOTOXICITY DUE TO CANCER/CHEMOTHERAPY BY TARGETING MICRO-RNAS |
| Publisher of your work | n/a |
| Expected publication date | Dec 2019 |
| Permissions cost | 0.00 USD |
| Value added tax | 0.00 USD |
| Total | 0.00 USD |
| Title | IDENTIFICATION OF EARLY BIOMARKERS OF CARDIOTOXICITY DUE TO CANCER/CHEMOTHERAPY BY TARGETING MICRO-RNAS |
| Institution name | n/a |
| Expected presentation date | Dec 2019 |
| Portions | Figure 1 |
| Requestor Location | Mr. Temitope R. Ogundipe<br>C/O Merriman and Bosman Street,<br>Mike De Vries Building<br>1st floor<br>STELLENBOSCH, WESTERN CAPE 7600<br>South Africa<br>Attn: Mr. Temitope R. Ogundipe |
| Publisher Tax ID | GB125506730 |
| Total | 0.00 USD |
| Terms and Conditions | |

**STANDARD TERMS AND CONDITIONS FOR REPRODUCTION OF MATERIAL FROM AN OXFORD UNIVERSITY PRESS JOURNAL**

1. Use of the material is restricted to the type of use specified in your order details.
2. This permission covers the use of the material in the English language in the following territory: world. If you have requested additional permission to translate this material, the terms and conditions of this reuse will be set out in clause 12.
3. This permission is limited to the particular use authorized in (1) above and does not allow you to sanction its use elsewhere in any other format other than specified above, nor does it

**Figure 7.17: Permission Letter for Figure 1.7.**




October 10, 2019

Temitope Richard Ogundipe
Physiological Sciences
Stellenbosch University
c/o Merriman and Bosman St
Mike De Vries Bldg. 1st Fl.
Stellenbosch
Western Cape 7600
South Africa

Email: 16597370@sun.ac.za

Dear Temitope Ogundipe:

This is to grant you permission to include the following figure in your thesis titled "IDENTIFICATION OF EARLY BIOMARKERS OF CARDIOTOXICITY DUE TO CANCER/CHEMOTHERAPY BY TARGETING MICRO-RNAS" for Stellenbosch University:

> Figure 4 from X Xu, HL Persson, and DR Richardson (2005) Molecular Pharmacology of the Interaction of Anthracyclines with Iron, *Mol Pharmacol*, 68(2): 261-271; DOI: https://doi.org/10.1124/mol.105.013383

Permission to reproduce the figure is granted for one-time use in any format or medium including print and electronic. The authors and the source of the materials must be cited in full, including the article title, journal title, volume, year, and page numbers.

Sincerely yours,

Richard Dodenhoff
Journals Director



**Figure 7.18: Permission Letter for Figure 1.8.**

**ELSEVIER LICENSE**
**TERMS AND CONDITIONS**

Oct 09, 2019

This Agreement between Mr. Temitope R. Ogundipe ("You") and Elsevier ("Elsevier") consists of your license details and the terms and conditions provided by Elsevier and Copyright Clearance Center.

| | |
|---|---|
| License Number | 4685010626863 |
| License date | Oct 09, 2019 |
| Licensed Content Publisher | Elsevier |
| Licensed Content Publication | European Journal of Pharmacology |
| Licensed Content Title | Molecular mechanism of doxorubicin-induced cardiomyopathy – An update |
| Licensed Content Author | Kaviyarasi Renu,Abilash V.G.,Tirupathi Pichiah P.B.,Sankarganesh Arunachalam |
| Licensed Content Date | Jan 5, 2018 |
| Licensed Content Volume | 818 |
| Licensed Content Issue | n/a |
| Licensed Content Pages | 13 |
| Start Page | 241 |
| End Page | 253 |
| Type of Use | reuse in a thesis/dissertation |
| Intended publisher of new work | other |
| Portion | figures/tables/illustrations |
| Number of figures/tables/illustrations | 1 |
| Format | electronic |
| Are you the author of this Elsevier article? | No |
| Will you be translating? | No |
| Original figure numbers | FIG 1 |
| Title of your thesis/dissertation | IDENTIFICATION OF EARLY BIOMARKERS OF CARDIOTOXICITY DUE TO CANCER/CHEMOTHERAPY BY TARGETING MICRO-RNAS |
| Expected completion date | Dec 2019 |
| Estimated size (number of pages) | 140 |
| Requestor Location | Mr. Temitope R. Ogundipe<br>C/O Merriman and Bosman Street,<br>Mike De Vries Building<br>1st floor<br>STELLENBOSCH, WESTERN CAPE 7600<br>South Africa<br>Attn: Mr. Temitope R. Ogundipe |
| Publisher Tax ID | ZA 4110266048 |
| Total | 0.00 USD |
| Terms and Conditions | |

**INTRODUCTION**

**Figure 7.19: Permission letter for Figure 4.1.**

## *APPENDIX M: TURNITIN REPORT*

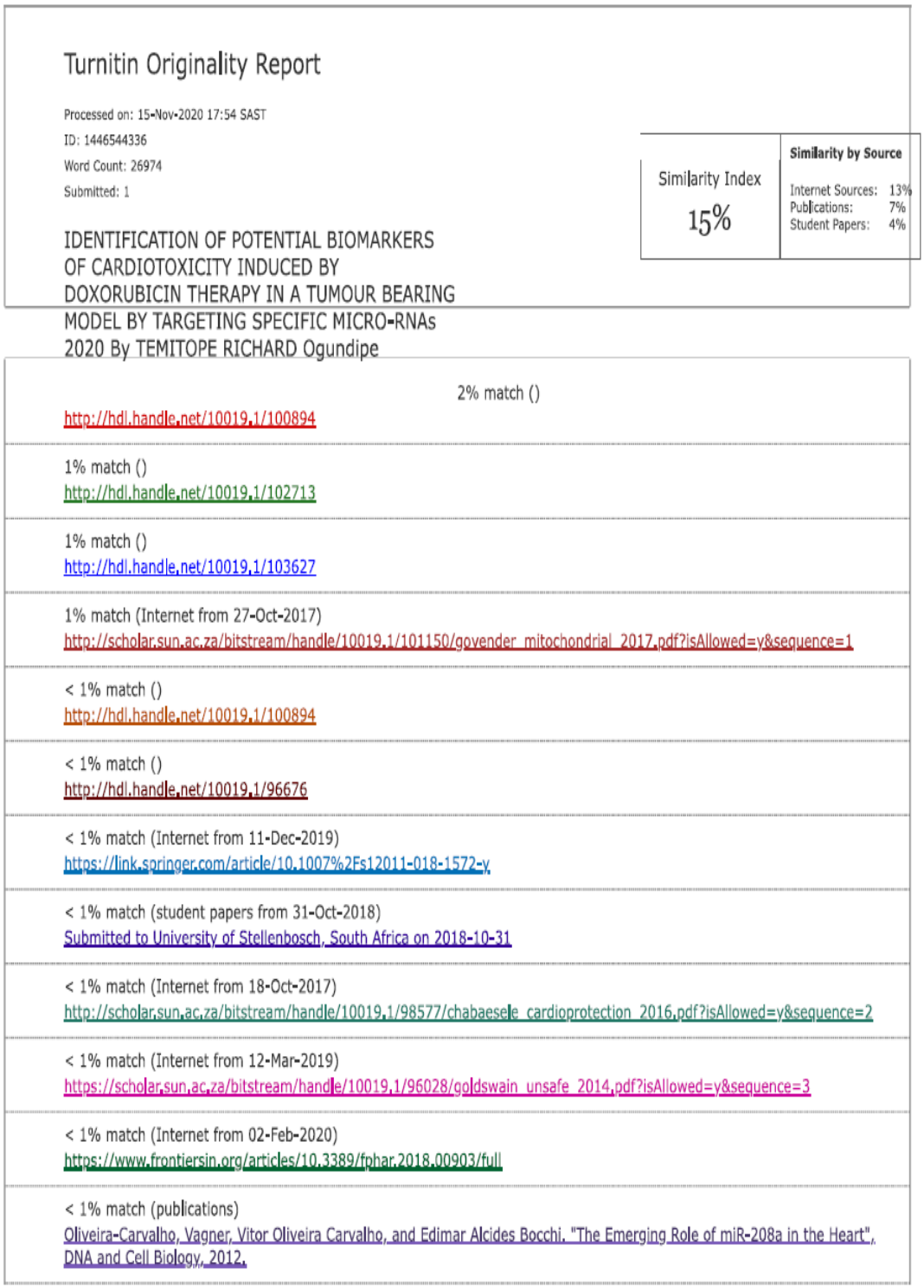

Turnitin Originality Report

Processed on: 15-Nov-2020 17:54 SAST
ID: 1446544336
Word Count: 26974
Submitted: 1

IDENTIFICATION OF POTENTIAL BIOMARKERS OF CARDIOTOXICITY INDUCED BY DOXORUBICIN THERAPY IN A TUMOUR BEARING MODEL BY TARGETING SPECIFIC MICRO-RNAs
2020 By TEMITOPE RICHARD Ogundipe

| Similarity Index | Similarity by Source |
|---|---|
| 15% | Internet Sources: 13%<br>Publications: 7%<br>Student Papers: 4% |

2% match ()
http://hdl.handle.net/10019.1/100894

1% match ()
http://hdl.handle.net/10019.1/102713

1% match ()
http://hdl.handle.net/10019.1/103627

1% match (Internet from 27-Oct-2017)
http://scholar.sun.ac.za/bitstream/handle/10019.1/101150/govender_mitochondrial_2017.pdf?isAllowed=y&sequence=1

< 1% match ()
http://hdl.handle.net/10019.1/100894

< 1% match ()
http://hdl.handle.net/10019.1/96676

< 1% match (Internet from 11-Dec-2019)
https://link.springer.com/article/10.1007%2Fs12011-018-1572-y

< 1% match (student papers from 31-Oct-2018)
Submitted to University of Stellenbosch, South Africa on 2018-10-31

< 1% match (Internet from 18-Oct-2017)
http://scholar.sun.ac.za/bitstream/handle/10019.1/98577/chabaesele_cardioprotection_2016.pdf?isAllowed=y&sequence=2

< 1% match (Internet from 12-Mar-2019)
https://scholar.sun.ac.za/bitstream/handle/10019.1/96028/goldswain_unsafe_2014.pdf?isAllowed=y&sequence=3

< 1% match (Internet from 02-Feb-2020)
https://www.frontiersin.org/articles/10.3389/fphar.2018.00903/full

< 1% match (publications)
Oliveira-Carvalho, Vagner, Vitor Oliveira Carvalho, and Edimar Alcides Bocchi. "The Emerging Role of miR-208a in the Heart", DNA and Cell Biology, 2012.

**Figure 7.20: Originality report generated by plaigairism checking software (Turnitin)**